Universidade de Lisboa

Faculdade de Farmácia

S-glutathionylation of Mitofusin 2 in the regulation of mitochondrial (dys)function in Parkinson's disease

Daria Alexandrovna Kovalchuk

Dissertation supervised by Andreia Margarida Gonçalves das Neves Carvalho, PhD
and co-supervised by Maria João Carlos da Silva Gama, PhD

Master in Biopharmaceutical Sciences

2022

Universidade de Lisboa

Faculdade de Farmácia

S-glutathionylation of Mitofusin 2 in the regulation of mitochondrial (dys)function in Parkinson's disease

Daria Alexandrovna Kovalchuk

Dissertation supervised by Andreia Margarida Gonçalves das Neves Carvalho, PhD
and co-supervised by Maria João Carlos da Silva Gama, PhD

Master in Biopharmaceutical Sciences

2022

Part of the results discussed in this dissertation were exhibited in the following meetings:

Kovalchuk D., Caria I., Anjo S.I., Branco V., Nunes M.J., Castro-Caldas M., Rodrigues E., Guedes R.C., Manadas B., Gama M.J., and Carvalho A.N. *Redox-signaling regulation of mitochondrial dynamics and function through post-translational modifications*. EMBO practical course "Characterization of post-translational modifications in cellular signalling", Odense, Denmark, May 05-12, 2022 [Abstract and oral communication].

Kovalchuk D., Caria I., Nunes M.J., Anjo S.I., Manadas B., Castro-Caldas M., Rodrigues E., Branco V., Guedes R.C., Gama M.J., and Carvalho A.N. *Redox-signalling regulation of Mitofusin 2 through S-glutathionylation in Parkinson's disease*. 13th iMed.Ulisboa Postgraduate Students Meeting, Lisbon, Portugal, July 04-05, 2022 [Abstract and Poster]

This work was supported in part by national funds from *Fundação para a Ciência e Tecnologia* (FCT) through UIDB/04138/2020 and project EXPL/BIA-BQM/0793/2021 (to A.N.C.).

Human brain samples used in this study were obtained from The Netherlands Brain Bank (NBB; open access: www.brainbank.nl).

ACKNOWLEDGMENTS

I would like to start by expressing my gratitude to Professor Cecília Rodrigues for providing me the opportunity to develop my dissertation at the Cell Function and Therapeutic Targeting Lab at the Research Institute for Medicines and for always be willing to support and help in any circumstance.

To my dearest supervisor Andreia, who gave me the opportunity to develop this work in the frame of such a remarkable project, thank you for believing in my capacities and for always welcoming my opinion and thoughts. I'll be forever grateful for helping me realize my passion for scientific research. I would also like to express my gratitude to my co-supervisor, Professor Maria João Gama, for assisting with the development of this dissertation and for always giving me words of encouragement. I am also very grateful to Professor Elsa Rodrigues, Professor Margarida Castro-Caldas and to Maria for hosting me at a group of powerful female scientists and for generously helping me in the complicated days at the laboratory and gave me wise advices. To all the other members and brilliant scientists of *CellFun*, namely, Marta, Simão, André, Vanda, Miguel and Joana, with whom I interacted every day during this year, thank you for all the support given. A special acknowledgement also to Professor Rita Guedes and to the incredible PhD students, namely, Pedro, Filipe and Silvestre, and to Patrícia at the Computational Medicinal Chemistry Laboratory, for kindly taught me so much and helped me in the *in silico* study.

To my dear colleagues Inês, Margarida and Joana, who I now have the pleasure to call friends, words can't express all the feeling of gratitude I have for you. Thank you for the infinite kindness, friendship and for sticking to each other since day one. Thank you for all the talks, laughs and cries and most of all for the everyday company and support. To Brian, Jan, André, Nicole and Gonçalo for the best moments in and outside the laboratory, for the nonstop laughs and long dinner talks, but also for encouraging each other in the sunny and rainy days at iMed.

Last but not least, I am incredibly grateful for my family and friends. To the woman of my life, my Mama, thank you for always being by my side and providing me the best education. Most importantly, thank you for the unconditional love and endless support. To my *Babushka*, who I known I make proud every day, to my brothers Vladimir and Andrey, and to António, thank you for always encouraging and supporting me in life. Finally, I would like to thank my best friends and soulmates Mariana and Carolina, with whom for so long, I have been sharing all the happy and sad moments, who give me everyday motivation and whose friendship is unexplainable.

ABSTRACT

Mitochondrial dysfunction and oxidative stress are key contributors to dopaminergic loss in Parkinson's disease (PD). Glutathione is an important antioxidant molecule able to induce S-glutathionylation, a redox post-translational modification that acts on signalling pathways, protects proteins from irreversible oxidative damage and modifies structure/function relationship. Mitofusin 2 (MFN2) is a mitochondrial dynamics' regulator which S-glutathionylation of specific cysteine residues was reported to drive mitochondrial hyperfusion as an early adaptive stress response. Mitochondrial function has been shown to largely depend on the redox regulation of mitochondrial dynamics through the remodelling of damaged organelles. However, it is still elusive the regulation of MFN2 by S-glutathionylation in the context of neurodegeneration in PD and if mitochondrial fusion is triggered in response to mitochondrial impairment and oxidative stress.

Herein, to understand if MFN2 is modulated by S-glutathionylation in an *in vitro* PD model, SH-SY5Y cells were exposed to the parkinsonism-triggering neurotoxin MPP^+ and in parallel to redox-modifying agents that impair glutathione levels. Results from the experimental PD model indicated a tendency to increased MFN2 expression and S-glutathionylation. Interestingly, MPP^+ led to a larger oligomerization of MFN2 which seems to be dependent on mitochondrial dysfunction and ROS overproduction and not exclusively on the reduced glutathione levels featured in PD patients. Together with the analysis of PD *post-mortem* samples that revealed several mitochondrial fusion clusters, results suggested an important regulation of MFN2 in response to the accumulation of dysfunctional mitochondria in PD. Moreover, a combination of bioinformatic and *in silico* approaches identified five cysteines in MFN2, targets of S-glutathionylation, and revealed possible structural and functional differences between MFN2 isoforms that may be critical for the efficiency of mitochondrial fusion.

Overall, our results gave insights on the processes coupling mitochondrial dynamics to the cellular stress response in PD, contributing to unravel possible novel targets for therapeutic intervention.

Keywords: Mitofusin 2; S-glutathionylation; Mitochondrial Dysfunction; Oxidative Stress; Parkinson's Disease

RESUMO

A disfunção mitocondrial e o stress oxidativo contribuem para a degeneração dos neurónios dopaminérgicos na doença de Parkinson (DP). O glutationo é um importante antioxidante que induz S-glutationilação, uma modificação pós-tradução que atua em relevantes vias de sinalização, protege as proteínas contra danos oxidativos irreversíveis e modifica a relação estrutura/função. A mitofusina 2 (MFN2) é uma proteína da dinâmica mitocondrial que é S-glutationilada levando à indução de hiperfusão mitocondrial como resposta adaptativa ao stress oxidativo. A função mitocondrial depende da regulação redox da dinâmica mitocondrial que é responsável pela remodelação de mitocôndrias danificadas. No entanto, a regulação da MFN2 por S-glutationilação na DP bem como a ativação da fusão mitocondrial em resposta à disfunção mitocondrial e ao stress oxidativo, não foram ainda esclarecidas.

Neste trabalho, de modo a explorar a regulação funcional da MFN2 pela S-glutationilação, um modelo *in vitro* de DP foi estabelecido expondo células SH-SY5Y à neurotoxina MPP^+ e, em paralelo, a agentes modificadores do estado redox celular e que alteram os níveis de glutationo. Os resultados indiciaram uma tendência para o aumento dos níveis de expressão da MFN2 e da sua S-glutationilação. Curiosamente, o MPP^+ levou à oligomerização da MFN2 dependente da disfunção mitocondrial e da sobreprodução de espécies reativas, e não exclusivamente dos níveis reduzidos de glutationo como ocorre na DP. Juntamente com a análise de amostras *post-mortem* de doentes com DP que revelou um possível aumento da fusão mitocondrial, os resultados sugeriram a regulação da MFN2 em resposta à acumulação de mitocôndrias danificadas. Combinando abordagens bioinformáticas e *in silico* identificaram-se cinco cisteínas potencialmente S-glutationiladas na MFN2 passíveis de modular a sua função. Além disso, as diferenças estruturais e funcionais que se identificaram entre as duas isoformas da MFN2, sugerem diferentes contribuições de cada isoforma para a eficiência na fusão mitocondrial.

Estes resultados elucidam os processos que associam a dinâmica mitocondrial e a resposta ao stress oxidativo na DP, contribuindo para a descoberta de possíveis novos alvos terapêuticos.

Palavras-chave: Mitofusina 2; S-glutationilação; Disfunção Mitocondrial; Stress Oxidativo; Doença de Parkinson

TABLE OF CONTENTS

INDEX OF FIGURES

INDEX OF TABLES

ABBREVIATIONS

PD Parkinson' disease

DAergic Dopaminergic

SNpc Substantia nigra pars compacta

DA Dopamine

SNCA α-synuclein

LRRK2 Leucine-rich repeat kinase 2

UCHL-1 Ubiquitin C-terminal hydrolase-L1

VPS35 Vacuolar protein sorting ortholog 35

CHCHD2 Coiled-coil-helix-coiled-coil-helix domain containing 2

PINK1 Phosphatase and tensin homolog (PTEN)-induced kinase 1

DJ-1 Protein deglycase DJ-1

ATP13A2 Probable cation-transporting ATPase 13A2

ATP Adenosine triphosphate

Ca^{2+} Calcium ion

L-DOPA Levodopa

MAO-B Monoamine oxidase B

OMM Outer mitochondrial membrane

IMM Inner mitochondrial membrane

IMS Intermembrane space

ROS Reactive oxygen species

DNA Deoxyribonucleic acid

RNA Ribonucleic acid

mtDNA Mitochondrial DNA

OXPHOS Oxidative phosphorylation

GTP Guanosine triphosphate

MFN1 Mitofusin 1

MFN2 Mitofusin 2

OPA1 Optic protein atrophy 1

DRP1 GTPase dynamin-1-like protein

MFF Mitochondrial fission factor

FIS1 Mitochondrial fission 1 protein

MID49/51 Mitochondrial dynamics proteins 49 and 51

HR1/2 Coiled-coil heptad-repeat domains 1 and 2

TMDs Transmembrane domains

CMT2A Charcot-Marie-Tooth Syndrome type 2A

ER Endoplasmic reticulum

MIRO1/2 Mitochondrial Rho GTPases 1 and 2

PGC-1α/β Peroxisome proliferator-activated receptor-gamma coactivator α and β

ERR Estrogen-related receptor

KO Knockout

LCFA Long-chain fatty acids

NADPH Nicotinamide adenine dinucleotide phosphate

NOXs NADPH oxidases

COXs Cyclooxygenases

LOXs Lipoxygenases

NADH/NAD$^+$ Nicotinamide adenine dinucleotide reduced and oxidized forms

MDA Malondialdehyde

8-oxo-dG 8-oxo-2'-deoxyguanosine

LPO Lipid hydroperoxide

SOD Superoxide dismutase

CAT Catalase

GSH Glutathione reduced form

GSSG Glutathione oxidized form

DAQs Dopamine quinones

MAMs Mitochondria-associated membranes

PRDx Peroxiredoxin

ADP Adenosine diphosphate

Redox-PTMs Redox post-translational modifications

LMW Low-molecular weight

GCL Glutamate-cysteine ligase

γ-GC L-γ-glutamyl-L-cysteine

GS Glutathione synthase

GPx Glutathione peroxidase

GR Glutathione reductase

PSSG S-glutathionylated proteins

DIC Dicarboxylate carrier

2OG 2-oxoglutarate carrier

CNS Central nervous system

CSF Cerebrospinal fluid

TTC Tricarboxylate carrier

p53 Nuclear phosphoprotein 53

JAK Janus kinase

NF-kB Nuclear factor-kB

AD Alzheimer's disease

Cys Cysteine residue

pK_a Acid dissociation constant

RNS Reactive nitrogen species

RSS Reactive sulphur species

GSTs Glutathione-S-transferases

GSTP Glutathione-S-transferase-P

GRx Glutaredoxin

TRx Thioredoxin

SRx Sulphiredoxin

PDIs Disulphide isomerases

MPP$^+$ 1-methyl-4-phenylpyridinium ion

MPTP 1-methyl-4-phenyl-1,2,3,6-tetrahydropyridine

TH Tyrosine hydroxylase

DAT Dopamine transporter

BSO Buthionine sulfoximine

6-OHDA 6-hydroxydopamine

tBHP *Tert*-butyl hydroperoxide

NO Nitric oxide

SEM Standard error of the mean

mRNA Messenger RNA

TOM20 Mitochondrial import receptor subunit 20 of the translocase mitochondrial outer membrane

NEM N-ethylmaleimide

qPCR Quantitative real-time polymerase chain reaction

RLP19/29 Ribosomal protein L19 and L29

PDB Protein Data Bank

MOE Molecular Operating Environment software

GOLD Genetic Optimisation for Ligand Docking software

MISR Mitofusin isoform specific region

I. INTRODUCTION

A. Parkinson's disease (PD)

1. Symptomatology, aetiology and pathophysiology

Parkinson's disease (PD) is a common chronic, age-associated, and often debilitating neurodegenerative condition characterized by the progressive degeneration of dopaminergic (DAergic) neurons in the substantia nigra pars compacta (SNpc) of ventral midbrain, resulting in dopamine (DA) deficiency in the striatum[1]; and the predominance of intracytoplasmic inclusions, i.e., Lewy bodies, in the surviving neurons which aggregate throughout disease progression [2]. The disease is named after the English doctor James Parkinson, who published the first detailed description of the disease in «*An Essay on the Shaking Palsy*» in 1817 [3]. PD is considered the second most common neurodegenerative disease, affecting approximately 1% of the population over the age of 60 and 5% over the age of 85 [4,5]. PD patients display common symptoms characterized by progressive motor deficits including bradykinesia, resting tremor, rigidity, and postural instability [6,7] caused by the loss of DAergic neurons and subsequent depletion of striatal DA. Although clinical diagnosis relies on the presence of these motor features, PD is also associated with many non-motor symptoms such as sleep disorders, depression, and impairment of cognitive functions by affecting cholinergic, serotonergic, and noradrenergic systems [8–10].

The aetiology of the sporadic form of PD remains elusive but studies over the past decades have identified responsible genes for the monogenic causes of familial PD (**Table I-1**). Genes associated to autosomal dominant forms of PD include α-synuclein (SNCA), leucine-rich repeat kinase 2 (LRRK2), ubiquitin C-terminal hydrolase-L1 (UCHL-1), vacuolar protein sorting ortholog 35 (VPS35) and coiled-coil-helix-coiled-coil-helix domain containing 2 (CHCHD2) [11]. The autosomal recessive associated inheritance PD genes include phosphatase and tensin homolog (PTEN)-induced kinase 1 (PINK1), E3 ubiquitin ligase Parkin, protein deglycase DJ-1, and probable cation-transporting ATPase 13A2 (ATP13A2) [11,12]. Several mutations in the identified genes have been directly linked to mitochondrial dysfunction and increased oxidative stress in PD [13–15] (**Table I-1**). Even though monogenic forms of PD represent 10-20% of the disease cases [16], investigating the cellular functions of the proteins encoded by these genes has been fundamental in identifying molecular pathways that mediate pathology in PD. This can be essential for providing insights also into the sporadic forms of the disease, as both forms of the PD often share common neuropathological features and underlying disease mechanisms. Moreover, external factors

including environmental stressors and neurotoxins by acting on the proteins implicated in monogenic PD, can be further linked to the sporadic cases [16].

Table I-1 Most common monogenic PD-related genes linked to mitochondrial dysfunction and oxidative stress. Mode of inheritance and PARK designed PD loci. N/A – not associated

Mode of Inheritance	Gene	PD locus
Autosomal dominant	SNCA	PARK1/4
	LRRK2	PARK8
	UCHL-1	PARK5
	VPS35	PARK17
	CHCHD2	N/A
Autosomal recessive	PARKIN	PARK2
	PINK1	PARK6
	DJ-1	PARK7
	ATP13A2	PARK9

Regardless the genetic associations, one of the major risk factors for neurodegenerative diseases such as PD, is advanced age [1]. Aging is marked by cumulative changes that are implied as common features in PD neuropathogenesis. This involves various molecular pathways and mechanisms such as deregulated proteostasis, mitochondrial dysfunction, oxidative stress, calcium (Ca^{2+}) homeostasis imbalance, defective axonal transport and neuroinflammation [17–21]. Hence, PD is now widely accepted as a complex, multifactorial disease that can have diverse genetic, biological, and environmental influences [1].

2. Current therapeutic approaches for PD

Remarkable progress has been made in understanding the neuropathogenesis and progression of PD as well as its symptoms. However, up-to-date, no cure for PD is known and therapies only aim to reduce symptomatology and improve patients' quality of life. Initial treatment is typically anchored on pharmacological substitution of striatal DA levels with medications including Levodopa (L-DOPA), monoamine oxidase B (MAO-B) inhibitors (e.g., selegiline, rasagiline) or DA agonists (e.g., pramipexole, ropinirole) [22–24]. Additional prescriptions include catechol-O-methyltransferase inhibitors (e.g., entacapone) and anti-cholinergic medication. Non-dopaminergic approaches to address both motor and non-motor symptoms rely on deep brain stimulation with microelectrodes for patients that are developing intractable pharmacological-related motor complications [25]. Diet changes and certain forms of rehabilitation have also shown some effectiveness at improving some of the motor and non-motor symptoms [26]. Most recently, experimental therapies have tried to restore striatal DA by cell-based approaches [27]. Certainly, understanding the molecular mechanisms underlying the disease and manipulating the disrupted cellular signalling

pathways provide new hope for the finding of therapeutic strategies to treat not only PD but other neurodegenerative conditions.

B. Mitochondrial dynamics

1. Mitochondria in neuron metabolism

Mitochondria are double-membrane organelles found in eukaryotic cells with structurally and functionally distinct outer (OMM) and inner (IMM) membranes, separating the intermembrane space (IMS) from the matrix [28]. The size, shape, and number of mitochondria can vary widely depending on the cell bioenergetic and functional requirements and on the environmental stress to which the cell is subjected [29]. Mitochondria are well-known to be required for a wide range of cellular processes such as the generation of adenosine triphosphate (ATP), the production of reactive oxygen species (ROS), the synthesis of key metabolites, Ca^{2+} homeostasis, and programmed and unprogrammed cell death [30]. Termed as the *powerhouses* of the cell, mitochondria convert most of the cell's energy to ATP by generating a proton (ΔpHm) and electrical (Δψm) gradient across the IMM through the electron transport chain, which is comprised of five polyprotein complexes, namely, complex I (NADH/ubiquinone oxidoreductase), complex II (succinate/ubiquinone oxidoreductase), complex III (ubiquinone/cytochrome *c* oxidoreductase), complex IV (cytochrome *c* oxidase), and complex V (ATP synthase) [31]. These complexes are considered vital components for cellular bioenergetics and survival. Mitochondria also possess their own transcriptional and translational machinery required for expression of mitochondrial DNA (mtDNA) which encodes proteins mainly related with oxidative phosphorylation (OXPHOS) [30].

The brain is extremely metabolically active and due to the limited glycolytic capacity of the neurons, a delicate maintenance of mitochondrial function in the neuronal network is required [32]. Besides being energetically demanding cells, neurons are highly polarized with complex cellular extensions (i.e., axons and dendrites). Thus, neurons need the timely and appropriate transport and distribution of mitochondria to provide energy and an internal Ca^{2+} storage pool for localized neuronal activities such as neurotransmission and plasticity, axonal and dendritic transport, and synaptic vesicle recycling [18,33]. Therefore, high-energy demands and the requirement to maintain homeostasis at sites distant to the cell body likely make neurons particularly vulnerable to mitochondrial dysfunction, which can have severe consequences for neuronal function [32].

The size, number, and location of mitochondria are critical for the complexity of its function. Thereby, mitochondria form an interconnected and highly dynamic network inside cells. This dynamism refers to changes in mitochondrial morphology through the events of

fusion and fission, to mitochondrial distribution achieved by mitochondrial trafficking, and to autophagic elimination known as mitophagy [34,35]. Changes in mitochondrial dynamics have been highly associated with various processes including development, cell division, apoptosis, and ultimately, neurodegeneration [36–39].

2. Mitochondrial fusion and fission

The overall shape of the mitochondrial tubular network is determined by the balance between the events of mitochondrial fusion and fission, which are regulated by several large dynamin-related GTPase proteins [40]. Mitochondrial fusion is the union of two adjacent mitochondria resulting in one mitochondrion, whereas mitochondrial fission is characterized by the division of one mitochondrion into two daughter mitochondria (**Figure I-1**).

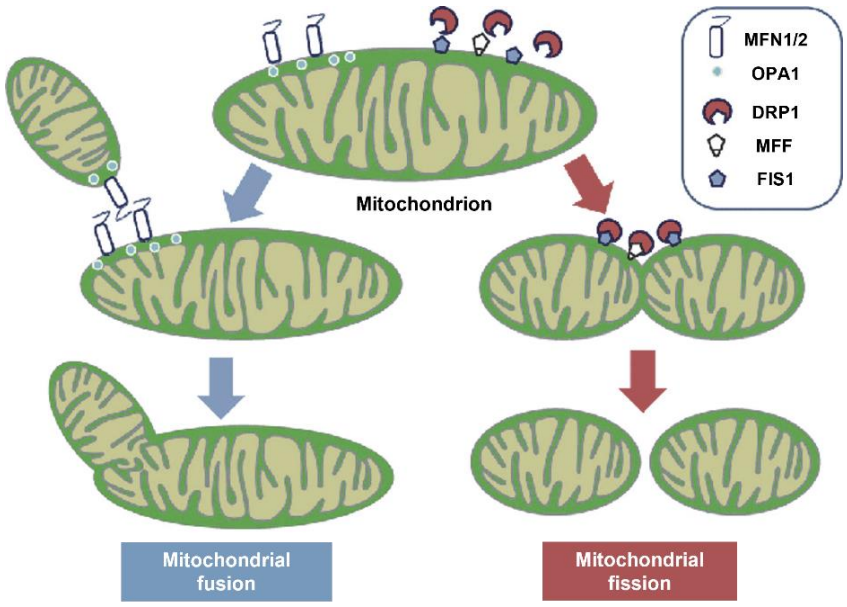

Figure I-1 Mitochondrial fusion (left) and fission (right) mechanisms under physiological conditions maintain cellular homeostasis. MFN1, MFN2 and OPA1 are the major mitochondrial fusion regulators, while DRP1 conducts mitochondrial fission. Mitochondrial fusion is a three-step process that firstly requires tethering of two adjacent mitochondria; secondly, OMM fusion mediated through interactions of coiled-coil domains of MFN1 and/or MFN2 and GTP hydrolysis; and finally, IMM fusion which involves OPA1. In mitochondrial fission, cytosolic DRP1 is recruited to the OMM by receptor proteins such as MFF and/or FIS1, followed by oligomerization into ring-like structures to constrict the mitochondrial membrane and thereby achieving the fragmentation. Adapted from *Saotome et al., 2014*.

The fusion of adjacent mitochondria is induced by homo- or heterodimers of the GTPases mitofusin 1 and 2 (MFN1/2) located at the OMM [41,42], while the fusion of the IMM is mediated by optic protein atrophy 1 (OPA1) [43] (**Figure I-1**). Generally, mitochondrial fusion is a three-step process: (1) the tethering of two adjacent mitochondria; (2) the fusion of the two

OMM due to conformational changes of MFNs induced by guanosine triphosphate (GTP) hydrolysis; and (3) IMM fusion [44]. On the other hand, the key regulator in the mitochondrial fission is the cytosolic GTPase dynamin-1-like protein (DRP1) [45]. After activation, DRP1 translocates to the OMM through recruitment by several receptors (e.g., mitochondrial fission factor (MFF), mitochondrial fission 1 protein (FIS1), mitochondrial dynamics proteins MID49/51), oligomerizes into a ring-like structure to encircle the mitochondrion by self-assembly and GTP hydrolysis, thereby, inducing mitochondrial fragmentation [46].

As mitochondria are relatively vulnerable to damage, irreversible defective mitochondria need to be cleared in a timely manner, and mitochondrial fission has been shown to precede the elimination of damaged organelles by mitophagy [47]. Additionally, mitochondrial fission can facilitate motility and is required for mtDNA replication [48] and mitochondrial redistribution during cell division [39]. Meanwhile, mitochondrial fusion can spare mitochondria from mitophagy by allowing an exchange of lipids, proteins and mtDNA between organelles [49], permitting the defective ones to regain essential components of the respiratory chain, and equally distribute metabolites to maintain a healthy population of mitochondria throughout cells [50]. Moreover, fusion and fission events are crucial for mitochondrial bioenergetics as mitochondrial dynamics regulators are directly involved in the assembly of OXPHOS complexes, which underlines their important role in regulating mitochondrial function [51]. Thus, mitochondrial fission and fusion are central to organelle quality control and a shift in the expression of genes controlling this dynamic can lead to significant mitochondrial morphological changes [50].

3. Mitofusin 2 (MFN2): structure and function

In mammals, MFN2 belongs to the large family of mitochondrial transmembranar GTPases and is mainly expressed in the heart, skeletal muscle and brain [42,52]. MFN2 shares about 80% similarity with MFN1 in humans and their most extensive homology exists in the relevant functional domains [44]. MFN1 consists of 741 and MFN2 of 757 amino acids and both contain an N-terminal exposed to the cytosol, which contains a GTPase domain followed by a coiled-coil heptad-repeat domain (HR1) and two transmembrane domains (TMDs) [44]. Only MFN2 harbours a proline-rich (PR) region between the HR1 and the TMDs (**Figure I-2A**). The C-terminal of both MFNs contains a second HR domain (HR2) which is most likely involved in protein–protein interactions, mainly, MFNs oligomerization [44,53–56].

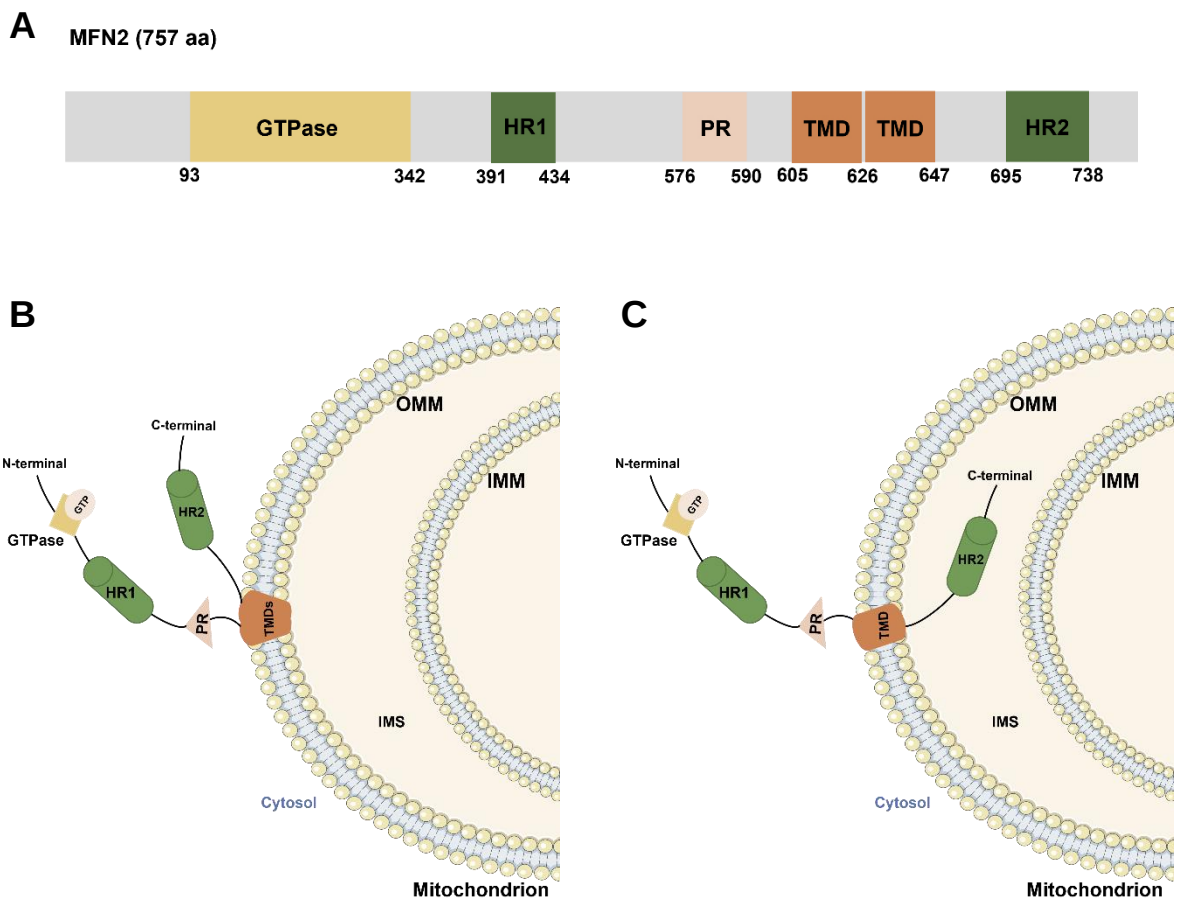

Figure I-2 MFN2 structure and topology. (A) Molecular architecture of MFN2 with the functional domains: GTPase domain, coiled-coil heptad-repeat (HR) regions 1 and 2, the proline-rich (PR) domain, and the two transmembrane domains (TMDs). The numbers below indicate the initial and the terminal amino acids of the corresponding domains. The two TMDs are separated by 15 amino acids. **(B)** N_{out}-C_{out} MFN2 topology in which C-terminal and HR2 domain are exposed to cytosol. **(C)** Recently demonstrated N_{out}-C_{in} MFN2 topology in which a single TMD keeps the N-terminal GTPase (with GTP-binding pocket) and HR1 domains in the cytosol but places the C-terminal and HR2 domain in the IMS. Adapted from *Zaman et al., 2022*. The schematics used in the figure were taken from Servier Medical Art by Servier.

It was proposed that MFNs can adopt either a constrained or permissive conformation for fusion, directed by intramolecular binding interactions [57]. According to this model, in the resting state MFNs are tethering-non-permissive, because of intramolecular, antiparallel HR1−HR2 interactions and a strict adherence of the GTPase domain to the OMM. In the tethering-permissive state, on the contrary, the destabilization of the intramolecular HR1−HR2 interaction allows the HR2 domain to extend into the cytosol, where it can encounter and bind HR2 domains of MFNs in the membrane of opposed mitochondria, mediating tethering as previously suggested [55]. The structural data requires the C-terminal and the HR1/2 domains to be cytoplasmic (N_{out}-C_{out} topology) and TMDs cross the OMM, which would result from a hairpin transmembrane anchor mediating the fusion process [55] (**Figure I-2B**). However, recent biochemical analysis instead suggested

that the membrane anchor is a single pass transmembrane helix, with the C-terminal and HR2 domain residing in the IMS (N_{out}-C_{in} topology) [53] (**Figure I-2C**).

The requirement for two topologies may serve specific functions, such as the coordination between OMM and IMM fusion, where MFNs with N_{out}-C_{in} topology might act as cofactors for MFNs with N_{out}-C_{out} topology [44,58,59]. Regardless of the topology in OMM, together with MFN1, the main function of MFN2 is to promote docking and mitochondrial fusion. The docking is induced by auto-oligomerization of MFNs in both *cis* (i.e., within the same membrane) and *trans* (i.e., across two opposing membranes) [54–56,60]. Although, *cis*-oligomerization is currently lacking structural insights, it has been linked to the N_{out}-C_{in} topology [53]. More specifically, *cis*-oligomerization of MFN2 was shown to be triggered by formation of disulphide bridges in HR2 domains, which stimulated mitochondrial fusion [53]. Therefore, HR2 domain seems to be important for the initial tethering between adjacent mitochondria through a dimeric antiparallel coiled-coil structure forming either homodimers (MFN1-MFN1 or MFN2-MFN2) or heterodimers (MFN1-MFN2) [55], while the GTPase domain is proposed to be critical for fusion completion [55]. The GTPase domain induces GTP hydrolysis to self-assembly and conformational changes which lead to membrane remodelling and the two opposite OMMs integration [61]. After GTP hydrolysis, MFN1 apparently loses its affinity to its counterpart but has greater GTP turnover activity, while MFN2 remain as dimers, making it a more effective tethering molecule [44].

The physiological relevance of the mitochondrial dynamics regulator MFN2 came to light with the discovery that mutations in this protein are associated with the inherited axonal neuropathy Charcot-Marie-Tooth Syndrome type 2A (CMT2A), affecting motor and sensory neurons [62]. The cellular and molecular mechanisms by which MFN2 mutations determine neuronal degeneration in CMT2A are still largely unclear. However, the importance of a regulated mitochondrial fusion event in cell physiology became clear when fibroblasts from patients with CMT2A were shown to present abnormalities in mitochondrial metabolism, characterized by lower mitochondrial coupling and impaired mitochondrial membrane potential [63]. Likewise, MFN2 depletion or deficiency in mammalian cells has been shown to induce mitochondrial dysfunction, characterized by a decrease in oxygen consumption coupled to ATP synthesis, increased production of ROS, and reduced coenzyme Q levels, thereby, leading to reduced glucose, pyruvate, and fatty acid oxidation [64–66]. Additional non-fusogenic functions of MFN2 include, for example, modulation of endoplasmic reticulum (ER)−mitochondria contacts [67], cell metabolism [68] and apoptosis [69]. MFN2 was also shown to play a key role in the heart as cardiac myocytes lacking MFN2 displayed a modest enlargement of mitochondria and attenuated cardiac cell death in response to ischemia-reperfusion injury [70]. Moreover, MFN2 acts as a receptor for PINK1/Parkin mediated

mitophagy [71], and is involved in mitochondrial transport via interactions with the mitochondrial transport machinery including the mitochondrial Rho GTPases 1 and 2 (MIRO1/2) [72]. Additionally, peroxisome proliferator-activated receptor-gamma coactivator (PGC)-1α and β are positive regulators of mitochondrial fusion activity under a range of physiological conditions and stimulate MFN2 expression by targeting the MFN2 promotor in an estrogen-related receptor (ERR)α-binding element-dependent manner [73]. MFN2 is also considered to be critical for embryonic development as complete loss of MFN2 is lethal in mice [74] as well as in *Drosophila melanogaster* [75]; and conditional MFN2 knockout (KO) severely impairs cerebellum development, which culminated in early movement defects in newborn mice, leading to evident reductions in dendritic outgrowth and spine formation in Purkinje cells [76].

Taken together, increasing evidence has demonstrated the contribution of MFN2 in a wide range of cellular signalling pathways and mechanisms, making clear the potential impact of MFN2 defects in the onset/progression of different pathological conditions.

C. Mitochondrial (dys)function and oxidative stress in PD

The majority of the PD-related proteins (**Table I-1**) are reportedly associated with mitochondria function, highlighting these organelles as one of the critical hubs in the mechanisms underlying the disease [11]. Mitochondrial dysfunction associated with PD pathogenesis is commonly linked to impairment of mitochondrial biogenesis, Ca^{2+} homeostasis, variations in mitochondrial dynamics, dysfunction of the electron transport chain, compromised trafficking, defective mitophagy, and to cellular oxidation-reduction (redox) homeostasis disruption in a cell and tissue-dependent manner [11,12,77] (**Figure I-3**). The complex interplay of these various functions leads to a vicious cycle of progressive cellular dysfunction ultimately leading to neurodegeneration that underlies PD [11].

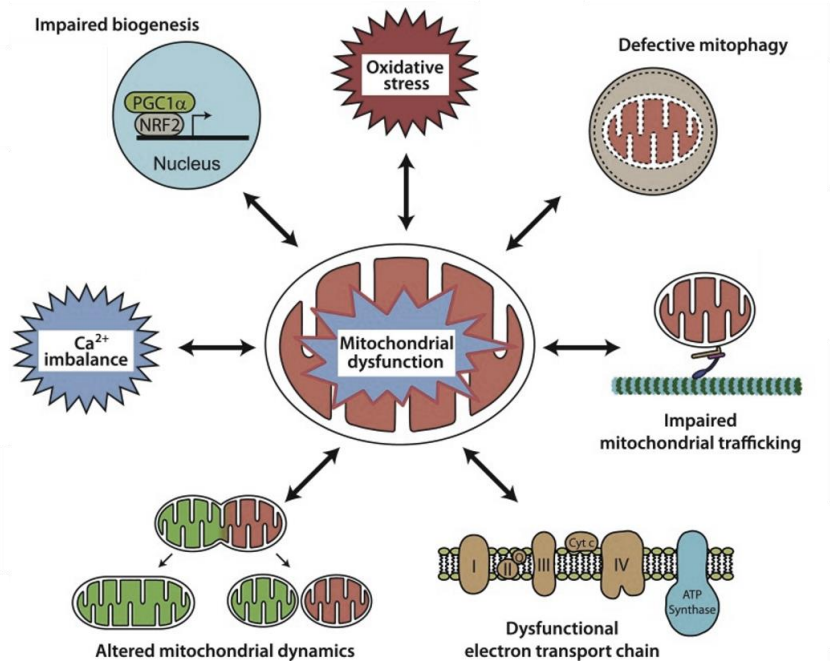

Figure I-3 The complex interplay between the various mitochondrial dysfunction pathways in PD neuropathogenesis. Adapted from *Park, Davis and Sue, 2018*.

1. Mitochondrial reactive species generation

From a quantitative viewpoint, mitochondria are thought to be the largest contributors to endogenous ROS production concurrently with other organelles such as the ER (particularly in the setting of ER stress) and peroxisomes (as part of their role in metabolizing long-chain fatty acids (LCFAs)), as well as various enzymes including NADPH oxidases (NOXs) and cyclooxygenases (COXs), cytochrome P450 enzymes and lipoxygenases (LOXs) [78]. Mitochondria can produce large amounts of superoxide radicals ($O_2^{\bullet-}$) and hydrogen peroxide (H_2O_2) almost entirely by OXPHOS (about 90%) [79]. Mitochondrial ROS production is physiologic but impairment in the electron transport chain can cause excessive ROS burden. Overproduction of ROS can occur under different conditions such as a high nicotinamide adenine dinucleotide reduced (NADH) and oxidized (NAD^+) forms ratio caused by inhibition or damage to complex I of the mitochondrial respiratory chain [80] or reverse electron transport due to a backlog of electrons during low ATP demand, cytochrome *c* loss, or inhibition of oxygen consumption [81]. Recent evidence has also identified complex II as one of the main ROS producers under certain conditions [82]. Likewise, complex III is an important ROS-producing source by both forward and reverse electron transfer primarily affecting the proteins of the OMM and IMS via oxidative modification, whereas the matrix proteins are rather targeted by ROS produced by complex I, indicating two separate redox-signalling pathways [83].

ROS production, especially by mitochondria, are now increasingly considered as important second messengers that regulate intracellular signal transduction under a variety of physiological and pathological conditions [84]. Consequently, the intricate relationship between mitochondrial function and overproduction of ROS has been intensively studied over the past decades in the context of the pathogenesis of human diseases, especially, neurodegenerative conditions.

2. Mitochondrial dysfunction, oxidative stress and abnormalities in mitochondrial dynamics: a complex interplay in PD

Although ROS are essential redox-signalling molecules, the oxidative damage such as lipid peroxidation, protein oxidation by cross-linking as well as DNA and RNA oxidation, occur within cells [12]. In neurodegenerative diseases such as PD, the required endogenous antioxidant defences are often diminished which results in excessive oxidative stress. Thus, DAergic neurons become more vulnerable to uncontrolled ROS production that ultimately leads to neuronal death by oxidative damage [85,86]. The connection between mitochondrial dysfunction and oxidative stress in PD is reported by the *post-mortem* analysis revealing complex I deficiency and increased oxidative stress markers (e.g., malondialdehyde (MDA); 8-oxo-2'-deoxyguanosine (8-oxo-dG); and lipid hydroperoxide (LPO)) accompanied with lower antioxidant activity (e.g., superoxide dismutase (SOD); catalase (CAT); and glutathione) in the SNpc of PD patients [87,88]. Evidence for oxidative damage in the brain of PD patients also includes the increase in H_2O_2 production by MAO-B as a by-product of its catalysis of oxidative deamination [89]. Auto-oxidation of DA seems to be increased in the early stages of PD when DA turnover is increased to compensate for the death of DAergic neurons, leading to the formation of DA quinones (DAQs) and $O_2^{\bullet-}$ radicals [90] which interact with ROS scavengers, respiratory chain complexes and PINK1/Parkin mitophagy pathway [77].

Oxidative stress can also disturb the mitochondrial fusion/fission balance causing a hyper-elongated mitochondrial network by stimulation of fusion and/or inhibition of fission or fragmented mitochondria by stimulation of fission and/or inhibition of fusion [91,92]. Functional studies on PD-causative mutations of Parkin, PINK1, DJ-1 and LRRK2 further indicated an interplay between mitochondrial dysfunction, oxidative stress, and mitochondrial dynamics in PD. Most of these proteins are localized to mitochondria or ER-mitochondria-associated membranes (MAMs), indicating their important role as additional regulators of mitochondrial dynamics [38]. Indeed, loss of PINK1, Parkin, or DJ-1 unanimously results in abnormal mitochondria morphology in DAergic neurons [14,93]. Moreover, mitochondrial fission has been reported to be induced by mutant forms of LRRK2 and α-synuclein in neurons that additionally exhibited greater vulnerability to mitochondrial dysfunction and display

overproduction of ROS [94]. Mitochondrial dynamics regulators themselves play essential roles in the neuropathogenesis of PD. For example, missense mutations in OPA1 (i.e., G488R, A495V) have been identified in patients with syndromic parkinsonism [36]. More recently, a study demonstrated that MFN2-KO mice developed severe and progressive DAergic neuron-specific mitochondrial dysfunction which triggered an early onset immune response, preceded with mitochondrial swelling, mtDNA depletion, respiratory chain deficiency and cell death, resulting in neurodegeneration and parkinsonism [95]. As mentioned above, MFN2 is a substrate of the PINK1/Parkin mitophagy pathway, whose mutations are linked to the familial forms of PD. MFN2 was reported to be especially increased in MAMs of fibroblasts from human PD patients with Parkin mutations [96]. A study also demonstrated that MFN2 is required for axonal projections of midbrain DAergic neurons *in vivo*; and Parkin translocation to mitochondria in MFN2-KO DAergic neurons was impaired, which led to accumulation of abnormal mitochondria [97]. In addition, a progressive loss of nigro-striatal projections was also seen in a similar model with disruption of MFN2 in DAergic neurons [98]. Mitochondrial fusion regulated by MFN2 is essential for the cellular homeostasis and it was demonstrated to be an early adaptive stress response in order to recycle damaged mitochondria [99].

In this regard, mitochondrial dynamics regulators such as MFN2 and PD-related proteins seem to play an important role in responding to the impairment in mitochondria by controlling mitochondrial quality control mechanisms and remodelling mitochondria damaged by ROS overproduction. Thus, mitochondrial dysfunction involved in neurodegenerative conditions such as in PD could highly empower alterations in mitochondrial morphology as part of response mechanisms to oxidative stress for maintenance of cellular homeostasis. Altogether, these findings likely suggest that there are important functional connections between the regulation of mitochondrial function, scavenge of ROS and mitochondrial dynamics to drive neurodegeneration in PD.

D. Glutathione

To combat oxidative stress, cells are equipped with various sophisticated antioxidant mechanisms. One of the primary cellular defences against oxidative stress is the presence of antioxidant enzymes with distinct and specific functions. For example, SODs act only on $O_2^{\bullet-}$ radicals, whereas CAT and the peroxiredoxin (PRDx) enzymes act exclusively on H_2O_2, lipid peroxides and peroxynitrite, respectively [100]. In addition to these enzymatic scavengers, cells have various non-enzymatic ways to combat reactive species such as the antioxidant molecule glutathione. Aside from the classical antioxidant enzyme-based mechanisms, the antioxidant responses can be invoked by mitochondria or achieved by negative feedback loops that inhibit ROS production, assembly and disassembly of supercomplexes, proton

leaks or redox post-translational modifications (redox-PTMs) of redox-sensitive proteins [92,101]. Altogether, these highly regulated mechanisms allow cells to use ROS for signalling whilst potentially avoiding its deleterious effects.

1. Glutathione system: biosynthesis, degradation and redox cycle

Glutathione (γ-glutamyl-L-cysteinyl-glycine) is a ubiquitously distributed tripeptide consisting of the three amino acids glycine, cysteine, and glutamic acid (**Figure I-4A**).

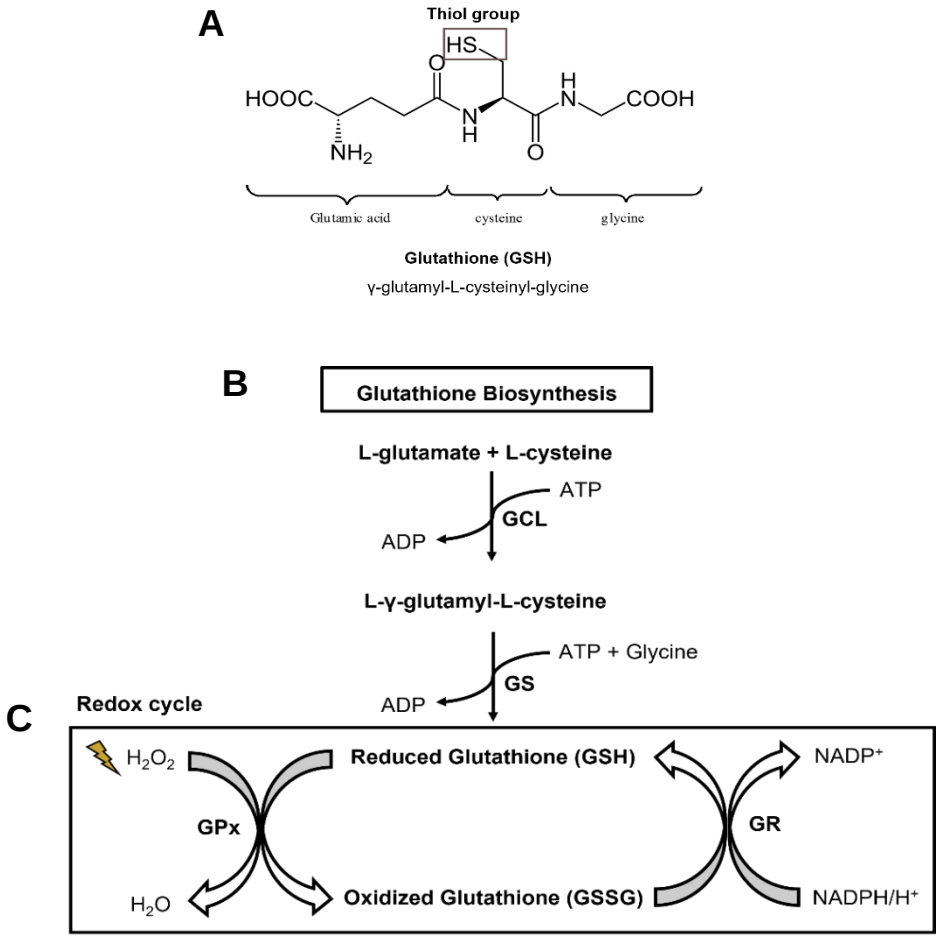

Figure I-4 Glutathione biosynthesis and redox cycle. (A) Glutathione reduced form (GSH). **(B)** Glutathione biosynthesis occurs by two mechanisms: *de novo* synthesis and recycling of oxidized glutathione (GSSG). *De novo* synthesis occurs in an ATP-dependent two-step process catalysed by two separate enzymes, glutamate-cysteine ligase (GCL) and glutathione synthase (GS). **(C)** The redox cycle is catalysed by two enzymes, glutathione peroxidase (GPx) which is a selenium-based enzyme that reduces H_2O_2 to water by oxidizing the formed GSH, and glutathione reductase (GR) that catalyses the reduction of GSSG back to GSH.

Among eukaryotes, glutathione is the predominant low-molecular-weight (LMW) cellular thiol [102] (**Figure I-4A**). In the cell reducing environment, LMW thiols are produced in high concentrations to serve as cofactors, reduce existing oxidative modifications, and form covalent linkages with protein free thiols [103]. Thus, due to its ability to donate reducing

equivalents, glutathione is essential for both direct and enzymatic neutralization of reactive species and for the maintenance of the cellular redox balance [104]. Besides its key role as endogenous antioxidant, glutathione participates in processes such as DNA synthesis and repair, stabilization of cell membranes, and detoxification of xenobiotics [104,105]. Under physiological conditions of cellular homeostasis, the tripeptide mainly exists in the reduced form (GSH) (**Figure I-4A**). However, the excessive ROS generation can lead to oxidation of GSH to oxidized glutathione (GSSG). The ratio between these two forms (GSH/GSSG) is normally used as a stress marker [105]. Thus, low cytosolic GSH/GSSG ratio is interpreted as evidence of redox imbalance and weakened reducing power in the cells [106].

Glutathione and various enzymes combine to form the glutathione system, which plays a crucial role in the utilization and regulation of reactive species [107]. Intracellular levels of glutathione are maintained by *de novo* synthesis and glutathione redox cycling [108]. Synthesis of glutathione in its reduced form (GSH) from L-cysteine and L-glutamate involves catalysis by glutamate-cysteine ligase (GCL) to form L-γ-glutamyl-L-cysteine (γ-GC) and the subsequent addition of glycine to γ-GC by glutathione synthase (GS) [109] (**Figure I-4B**). The antioxidant function of glutathione is largely accomplished by its role as substrate for the reactions catalysed by glutathione peroxidase (GPx) which reduces reactive species (e.g., H_2O_2), while synthetized GSH is oxidized to GSSG [109] (**Figure I-4C**). GSSG in turn can be reduced back to GSH by glutathione reductase (GR) at the expense of NADPH, thereby, forming a redox cycle [109] (**Figure I-4C**). The ability of the cell to recycle GSSG to GSH may be overcome during severe oxidative injury, leading to an accumulation of GSSG. To prevent a major shift in the redox equilibrium due to GSSG elevated pool, GSSG can be actively exported out of the cell [110] or react with a protein sulfhydryl group (-SH) leading to the formation of a mixed disulphide or S-glutathionylated protein (PSSG) [110]. This is a mechanism set mainly to protect sensitive protein free thiols from irreversible oxidation and may also serve to prevent loss of GSH levels under oxidative stress conditions [110].

The extra- and intracellular glutathione contents are regulated by the balance between the consumption, transportation, and production of glutathione [110]. Once synthesized in the cytosol, glutathione in its reduced form (GSH) is distributed to organelles such as the nucleus, ER and mitochondria, where distinct redox pools in terms of GSH=GSSG distribution is present. In most cells, GSH is present at concentrations of 1-10 mM in the cytosol [105], while GSSG levels do not exceed 1% of its total intracellular content [111]. In terms of mitochondria, the diffusion of GSH between IMS and cytosol is carried by porins present in OMM [112] and the passage from IMS to matrix requires carrier-mediated transports such as dicarboxylate carrier (DIC) and the 2-oxoglutarate carrier (2OG) [111–113]. On the other hand, in

humans and mouse, GSH degradation is achieved by two ChaC-like proteins in the cytosol (i.e., ChaC1 and ChaC2) [114,115] that function as γ-glutamyl cyclo-transferases acting specially to degrade GSH.

2. Glutathione in the brain

The redox homeostasis in the brain is crucial, since being an extremely metabolically active organ it displays consumption of high levels of oxygen which leads to the production of harmful free radicals, including $O_2^{\bullet-}$ radicals, hydroxyl (•OH), lipoperoxide (LOO•), nitric oxide (NO•) and nitrogen dioxide (NO_2•) radicals [112]. Organs where cells generate such high levels of free radicals require efficient antioxidant defence systems to protect cellular structures from oxidative damage. In the mammalian central nervous system (CNS), the highest concentration of the antioxidant molecule glutathione is found in glial cells of the cortex [116]. Glutathione is also highly present in both extracellular fluid and in the cerebrospinal fluid (CSF) [116]. Astrocytes are essential for upregulation of glutathione biosynthesis in the brain, most likely due to the transfer of cysteine precursors to nearby neurons [117]. Roughly 10 to 20% of glutathione in neural cells is localized in the mitochondria [118], being imported from the cytosol effectively by the specific glutathione carrier tricarboxylate (TTC) found in neurons and astrocytes [116]. Intriguingly, the tripeptide structure of glutathione can interfere with neuronal signalling through glutamate receptors as the conformational flexibility of glutathione allows for its binding to all classes of glutamate receptors via its glutamyl residue due to its similarity to the natural receptor agonist, L-glutamate [107].

Depletion of glutathione, especially in the brain, can trigger a series of processes including the amplification of oxidative and nitrosative cell damage; increased levels of inflammation; disturbances in intracellular signalling pathways of nuclear phosphoprotein p53, Janus kinases (JAK), and nuclear factor-kB (NF-kB); as well as decreased DNA synthesis and cell proliferation; inactivation of complex I of the electron transport chain; compromised epigenetic regulation of gene expression; and impaired control of energy production in different cell types [104,105,107]. Indeed, a low GSH/GSSG ratio is a well-established manifestation of the aging process and is widely reported in neurodegenerative disorders including PD and Alzheimer's disease (AD) [107,119].

3. Glutathione system in PD

Increased oxidative damage in neurodegenerative tissue is often accompanied by markers of deregulated antioxidant scavenging systems (non-enzymatic and enzymatic) as

previously discussed in **I.C.2**. Analysis of *post-mortem* brain tissues from PD patients has revealed decreased levels of glutathione in SNpc [88,120,121]. Under increased oxidative stress in PD, the oxidation of GSH to GSSG in DAergic neurons leads to the formation and extrusion of conjugates of GSH with electrophilic by-products of lipid oxidation [88,120]. Additionally, in the context of PD neurodegeneration, the rate of aggregation of α-synuclein was reported to be accelerated by GSSG levels [122]. Although in literature, there is a wide variability in the reported GPx levels in PD patients, in general, increased levels of GPx activity are interpreted to be a compensatory protective mechanism against oxidative stress [123]. Nevertheless, changes in glutathione metabolism may be a consequence of the neuroinflammatory modifications present in PD rather than a causal factor in the pathophysiology of PD [124]. Individuals with PD also present lower activities of GR [125]. Moreover, silencing the rate-limiting enzyme GCL induced gradual and progressive degeneration of nigral DAergic neurons, and overexpression of the enzyme led to aberrant S-glutathionylation of neuronal proteins [126].

Altogether, these findings suggested that the glutathione system in PD is considerably altered. Consequently, this justifies the impaired antioxidant defences in DAergic neurons that cannot effectively fight against the increased oxidative stress which ultimately intensifies the chronic inflammatory reactions, leads to oxidative damage in DNA and proteins and contributes to the neurodegeneration [124,125].

E. Redox post-translational modifications (redox-PTMs)

ROS may function as important second messengers within intracellular redox-dependent signalling pathways [127], which are well-conserved and primarily based on redox-PTMs [100]. PTMs of specific amino acids such as phosphorylation of serine (Ser) and tyrosine (Tyr) residues, ubiquitylation and SUMOylation of lysine (Lys), and S-glutathionylation of cysteine (Cys) residues, regulate the function and activity of many redox-sensitive proteins, which is important for rapidly adjusting the cellular physiology to diverse challenges in order to maintain homeostasis [128,129].

1. Cysteine as redox thiol switch

Despite its low abundance, with 2.2% in complex eukaryotes [130], cysteine residues are present within functional sites in proteins where they serve catalytic, regulatory and structural functions [131]. In addition, cysteine is one of the most commonly post-translationally modified amino acids due to the chemical and physical properties of its sulphur-based functional group – thiol group (-SH). The thiol group allows cysteine to participate in unique

redox reactions, forming post-translationally modified structures that exhibit significantly altered functions [131].

Cysteine residues can be distributed on protein surface exposed to an aqueous environment or deeply buried inside globular domains [132]. In aqueous solution, the thiol of cysteine is subject to deprotonation to form negatively charged thiolate ($-S^-$). Although both forms of the sulphur-based group are nucleophilic, thiolates are much more reactive than thiols [133]. At any given pH, the ratio of thiol/thiolate is determined by the acid dissociation constant (pK_a) of the group. The pK_a of the unperturbed cysteine thiol group is approximately 8.3 [133], indicating that only a relatively small proportion of lone residues would be in their thiolate forms at physiological pH (7.0-7.4). However, thiols and thiolates can be strongly influenced by the local microenvironment and exhibit a wide range of pK_a values [133]. For instance, vicinity of the basic amino acids lysine (Lys), arginine (Arg), and histidine (His) stabilize the thiolate anion by decreasing its pK_a (usually to 5.0-7.0, which makes thiols dissociate at physiological pH) and increasing the reactivity of the cysteine [133].

Protein sulphydryl groups have gained particular attention for their ability to transform oxidant signals into biological responses [134]. Nevertheless, it is important to note that about 10-20% of the total cellular cysteine thiols are readily oxidized under aerobic conditions, while the remaining are thought to be relatively inert to redox-reactions [134]. Under stress conditions, oxidation of thiols by free radicals leads to formation of thiyl groups ($-S\bullet$) (**Figure I-5**). Redox reactions of thiols or thiolates may also lead to other various reversible and regulatory modifications including S-glutathionylation (-SSG), formation of intra- and intermolecular disulphide bonds (-SS-), S-sulphenylation (-SOH), S-sulphydration (-SSH) or polysulphidation ($-SS_{(n)}H$), and S-nitrosylation (-SNO) [135] (**Figure I-5**). Besides, the thiosterification reaction could lead to S-palmitoylation through reversible addition of one or multiple palmitoyl moieties to the thiol group [135] (**Figure I-5**). Although, S-sulphenylation is considered a reversible modification, it can easily oxidize to generate sulphinic ($-SO_2H$) and sulphonic ($-SO_3H$) acids, which are known to be irreversible modifications causing permanent loss of protein activity [136] (**Figure I-5**).

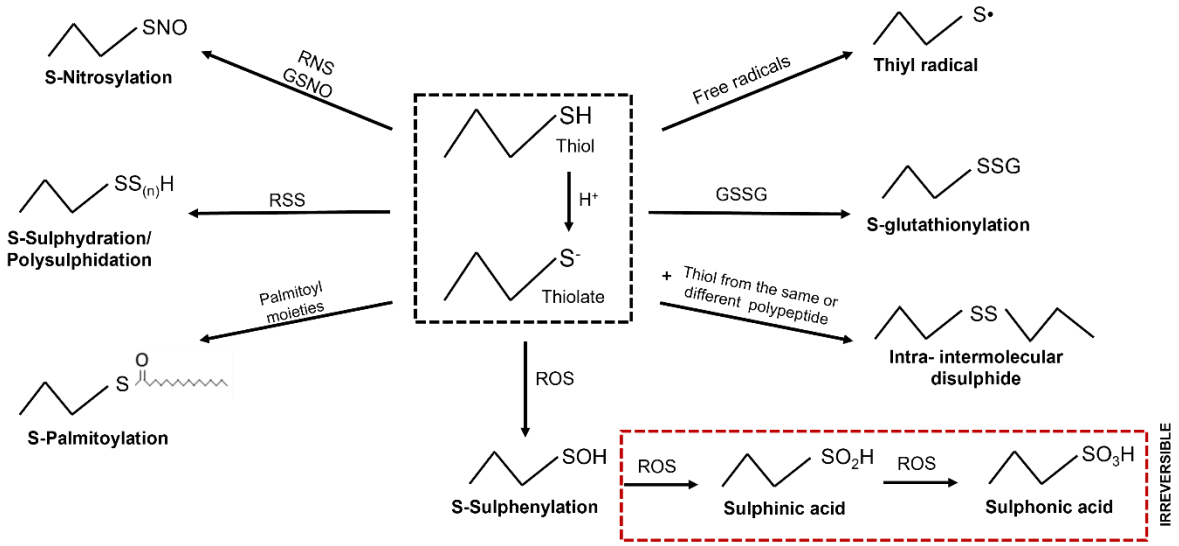

Figure I-5 Possible pathways for cysteine thiol redox modifications. Deprotonation of a free thiol (-SH) in a protein leads to the formation of a thiolate ($-S^-$). Both thiol and thiolate are redox sensitive which oxidation can result in several different redox modifications. Free radicals attack on protein thiol group leads to the formation of thiyl radical (-S•). Moreover, thiols can be S-glutathionylated (-SSG) by GSSG via thiol-disulphide exchange; form inter- intramolecular disulphide bridges (-SS-) through exchange with the sulphur group on the same or another protein; S-sulphenylated (-SOH) by ROS (e.g., H_2O_2) which can be subsequently and irreversibly oxidized to sulphinic acid (SO_2H) and, under severe oxidizing conditions, to sulphonic acid (SO_3H); S-palmitoylated by covalent linking of palmitoyl moieties; S-sulphydrated or polysulphidation ($-SS_{(n)}H$) by RSS; and S-nitrosylated (-SNO) by RNS (e.g., nitric oxide (NO)) or trans-nitrosylation by NO containing species such as S-nitrosoglutathione (GSNO).

This subset of modifications at critical thiol groups can act as redox switches, which elicit functional effects in response to changes in the cellular redox status [137]. Indeed, proteins containing free thiols exhibit reactivity towards ROS, reactive nitrosative (RNS) and sulphur species (RSS) [137].

2. S-glutathionylation of proteins

a) Thiol-disulphide exchange

Of all cysteine redox modifications that may occur, S-glutathionylation likely represents the common steady-state derivative due to cellular abundance of glutathione [129]. A common mechanism proposed for protein S-glutathionylation is the thiol-disulphide exchange between a reactive thiol on a specific protein cysteine residue and a GSSG molecule, leading to formation of S-glutathionylated proteins (PSSG) [138] (**Figure I-6**). An alternative mechanism involves the initial oxidative modification of a reduced protein thiol (e.g., -S•, -SOH, -SNO) which may then react with a GSH molecule to the mixed disulphide [138].

Thiol-disulphide exchange primarily relies on the redox state of cellular glutathione. In principle, oxidative stress leads to the oxidation of GSH molecules to form GSSG, shifting the GSH/GSSG redox balance toward a more oxidizing state. As a result, the accumulation of GSSG can lead to a spontaneous thiol-disulphide exchange between protein free thiols and GSSG, thereby, yielding the corresponding protein-mixed disulphide along with GSH. However, for most protein free thiol groups, the GSH/GSSG ratio would have to decline significantly to drive S-glutathionylation by thiol-disulphide exchange [129]. Thus, although the protein thiol–disulphide exchange may occur spontaneously, the reaction is slow due to a lack of extreme conditions [102] therefore, it normally takes place under pathological conditions [139].

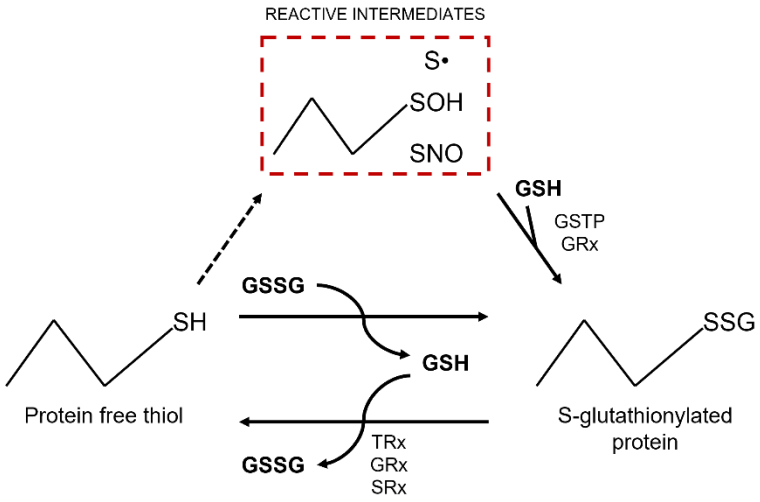

Figure I-6 Protein S-glutathionylation and deglutathionylation cycle. S-glutathionylation of protein free thiol groups proceeds either spontaneously by thiol-disulphide exchange or enzymatically with glutathione-S-transferase P (GSTP) or glutaredoxin (GRx). The thiol-disulphide exchange can proceed between protein free thiol and oxidized glutathione (GSSG) molecule; or between reactive intermediate thiol derivate such as thiyl radical (-S•) or resulted from S-sulphenylation (-SOH) and S-nitrosylation (-SNO), and a GSH molecule. The rate and magnitude of protein S-glutathionylation are greatly enhanced by catalytic activity of GSTP and GRx. S-glutathionylation can be reversed by the action of thiol-modifying enzymes such as GRx, thioredoxins (TRx) and sulphiredoxins (SRx).

b) Enzymatic S-glutathionylation

Due to the slow rate and extent of S-glutathionylation by the thiol-disulphide exchange mechanism, the participation of enzymes increases, among which glutathione-S-transferase P (GSTP) and glutaredoxins (GRx; in particular the isoform GRx2) play the most relevant roles [140–143] (**Figure I-6**). Glutathione S-transferases (GSTs) are an abundant family of detoxification enzymes that catalyse the conjugation of GSH to chemically reactive electrophilic compounds [144]. This enzymatic S-glutathionylation is proposed to be triggered by oxidants such as diamide and *tert*-butyl hydroperoxide tBHP) [145]. On the other hand, GRx functions comprise the ability to catalyse GSH-dependent redox regulation via S-

glutathionylation, the conjugation of GSH to a substrate, and its reverse reaction, deglutathionylation [146] (**Figure I-6**). It must be underlined that biochemically the thiol-transferase activity is different from the GSTP because the reactions catalysed by GRx are redox rather than transferase reactions [146]. Yet, how GRx is activated to drive forward S-glutathionylation still remains to be clarified.

c) Deglutathionylation

Levels of protein S-glutathionylation can be controlled by enzymatic regulators of protein deglutathionylation. The family of these enzymatic regulators consist of GRx/GRx reductase system which deglutathionylate proteins and thiol-disulphide bonds [147]; thioredoxins (TRx)/TRx reductase system that can reduce thiol-disulphide bonds and sulphenic acids [148]; and sulphiredoxins (SRx) which also deglutathionylate proteins [149] (**Figure I-6**). All these enzymes are known to mediate reduction of protein thiols, by concomitantly oxidizing their own cysteines. They act as intracellular antioxidants so that protein function can be recovered upon resolution of oxidative stress or termination of redox processes [103]. Additionally, protein disulphide isomerases (PDIs) catalyze the formation and breakage of disulphide bonds between cysteine residues within proteins as they fold [150].

3. Redox regulation by S-glutathionylation

S-glutathionylation serves both to protect proteins from oxidative irreversible damage and modify structure/function relationship. By introducing the tripeptide glutathione with additional ionic charges into a protein, S-glutathionylation resembles the well-characterized mechanism of protein phosphorylation [129], preventing the degradation from sulphydryl overoxidation or proteolysis [151]. Indeed, the irreversible modifications by sulphinic and sulphonic acids can be prevented by immediate S-glutathionylation of the free thiols [152]. Under oxidative stress, S-glutathionylation can act as an adaptive cellular response to reactive species and regulate the function of intracellular signalling proteins as well as transcription factors related to energy metabolism, cytoskeleton organization, Ca^{2+} homeostasis, mitochondrial quality control, protein folding and apoptosis cascades [129,151,152]. Generally, the criteria for S-glutathionylation as a regulatory mechanism are (1) occurs at a specific cysteine residue and (2) is reversible, thus allowing reversion of the redox signal and providing an additional layer of regulation for controlling cellular processes [128,129]. Therefore, the cyclical nature of protein S-glutathionylation allows regulation of signalling pathways to occur during variations in the redox status of the cell.

Important cysteine residues as redox-switches have been shown to be conserved over different taxa [130], justifying important protein function features through regulation by

redox-PTMs. Evolutionarily conserved cysteine residues in MFN2 (i.e., Cys132, Cys188, Cys217, Cys348, Cys684 and Cys700) have been identified to likely represent sites of physiologically relevant redox-PTMs [153]. In particular, Cys684 and Cys700, through formation of dimers and oligomers by disulphide bridges was shown to mediate mitochondrial hyperfusion under oxidative stress characterized by elevated GSSG levels [53,99,154]. Unlike Cys684 and Cys700, the role of other cysteine residues in MFN2 remains unclear with regard to their function as potential redox sites targeted by glutathione. Redox regulation by S-glutathionylation contributes to physiological processes which have been associated with various human pathologies [129,139]. Concretely, research has pointed out that disruption of sulphydryl homeostasis likely contributes to onset/progression of neurodegeneration [155]. The basal levels of S-glutathionylated proteins in cells are at least an order of magnitude lower than those in cells under oxidative stress [156]. Therefore, identification of selectively S-glutathionylated proteins in a quantitative manner can provide new insights about the use of redox modified proteins as biomarkers [157–159].

F. Possible therapeutic approaches targeting mitochondrial dynamics in PD

The understanding of redox-mediated mechanisms is crucial to unravel the neuropathological events in PD where redox homeostasis and mitochondrial function seen to be disturbed, as well as to develop successful therapeutic strategies. Restoring the levels of glutathione in PD has been studied as one strategy to prevent damages of oxidative stress in DAergic neurons. Although glutathione administration has the ability to slightly improve motor function in PD patients, it does not have the potential to improve cognitive function, behaviour, mood or the ability to perform daily activities [160]. Therefore, while further investigation is required for the use of glutathione as potential treatment for PD-related symptoms, better understanding of molecular mechanisms involved in the disease is essential for the exploration of novel cell- and tissue-based therapies that may not only improve symptoms but could target the deregulated mechanism. In fact, recent studies have been demonstrating the possibility of intervention in mitochondrial dynamics processes such as fission and fusion to become alternative therapeutic approach for PD. For instance, Mallach *et al*. recently reported, after a *post-mortem* analysis of striatal DAergic structures, that mitochondrial volume was significantly higher in the brains of patients that undergone deep brain stimulation procedure [161]. These results were associated with increased mitochondrial biogenesis, decreased fission and increased fusion [161] and were suggested to be further encouragement for therapies targeting mitochondrial dynamics [162]. Moreover, in PD genetic models, the inhibition of mitochondrial fission alone was sufficient to greatly alleviate mitochondrial dysfunction and enhanced mitochondrial trafficking, which strongly

suggested that mitochondrial movement impairment in PD could also be the downstream effect of altered fusion and fission dynamics [36,38]. These results suggested that reversal of mitochondrial fragmentation to enhance mitochondrial fusion possibly by genetic or pharmacological modulation with endogenous antioxidant levels or application of cell-permeable exogenous antioxidants could be a promising therapeutic strategy in PD [163].

Thus, the continuous investigation and discovery of new disease molecular pathways together with the growing development in the pharmacological research area, are essential for future use of potential biomarkers (e.g., S-glutathionylated proteins) that would provide clues of impaired cellular processes and would give an opportunity for targeted therapeutic intervention.

G. *In vitro* experimental model

1. SH-SY5Y cell line

A cellular model was chosen for the current study as these models have the advantage of a quicker pathology development; are less costly and do not require ethical approval; and genetic or pharmacological manipulations are easier and more reliable [164].

The human neuroblastoma SH-SY5Y cell line was used. This cell line was originally derived in 1970 from a metastatic neuroblastoma and is a subclone of the SK-N-SH neuroblastoma cells that present two phenotypes characterized by different morphological and biochemical features: one is defined as N-type (neuroblastic) and the other is called S-type (epithelial, adherent) [165,166]. SH-SY5Y cell line provides an unlimited supply of cells of human origin with similar biochemical characteristics to neurons [165,166]. However, as undifferentiated cells, they are not DAergic cells, having instead a catecholaminergic phenotype, as they can synthesize both DA and noradrenaline [165,166]. Nevertheless, even when undifferentiated, they present activity of DA-β-hydroxylase, tyrosine hydroxylase (TH) and expression of dopamine transporter (DAT) [165,166]. In this study, undifferentiated SH-SY5Y cells were used as according to the literature differentiation agents may alter the susceptibility of the cells to neurotoxins [167].

SH-SY5Y cell line has been widely utilized to study mechanisms of 1-methyl-4-phenylpyridinium (MPP^+)-induced neurotoxicity and the pathogenesis underlying MPP^+-induced PD mimics [168] because DAT is a prerequisite for MPP^+ incorporation into neurons [165,166]. However, it is important to note that as SH-SY5Y have cancerous properties that may influence its viability, growth performance, metabolic properties and genomic stability [165,166].

2. Glutathione depletion compound buthionine sulfoximine (BSO)

Buthionine sulfoximine (BSO) was used in order to deplete levels of glutathione in the *in vitro* model. The compound is a sulfoximine derivative and an analogue of the glutamate-cysteine ligase inhibitor, methionine sulfoximine [169]. Administration of BSO effectively inhibits GCL, the enzyme required in the first step of glutathione biosynthesis [169] (**Figure I-7**).

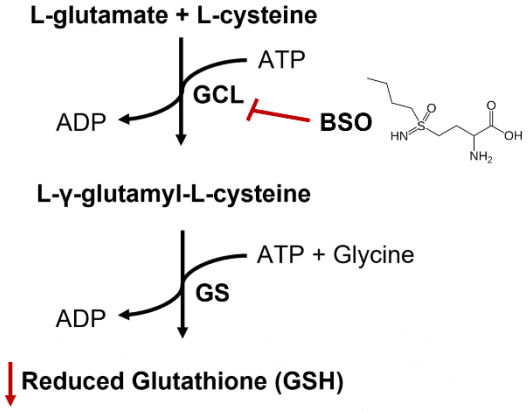

Figure I-7 Mode of action of BSO in the depletion of glutathione levels. The initial steps of glutathione biosynthesis pathway leading to the formation of reduced glutathione (GSH) by the action of GCL is inhibited by BSO.

Agents that inhibit the synthesis of glutathione such as BSO have been particularly useful in elucidating the regulatory pathways induced or altered by levels of glutathione [170–173]. Treatment with BSO has shown to produce dose-dependent decreases in total glutathione levels *in vitro* [171,173]. Moreover, administration of BSO *in vivo* sufficient to reduce glutathione levels by 40–60%, similar to the loss that occurs in PD, enhanced the neurodegeneration when the rodents are treated with other toxins such as 6-hydroxydopamine (6-OHDA) or MPP^+ [172,174].

3. Oxidant stimulus by *tert*-butyl hydroperoxide (tBHP)

Tert-butyl hydroperoxide (tBHP) is an oxidative agent commonly used as a model substance for evaluation of mechanisms and cellular alterations resulting from oxidative stress in cells and tissues [175–178]. There are two pathways by which tBHP is metabolized and both of them induce oxidative stress. First, tBHP can be detoxified to *tert*-butanol (tBOH) by the action of GPx which oxidizes GSH into GSSG [145,179] (**Figure I-8**). Thereby, tBHP affects cellular GSH in a similar manner as H_2O_2 but is not degraded by CAT providing a stimulus more prolonged in time [179]. Alternatively, tBHP can be converted into *tert*-butoxyl radicals

(tBO•) by iron-dependent reactions which initiates lipid peroxidation of membrane phospholipids with subsequent alterations to membrane fluidity and permeability [180] (**Figure I-8**). Altogether, these are general mechanisms involved in cell injury caused by oxidative stress, thus the usage of exogenous stress inducers such as tBHP can simulate augmented oxidative stress in various experimental models, mimicking a situation than may occur *in vivo* as in PD.

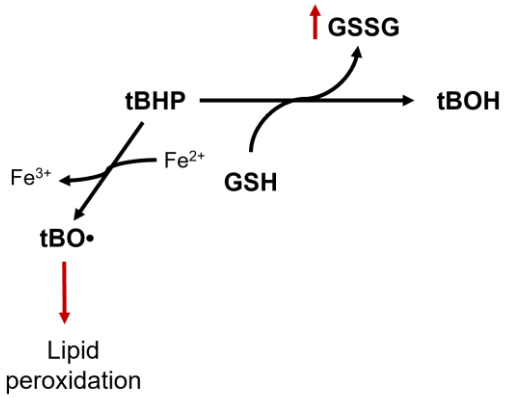

Figure I-8 Proposed mechanism of oxidative stress induced by tBHP. The action of tBHP in the cells involves reduction of GSH levels and accumulation of GSSG; and, alternatively, the lipid peroxidation through iron-dependent reactions. tBOH *tert*-butanol; tBO• *tert*-butoxyl radical. Adapted from *Martín et al., 2001.*

4. Parkinsonism-triggering neurotoxin MPP^+

The connection between mitochondrial dysfunction and oxidative stress in PD was firstly demonstrated by the discovery of 1-methyl-4-phenyl-1,2,3,6-tetrahydropyridine (MPTP)-induced Parkinsonism among drug abusers [181]. MPTP is converted in the brain into 1-methyl-4-phenyl-2,3-dihydropyridinium ($MPDP^+$) by the enzyme MAO-B [168,182] located in the OMM, which catalyses the oxidative deamination of biogenic and xenobiotic amines [89]. This metabolic process occurs predominately in glial cells such as astrocytes in the brain. Although the mechanism is still elusive, MPDP+ is probably spontaneously oxidized and is then converted to the active toxic molecule, 1-methyl-4-phenylpyridinium (MPP^+) and released into the extracellular space [183]. It was described that MPP^+ enters DAergic neurons due to its high affinity for DAT. In SH-SY5Y cells, MPTP cannot be metabolized to MPP^+; however, these cells have the capacity to uptake MPP^+. Moreover, MPTP is extremely toxic, and is able to cross the BBB being potentially dangerous to manipulate. Therefore, in cellular models the metabolite is preferably used rather than MPTP. Once inside the DAergic neurons, MPP^+ can siphon electrons from the mitochondrial electron transport chain at complex I and be reduced in the process forming free radicals namely $O_2^{\bullet -}$ radicals which go

on to cause further generalized cellular damage [184,185] (**Figure I-9**). In addition, the overall inhibition of the electron transport chain eventually leads to stunted ATP production and eventual death of the DAergic neurons, which ultimately displays itself as clinically pathological features of PD [182,184,185].

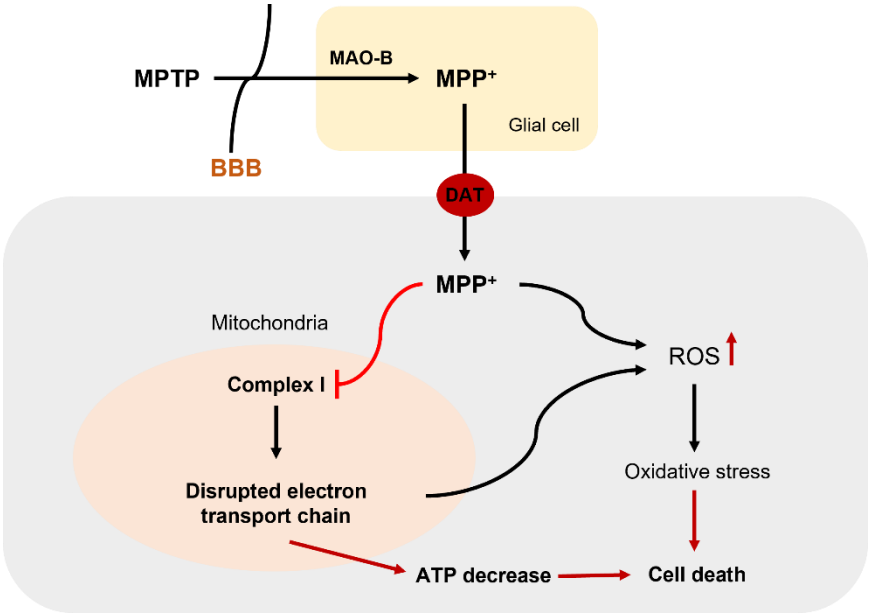

Figure I-9 MPTP/MPP⁺ action in cell metabolism. MPTP crosses the blood-brain barrier (BBB). Once inside the brain, MPTP is metabolized into MPP^+ by enzyme MAO-B in the glial cells and is transported to the neurons through DAT. Inside the neuron MPP^+ interferes with complex I of the electron transport chain which causes the ROS burden as well as ATP decrease, ultimately leading to cell death. Adapted from *Muramatsu et al., 2002.*

H. Main objectives

The main objective of the current study was to understand how S-glutathionylation of MFN2 is regulated under mitochondrial dysfunction and stress-altered glutathione levels in an *in vitro* PD experimental model, potentially impacting its expression and function as mitochondrial fusion mediator. Moreover, by predicting S-glutathionylated cysteine residues in MFN2, we aimed to provide insights into the complex relation between redox-PTMs, mitochondrial (dys)function and dynamics in neurodegeneration context of PD.

The specific goals of the workplan were:

- Understand how S-glutathionylation of MFN2 is regulated by changes induced by the different redox-modifying agents that act on mitochondrial function, redox status and alter glutathione levels in SH-SY5Y cells

- Evaluate the mitochondrial morphology changes in *post-mortem* PD samples, specifically, the modulation of mitochondrial fusion by MFN2, providing a link between the redox regulation of MFN2 in the *in vitro* model and mitochondrial dynamics in PD patients

- Identify potentially S-glutathionylated cysteine residues in MFN2 using bioinformatic tools and simulation of S-glutathionylation of the predicted residues by *in silico* approaches

II. MATERIALS AND METHODS

A. Materials

1. Reagents

Minimum essential Eagle's medium (MEM), Ham's nutrient mixture F-12, penicillin/streptomycin, L-glutamine, MEM non-essential amino acids, Dulbecco's phosphate buffered saline without calcium (Ca^{2+}) and magnesium (Mg^{2+}) (DPBS), and molecular grade water were acquired from Corning® (Manassas, VA, USA). Heat-inactivated fetal bovine serum (FBS), TrypLE™ Express and Hank's balanced salt solution (HBSS) were purchased from GIBCO® (Life Technologies, Inc., Grand Islands, USA). 1-methyl-4-phenylpyridinium iodide (MPP^+), L-buthionine sulfoximine (BSO), Luperox® TBH70X *tert*-butyl hydroperoxide (tBHP), L-glutathione oxidized (GSSG), β-mercaptoethanol, 1,4-dithiothreitol (DTT), sodium orthovanadate (Na_3VO_4), ammonium persulfate (APS), sodium fluoride (NaF), Amido Black staining solution, bovine serum albumin (BSA), glutathione reductase (GR), L-glutathione reduced (GSH), 2-vinylpyridine, 5-sulfosalicylic acid dihydrate, Triton™ X-100, triethanolamine, meta-phosphoric acid (HPO_3), sodium borohydride ($NaBH_4$), β-nicotinamide adenine dinucleotide 2'-phosphate reduced tetrasodium salt hydrate (β-NADPH), 5,5'-dithiobis(2-nitrobenzoic acid) (DTNB), ethylenediaminetetraacetic acid disodium salt dihydrate (EDTA), sodium deoxycholate, Tween-20, IGEPAL®, dimethyl sulfoxide (DMSO), 3-(4,5-dimethylthiazol-2-yl)-2,5-diphenyltetrazolium bromide (MTT), hydrochloric acid (HCl), chloroform, glycerol and xylene were acquired from Sigma-Aldrich® (St. Louis, MO, USA). N-ethylmaleimide (NEM) was acquired from ACROS Organics (New Jersey, USA). Acrylamide/bis-acrylamide (30%), Bio-Rad's protein assay reagent, pre-stained protein ladder molecular weight marker, goat-serum, horseradish peroxidase-conjugated anti-mouse secondary antibody and horseradish peroxidase-conjugated anti-rabbit secondary antibody were acquired from Bio-Rad Laboratories Inc., (Hercules, CA, USA). Tris(hydroxymethyl)aminomethane (Tris), glycine, sodium dodecyl sulphate (SDS), isopropanol, methanol, absolute ethanol, and acetic acid were obtained from VWR® (Radnor, PA, USA). N,N,N',N'-tetramethyl ethylenediamine (TEMED), potassium dihydrogen orthophosphate (KH_2PO_4), dipotassium hydrogen orthophosphate (K_2HPO_4) and recombinase DNase I enzyme were purchased from Merck (Kenilworth, NJ, USA). WesternBright™ ECL HRP Substrate was acquired from Advansta (San Jose, CA, USA). SuperSignal™ West Femto Maximum Sensitivity Substrate and BSA ampules (2 mg/mL) were obtained from Thermo Fisher Scientific Inc., (Rockford, USA). cOmplete™ Protease Inhibitor Cocktail was acquired from Roche Diagnostics (Penzberg, Germany). ATP-Glo™ Bioluminometric Cell Viability Assay Kit and 4′,6-diamidino-2-phenylindole (DAPI) were purchased from Biotium Inc., (Freemont, CA, USA). 2',7'-dichlorofluorescein diacetate

(H_2DCF-DA) and MitoSOX™ Red mitochondrial superoxide indicator were acquired from Molecular Probes Inc., Invitrogen™ (Eugene, OR, USA). Sodium chloride (NaCl) and potassium chloride (KCl) were acquired from Fisher Chemical (Hampton, NH, USA). Protein A/G PLUS-agarose beads were obtained from Santa Cruz Biotechnology Inc., (Dallas, TX, USA). TRIzol® reagent, anti-rabbit IgG secondary antibody conjugated with Alexa Fluor® 488 and anti-mouse IgG secondary antibody conjugated with Alexa Fluor® 555 were acquired from Invitrogen™ Life Technologies (Carlsbad, CA, USA) and SensiFAST™ SYBR® Hi-ROX kit from Bioline (London, UK). Citric acid monohydrate was purchased from AnalaR NORMAPUR© and bromophenol blue from BDH® Chemicals. Primers (forward and reverse) were acquired from STAB Vida Lda. (Caparica, Portugal). Random hexamers mix for reverse transcribed complementary DNA (cDNA), dNTPs NZY mix and NZY First-Strand cDNA Synthesis Kit were acquired from NZYTech Lda., (Lisbon, Portugal).

2. Antibodies

Table II-1 List of the primary antibodies used in immunoblotting (IB), immunoprecipitation (IP) assays and immunofluorescence analysis (IF).

Antibody	Commercial source	Reference	Host	Dilution			Molecular Weight (kDa)
				IB	IP	IF	
MFN2	Sigma-Aldrich® (St Louis, MO, USA)	HPA030554	Rabbit	1:2000	-	1:200	75; 55
	Cell Signalling Technology® (Boston, MA, USA)	11925S		-	2 µL	-	n.a.
MFN1		14739S		1:1000	-	-	84
Glutathione	Enzo Life Sciences Inc., (Farmingdale, New York, USA)	ADI-SPA-542-E	Mouse	1:1000	-	-	n.a.
GSTP	BD Transduction Laboratories™	610719		1:1000	-	-	23
Total OXPHOS	Abcam® (Cambridge, UK)	AB110413		1:200	-	-	55; 48; 40; 30; 20
TOM20	Santa Cruz Biotechnology, Inc. (Dallas, TX, USA)	sc-17764		-	-	1:50	n.a.

n.a. – not applicable

3. Equipment and consumables

Heracell™ 150 incubator (Thermo Fisher Scientific Inc., Waltham, MA, USA); Micro Star 17R centrifuge VWR® (Radnor, PA, USA); Varioskan LUX multimode microplate reader (Thermo Fisher Scientific Inc., Rockford, USA); FB12 luminometer (Berthold Detection Systems, Pforzheim, Germany); ultrasonic processor UP100H (Hielscher Ultrasound Technology, Teltow, Germany; cycle: 1, amplitude: 100%); ChemiDoc™ MP Imaging

System (Bio-Rad Laboratories Inc., Hercules, CA, USA); NanoDrop® 1000 spectrometer (Thermo Fisher Scientific Inc., Rockford, USA); Thermal Cycler XT^{96} VWR® (Radnor, PA, USA); QuantStudio™ 7 Flex Real-Time Polymerase Chain Reaction (qPCR) System (Thermo Fisher Scientific Inc., Waltham, MA, USA); Leica DMi8 Confocal Fluorescence Microscope (Leica Microsystems, Wetzlar, Germany). All sterile cell culture material including 75 cm^2 flasks; culture plates and 96 multi-well microplates were obtained from Falcon™ BD Biosciences (San Jose, California, EUA). Polyvinylidene difluoride (PVDF) membranes were acquired from Milipore® (Burlington, MA, USA).

B. Methods

1. SH-SY5Y cell line culture

Undifferentiated human neuroblastoma SH-SY5Y cells obtained from American Type Culture Collection (ATCC®) were maintained in complete culture medium containing 1:1 mixture of minimum essential Eagle's medium (MEM) and Ham's nutrient mixture F-12, supplemented with 10% heat-inactivated fetal bovine serum (FBS), 1% MEM non-essential amino acids, 2 mM L-glutamine and 100 µg/mL streptomycin and 100 units/mL penicillin. All adherent cells were kept at 37ºC in a humidified 5% CO_2 incubator in 75 cm^2 sterile culture flasks. Cell sub-culturing (when reaching about 80-90% confluence) was achieved by enzymatic dissociation using TrypLE™ Express to promote detachment of adherent cells from the flasks. The collected cell suspension was centrifuged, and cells were then transferred into new flasks with new growth medium and/or counted and plated overnight before proceeding to experiments. For different assays, cells were plated at a density of 2.5x10^4 cells per well in 96 multi-well microplates, 1x10^6 cells per plate in 60x15 mm cell culture plates and 3.5x10^6 cells per plate in 100x20 mm cell culture plates.

2. SH-SY5Y cells treatment protocol

In the course of the study, after dose-dependent cell viability assays (see **Figure S 1**), seeded SH-SY5Y cells were grown overnight to 70-80% confluence and divided into control (untreated cells) and five different treatment groups: (1) cells exposed to BSO in a final concentration of 100 µM for 24 hours; (2) cells exposed to MPP^+ with a final concentration of 500 µM for 24 hours; (3) cells exposed to tBHP with a final concentration of 50 µM for 3 hours; or (4) to tBHP in a final concentration of 50 µM for 3 hours after a 21 hours pre-treatment with 100 µM BSO; and (5) cells treated with oxidized glutathione (GSSG) with a final concentration of 1 mM for 24 hours. The concentration and time-point treatment with BSO were based on previous experiments from our lab and further literature [99]. The timeline of the treatment protocol is shown in **Figure II-1**. All compounds were freshly prepared from sterile stock solutions.

Figure II-1 Representative scheme of the SH-SY5Y cells treatment timeline. SH-SY5Y cells were plated 24 hours before initiating treatments with 100 µM BSO; 500 µM MPP^+ or 1 mM GSSG for 24 hours; and 50 µM tBHP for 3 hours or 50 µM tBHP for 3 hours after 21 hours pre-treatment with 100 µM BSO.

3. Cell viability assay

To measure the metabolic activity of the cells, as an indicator of their viability, the MTT (3-(4,5-dimethylthiazol-2-yl)-2,5-diphenyltetrazolium bromide) assay was implemented. This colorimetric assay is based on the reduction of the tetrazolium salt to the formazan product with a correspondent change in colour from yellow to purple and the formation of crystals, which only occurs in the presence of oxidoreductases, in metabolically active cells. 2 hours before the end of each treatment as described in **II.B.2**, MTT was added to each well of a 96 multi-well microplate containing seeded SH-SY5Y cells to a final concentration of 0.5 mg/mL and allowed to incubate at 37ºC in a humidified 5% CO_2 atmosphere protected from light for 1 hour. Afterwards, cell culture medium with MTT was removed and DMSO was added into each well of the microplate which then was subjected to vigorous agitation to facilitate the MTT formazan product solubilization process. Concentration of solubilized formazan was used as a direct marker of viable cells and determined by measuring absorbance using a microplate reader at 570 nm with a reference absorbance of 620 nm.

4. Measurement of ATP levels

The ATP content in SH-SY5Y cells was measured using the ATP-Glo™ Bioluminometric Cell Viability Assay Kit (Biotium Inc.) according to the manufacturer's protocol. Briefly, after the end of the treatment protocol as described in **II.B.2**, the culture medium from each well of a 96 multi-well microplate containing seeded SH-SY5Y cells was replaced with sterile molecular grade water to lyse the cells. The microplate was then stored at -80ºC until further use. The kit is based on the luciferin-luciferase reaction, thereby an assay buffer solution containing D-luciferin with a concentration of 0.4 mg/mL was previously prepared and before microplate reading, luciferase was added to the buffer solution in a proportion of 1:100. The samples corresponding to the control and to each treatment group were diluted in molecular grade water (1:10) and together with the buffer containing luciferase, previously heated at 37ºC, were added (1:1) to each appropriated assay tube. The reaction sample + buffer with luciferase was quickly mixed and then read in a luminometer with a 10 second delay time. Intracellular ATP levels were determined based on

luciferase activity as it is directly dependent on consumption of the ATP content in the cells. An ATP standard curve was generated by plotting the luminescence readings against known concentrations of ATP (1 nM – 1000 nM). The value of the background control containing only molecular grade water and assay buffer solution (1:1) was subtracted to each obtained value in order to abrogate any unspecific luciferase activity.

5. Measurement of intracellular ROS

To assess ROS production within SH-SY5Y cells, the cell-permeant fluorescent probe 2',7'-dichlorodihydrofluorescein diacetate (H_2DCF-DA) was employed. After the end of the treatment protocol as described in **II.B.2** the cell culture medium was removed from each well of a black 96 multi-well microplate (appropriate for fluorescent assays) and the H_2DCF-DA probe prepared in culture medium was added to each well at a final concentration of 20 µM. SH-SY5Y cells were then incubated for 35-45 minutes at 37ºC and 5% CO_2 atmosphere protected from light. Afterwards, the culture medium from each well containing the probe was replaced with HBSS and microplate readings were performed with a filter for maximum excitation λ of 495 nm and a maximum emission λ of 527 nm. After diffusion into cells, H_2DCF-DA is deacetylated by esterases, which are later oxidized by ROS into a highly fluorescent compound DCF-DA [186]. Therefore, determination of ROS production within SH-SY5Y cells was based on the fluorescence values obtained from treated and untreated cells.

6. Measurement of mitochondrial superoxide

The mitochondrial redox status in the SH-SY5Y cells was evaluated using MitoSOX™ Red mitochondrial superoxide indicator (Molecular Probes Inc., Invitrogen™) according to the manufacturer's protocol. Briefly, after the end of the treatment protocol as described in **II.B.2**, the cell culture medium was removed from each well of a black 96 multi-well microplate (appropriate for fluorescent assays) and the MitoSOX™ probe prepared in culture medium was added at a final concentration of 5 µM. After incubation for 20-30 minutes at 37ºC and 5% CO_2 atmosphere protected from light, the culture medium from each well containing the probe was replaced with HBSS and microplate readings were performed with a proper filter for maximum excitation λ of 510 nm and a maximum emission λ of 580 nm. This probe is live-cell permeant and is rapidly targeted to the mitochondria where it is oxidized by superoxide and exhibits red fluorescence. Therefore, the mitochondrial superoxide generation was determined by the proportion of the highly fluorescent oxidation product indicated by the fluorescence values obtained for the treated and untreated cells.

7. Assessment of glutathione levels

Total levels of both oxidized (GSSG) and reduced (GSH) forms of glutathione were determined with an enzymatic assay according to Rahman *et al* [187]. Succinctly, after the end of the treatment protocol as described in **II.B.2**, SH-SY5Y cells seeded in 60x15 mm culture plates were washed twice with cold Ca^{2+}/Mg^{2+} free PBS 1x, removed with cell scraper and pelleted by centrifugation at 1000 *g* for 5 minutes at 4ºC. The pellets were then deproteinized in freshly prepared ice-cold extraction buffer (0.1% Triton X-100 and 0.6% 5'-sulfosalicylic acid hydrate in potassium phosphate (KPE) buffer (0.1 M potassium phosphate buffer with 5 mM EDTA disodium salt, pH 7.5)) and homogenized with Teflon pestles. For proper cell lysis, the suspensions were then sonicated for 2-3 minutes with alternate vortexing every minute and froze at -80ºC and defrost on ice twice. Following the freeze-thaw cycle, cell suspensions were centrifuged at 3000 *g* for 5 minutes at 4ºC and the supernatants immediately transferred to pre-chilled Eppendorf tubes. These supernatants were assayed for glutathione content and the pellets were used for quantification of GSH released from protein-thiols (see next section **II.B.8**). The supernatant of each sample was then divided into two different Eppendorf tubes, one for the GSH and the other for GSSG quantification. For the determination of GSSG content, supernatants were treated with 2-vinylpyridine (dilution 1:10 in KPE buffer) at room temperature (r.t) and in fume hood, 1 hour before performing the enzymatic assay. The derivatization process with 2-vinylpyridine allows the alkylation of GSH molecules leaving only GSSG in the sample. Afterwards, triethanolamine (dilution 1:6 in KPE buffer) was added to the samples and allowed 10 minutes for the neutralization process. GSSG (containing 2-vinylpyridine and triethanolamine) and GSH standards were prepared with the following concentrations: 26.4 nM/mL; 13.2 mM/mL; 6.6 nM/mL; 3.3 nM/mL and 0.103 nM/mL. Equal volume of each standard, sample (either for GSH or GSSG quantification) and blanks containing only KPE buffer and/or 2-vinylpyridine and/or triethanolamine were added to a 96 multi-well microplate.

The assay involves the oxidation of GSH by the sulphydryl reagent 5,5'-dithio-bis(2-nitrobenzoic acid) (DTNB) to form a yellowish derivative 5'-thio-2-nitrobenzoic acid (TNB), measurable at 412 nm [187]. The GSSG formed can be recycled to GSH by GR in the presence of β-NAPDH. For GSSG quantification, as the GSH molecules are masked by 2-vinylpyridine, GSSG is reduced by GR to GSH. Equal volumes of freshly prepared DTNB (2 mg of DTNB in 3 mL of KPE buffer) and GR (40 µl of GR (250 units mL^{-1}) in 3 ml KPE) solutions were mixed together (1:1) and added to each well and allowed a 30 seconds GSH to GSSG conversion before adding equal volume of freshly prepared β-NAPDH (2 mg of β-NAPDH in 3 mL of KPE buffer). The absorbance at 412 nm was then immediately read every 30 seconds for 2 minutes in a microplate reader. The rate of TNB formation (change in

absorbance $\Delta_{Abs412\ nm}$ min^{-1}) is proportional to the concentration of total glutathione in the sample. Because GR reduces the GSSG formed into 2GSH, the amount of total GSH measured represents the sum of GSH and GSSG in the sample ($[GSH]_{total}$ = [GSH] + 2x [GSSG]). The total GSH and GSSG concentrations in the unknown samples were determined by calculating from the regression curve generated from the standards. The GSH levels were obtained by the equation mentioned above. Both GSH and GSSG concentrations per well ([GSSG] or [GSH] in 20 µl of sample in the well) were then converted to nmoles per 1 mL of sample and represented in µM. The blank values including KPE buffer, 2-vinylpyridine and triethanolamine were subtracted. All solutions were prepared in cold 0.1 M KPE buffer and pH cautiously controlled. The samples and standards were kept on ice during the procedure and all reagents protected from light.

8. Quantification of GSH released from protein-bound thiols (PSSG)

To quantify GSH released from protein-bound thiols (PSSG), pellets from the previous glutathione levels microplate assay (see previous section **II.B.7**) were homogenized with 1% sodium borohydride ($NaBH_4$) to remove GSH from proteins according to Rahman *et al* [187]. The samples were then neutralized with 30% meta-phosphoric acid (HPO_3) and centrifuged at 1000 *g* for 15 minutes at 4ºC. The supernatants were used for the GSH levels determination by the DTNB-GSSG reductase recycling method as previously described in **II.B.7**.

9. Western Blot analysis

Following treatment protocol as described in **II.B.2**, SH-SY5Y cells seeded in 100x20 mm culture plates were washed twice with cold PBS 1x, removed with cell scraper and pelleted by centrifugation at 500 *g* for 5 minutes at 4ºC. Cell homogenates were prepared in lysis buffer (50 mM Tris-HCl pH 7.4, 180 mM NaCl, 1 mM EDTA, 1% Triton X-100) with addition of the cOmplete™ Protease Inhibitor Cocktail. Under reducing conditions, the lysis buffer was supplemented with 1 M sodium fluoride (NaF), 200 mM sodium orthovanadate (Na_3VO_4) and 1 M 1,4-dithiothreitol (DTT). Under non-reducing conditions, the reducing agents were absent and, additionally, to prevent oxidation artifacts that can occur during sample preparation, free thiols present in samples were blocked with 400 nM N-ethylmaleimide (NEM). The lysates were sonicated 3x5 seconds and then centrifuged at 13 000 rpm for 15 minutes at 4ºC. Protein concentration was determined following the Bradford's protein quantification assay [188]. For Western Blot, 80 µg of total protein extracts were used and Laemmli buffer (Tris-HCl pH 6.8, 4% SDS, 4% glycerol and bromophenol blue) either reducing (with 1% β-mercaptoethanol) or non-reducing (without β-mercaptoethanol) was added. In addition, protein extracts were either non-denatured or

denatured for 5 minutes at 95ºC using a dry bath. Independently of the preparation condition, samples were resolved by 10% SDS-PAGE of 30% acrylamide/bis-acrylamide and prepared with addition of polymerization catalysts tetramethyl ethylenediamine (TEMED) and 10% ammonium persulphate solution (APS). The electrophorese system containing running buffer solution (25 mM Tris, 192 mM glycine, 0.1% SDS at pH 8.8) was under refrigeration and for each gel an electric current of 35 mA was applied for approximately 4 hours. Proteins were electro-transferred to PVDF membranes previously activated in methanol and equilibrated in transfer buffer (25 mM Tris, 192 mM glycine and 10% methanol). The system containing transfer buffer was under refrigeration and an electric current of 500 mA was applied for approximately 2 hours. The membranes were then stained with Amido Black staining solution for control of loaded samples and transfer efficiency.

For immunodetection, membranes were reactivated in absolute ethanol, washed in distilled water and in Tris-buffered saline solution with 0.1% Tween-20 (TBS-T; 25 mM Tris, 137 mM NaCl, 2.7 mM KCl at pH 7.5). The membranes were then blocked with 5% (w/v) non-fat dry milk in TBS-T for minimum 1 hour at r.t. and incubated overnight at 4ºC with specific primary antibodies (listed in **Table II-1**). Afterwards, membranes were incubated with horseradish peroxidase-conjugated anti-mouse or anti-rabbit secondary antibodies (1:5000) for 1 hour at r.t. and then washed again with TBS-T. For detection of chemiluminescent immunocomplexes, WesternBright™ ECL HRP Substrate or SuperSignal™ West Femto Maximum Sensitivity Substrate were used and the detection analysis was performed through Image Lab 5.1 Beta software (Bio-Rad Laboratories Inc., Hercules, CA, USA) after scanning with ChemiDoc™ MP Imaging System (Bio-Rad Laboratories Inc., Hercules, CA, USA). Before re-probe the membranes, a stripping solution (1.5% glycine, 40% glacial acetic acid, 0.01% SDS and 1% Tween-20) was applied for approximately 10-15 minutes and membranes were properly washed with distilled-water and TBS-T.

10. Co-immunoprecipitation assay

SH-SY5Y cells were grown in 100x20 mm culture plates and after the end of the treatment protocol as described in **II.B.2** were washed with ice-cold PBS 1x and pelleted by centrifugation at 500 *g* for 5 minutes at 4ºC. Cell homogenates were prepared in lysis buffer (50 mM Tris-HCl pH 7.4, 180 mM NaCl, 1 mM EDTA, 1% Triton X-100) supplemented with 50 mM NEM and with protease inhibitors, for approximately 30 minutes on ice. Lysates were centrifugated at 14 000 *g* for 30 minutes at 4ºC to pellet the cell debris and the supernatants were transferred to new pre-chilled Eppendorf tubes. Protein concentration was determined in the cell lysates following the Bradford's protein quantification assay [188] and 1 mg of total protein extract was used.

For co-immunoprecipitation of MFN2, 50 µL of protein A/G PLUS-agarose beads were washed 3x with 300 µL of lysis buffer and incubated with 2 µL of anti-MFN2 antibody (listed in **Table II-1**) for 4h at 4ºC under gentle rotation. In parallel, another 50 µL of pre-cleared beads were incubated with the cell lysates. After centrifugation at 1000 *g* at 4ºC for 2 minutes the cleared cell lysates were then added to the tubes with the beads + anti-MFN2 antibody and incubated overnight at 4ºC under gentle rotation. After this incubation, the samples were washed 3x with cell lysis buffer. Samples were then recovered in Laemmli buffer without 1% β-mercaptoethanol and denatured for 5 minutes at 100ºC using a dry bath. Finally, samples were centrifuged at 1000 *g* at 4ºC for 2 minutes and the supernatants collected for Western Blot analysis as described previously (see **II.B.9**). The inputs were also collected ran in parallel as a loading control. The membranes were first incubated overnight at 4ºC with anti-glutathione antibody to detect S-glutathionylated MFN2 and re-probed with anti-MFN2 antibody as a control of the immunoprecipitation efficiency.

11. RNA isolation and Quantitative Real-Time PCR (qPCR)

SH-SY5Y cells were seeded in 60x15 mm culture plates and after the end of the treatment protocol as described in **II.B.2**, cells were washed twice with cold PBS 1x and TRIzol® reagent added to the cells. The RNA extraction was performed according to the manufacturers' instructions as follows: firstly, cells were scrapped, transferred into sterile Eppendorf tubes and chloroform (200 µL per 1 mL of TRIzol®) added to each sample. The samples were then briefly vortexed, left at r.t. for 3 minutes and centrifuged at 12 000 *g* for 15 minutes at 4ºC. In order to precipitate the RNA, isopropanol (500 µL per 1 mL of TRIzol®) was added to the aqueous phase of each sample, mixed by inversion, incubated at r.t. for 10 minutes and centrifugated at 12 000 *g* for 10 minutes at 4ºC. The RNA pellets were then washed in 70% ethanol, briefly vortexed, centrifuged at 12 000 *g* for 10 minutes at 4ºC and left to air dry before resuspending in sterile molecular grade water. Finally, the RNA pellets were incubated at 55ºC for 10 minutes to help its solubilization.

RNA quantification (ng/µL) was achieved by using a NanoDrop® 1000 spectrometer. Before proceeding to qPCR, samples were treated with DNase to remove possible contaminations with DNA. For each sample, 1 µg of RNA was used and added equal volume of a prepared mix containing DNase buffer 1x and recombinant DNase I enzyme (10 U/µL). All samples were incubated in a thermocycler following a cycle of 20 minutes at 37ºC and 75ºC for 10 minutes. In order to synthesize the cDNA, the NZY First-Strand cDNA Synthesis Kit (NZYTech Lda., Lisbon, Portugal) was used according to the manufacturer's instructions. Succinctly, 500 ng of RNA from each sample treated with DNase were mixed with random hexamers (25 µg/500 µL) and dNTPs (25 mM). This mixture was incubated for 5 minutes at

65ºC before adding equal volumes of reverse transcriptase enzyme and buffer 1x. The cDNA synthesis followed a program of 10 minutes at 25ºC, 50 minutes at 50ºC and 5 minutes at 85ºC in the thermocycler.

For qPCR, a mix containing SensiFAST™ (1x) and 500 nM of the forward and reverse primers was prepared to amplify each target gene (**Table II-2**) and added to each well of a 384-well microplate with corresponding cDNA sample. All samples were assayed in duplicate as well as the negative control for each primer mix. Finally, microplate was covered with a transparent adhesive, centrifuged at 500 *g* for 1 minute and placed into the QuantStudio™ 7 Flex Real-Time PCR System with the following amplification program: 2 minutes at 95ºC, 40 cycles of 5 seconds at 95ºC and 30 seconds at 60ºC. A melting curve analysis was considered and in order to quantify the amplified gene sequences in each sample, the comparative ΔΔCT method was used [189]. The relative mRNA levels of the genes of interest were normalized to the relative mRNA levels of endogenous ribosomal proteins L19 (RPL19) and L29 (RPL29) and expressed as fold induction over control.

Table II-2 Sequences of primers (forward and reverse) used for qPCR analysis.

Gene (Human)	Forward primer (5' → 3')	Reverse primer (5' → 3')
RPL19	GGG CAT AGG TAA GCG GAA GG	TCA GGT ACA GGC TGT GAT ACA
RPL29	CGA CTT GCC TAC ATT GCC	CCT GAG CTG GAA CTG AAG
MFN2	CCT TCC TTG AAG ACA CGT ACA G	GAT GCC TCT CAC TTT GGA TAG G
MFN1	GCA ACT GAA AAA CTG AGG AT	ACT TGT TGG CAC AGG CGA GC

12. Acquisition of human *post-mortem* brain samples

Human brain samples used in this study were obtained from The Netherlands Brain Bank (NBB; open access: www.brainbank.nl) upon approval of the project by the NBB and in compliance with their ethical guidelines. The study was approved by the institutional ethics review board and all material had been collected from donors from whom a written consent for a brain autopsy and the use of material and clinical information for research purposes had been obtained by the NBB. Mesencephalon tissue samples of 4 PD patients (age range: 65-83; m/f; 2/2) and 4 control subjects (age range: 56-84; m/f; 2/2) obtained with a short *post-mortem* delay were selected based on clinical diagnosis and confirmed by neuropathological evaluation. Control cases had no known clinical history of dementia or motor disturbance and the cause of death was unrelated to the CNS. Formalin-fixed paraffin-embedded tissue samples were sectioned, and 5 µm-thick sections were obtained for immunohistochemistry analysis.

13. Immunohistochemistry analysis of human *post-mortem* brain samples

Immunofluorescence staining of mesencephalon tissue sections of 4 PD patients and 4 control subjects were prepared and observed using a confocal laser scanning microscope. Briefly, sections were deparaffinated following a cycle of washes with xylene (2x5'), 100% ethanol/xylene solution (1:1) (30''), 100% ethanol (30''), 96% ethanol (30''), 80% ethanol (30'') and finally with 70% ethanol (30''). Samples were then washed with PBS before boiled for 20 minutes in citrate buffer (10 mM citric acid, 0.05% Tween-20, pH 6.0) for antigen retrieval. After cooling at r.t., sections were washed (3x) with PBS/0.05% Tween-20 and blocked with 10% goat-serum in PBS/1% BSA/0.05% Tween-20 for 30 minutes. Sections were then incubated overnight at 4ºC with anti-MFN2 and anti-TOM20 antibodies (listed in **Table II-1**). After this incubation, the tissue sections were washed (3x) with PBS/0.05% Tween-20 and incubated for 1 hour at r.t. with anti-rabbit IgG secondary antibody conjugated with Alexa Fluor® 488 (1:400) and anti-mouse IgG secondary antibody conjugated with Alexa Fluor® 555 (1:400). Following this incubation, sections were washed (3x) with PBS/0.05% Tween-20. Finally, tissue sections were stained with DAPI (1:10000) in PBS for 15 minutes at r.t. All antibodies were diluted in PBS/1% BSA/0.05% Tween-20/1% goat-serum which also served as a negative control. After washing with PBS, tissue samples were mounted with Fluoromount™ Aqueous Mounting Medium (Sigma-Aldrich, St Louis, MO, USA) and observed using Leica DMi8 Confocal Fluorescence Microscope with Leica Application Suite X (LAS X) software for image acquisition. A series of images derived from merged Z-stack imaging were obtained and analysed with ImageJ software (https://imagej.nih.gov/ij/). The percentage of fluorescent occupancy for each antibody and the percentage of colocalization of both anti-MFN2 and anti-TOM20 were determined using an ImageJ macro developed by Dr. Jorge Valero Gómez-Lobo (Copyright© 2020 Jorge Valero Gómez-Lobo; jorge.valero@achucarro.org). A fluorescence intensity threshold was defined for each region of interest (ROI) which helped define specific from nonspecific staining above background. The values corresponding to the percentage of fluorescent occupancy and colocalization were calculated based on the total area of fluorescent occupancy of both antibodies and the area corresponding to each antibody.

14. Prediction of S-glutathionylation sites in MFN2

For the prediction of potentially modified cysteine residues in MFN2 by S-glutathionylation, three integrative web servers/databases were used: DeepGSH [190] (http://deepgsh.cancerbio.info/), iCysMod [191] (http://icysmod.omicsbio.info/) and pCysMod [192] (http://pcysmod.omicsbio.info/). The web servers/databases were chosen as they are the most recent and up-to-date bioinformatics tools to predict S-glutathionylation sites, performing better than their predecessors (e.g., *GSHsite, PGluS, dbGSH*). The tools adopt

four feature extraction methods to extract the sequence information and use a deep neural network to learn it. PSO (Particle Swarm Optimizer) algorithm is used to fine-tune the hyperparameters such as learning rate, layer numbers, and activation functions [190]. DeepGSH predicts possible S-glutathionylated sites in proteins [190] and additional three fundamental properties of protein sequence are outputted including disorder and secondary structure. iCysMod and pCysMod were used to predict additional cysteine oxidative modifications in MFN2 including S-nitrosylation, S-palmitoylation, S-sulphydration, S-sulphenylation and S-sulphinylation. For all web servers/databases, the canonical sequence of the MFN2 in FASTA format (**Table II-3**) retrieved from UniProt (ID O95140), the Universal resource of protein sequence and functional information (http://www.uniprot.org/), was submitted in order to predict potential redox-modified sites.

Table II-3 Information regarding MFN2 in humans including UniProt ID and the FASTA format sequence used in bioinformatic tools to predict potentially redox-modified sites.

Organism	*Homo sapiens*
UniProt ID	O95140_HUMAN
Gene name	MFN2
Protein name	Mitofusin 2
FASTA format sequence:	
>O95140_HUMAN MSLLFSRCNSIVTVKKNKRHMAEVNASPLKHFVTAKKKINGIFEQLGAYIQESATFLEDTYRNAELDPVTTEEQVLD VKGYLSKVRGISEVLARRHMKVAFFGRTSNGKSTVINAMLWDKVLPSGIGHTTNCFLRVEGTDGHEAFLLTEGSE EKRSAKTVNQLAHALHQDKQLHAGSLVSVMWPNSKCPLLKDDLVLMDSPGIDVTTELDSWIDKFCLDADVFVLVA NSESTLMQTEKHFFHKVSERLSRPNIFILNNRWDASASEPEYMEEVRRQHMERCTSFLVDELGVVDRSQAGDRI FFVSAKEVLNARIQKAQGMPEGGGALAEGFQVRMFEFQNFERRFEECISQSAVKTKFEQHTVRAKQIAEAVRLIM DSLHMAAREQQVYCEEMREERQDRLKFIDKQLELLAQDYKLRIKQITEEVERQVSTAMAEEIRRLSVLVDDYQMD FHPSPVVLKVYKNELHRHIEEGLGRNMSDRCSTAITNSLQTMQQDMIDGLKPLLPVSVRSQIDMLVPRQCFSLNY DLNCDKLCADFQEDIEFHFSLGWTMLVNRFLGPKNSRRALMGYNDQVQRPIPLTPANPSMPPLPQGSLTQEEFM VSMVTGLASLTSRTSMGILVVGGVVWKAVGWRLIALSFGLYGLLYVYERLTWTTKAKERAFKRQFVEHASEKLQL VISYTGSNCSHQVQQELSGTFAHLCQQVDVTRENLEQEIAAMNKKIEVLDSLQSKAKLLRNKAGWLDSELNMFTH QYLQPSR	

15. Molecular docking studies

S-glutathionylation of predicted cysteine residues in MFN2 was computationally evaluated through molecular docking studies (covalent binding) using the Cambridge Crystallographic Data Centre's Genetic Optimisation for Ligand Docking software (GOLD, version 5.7, https://www.ccdc.cam.ac.uk/) [193]. At the time of this study, there were three different crystallographic structures of MFN2 (PDB IDs: 6JFM, 6JFL, 6JFK; resolution between 1.997-2.806 Å) available on the Protein Data Bank (http://www.rcsb.org/pdb/). However, these structures were not suitable for further studies since variable regions of the genomic sequence were missing, where some of the predicted cysteine residues are located (i.e., Cys8, Cys482, Cys684 and Cys700). Therefore, the missing MFN2 structure was

generated computationally by homology modelling using the Molecular Operating Environment software package (MOE, Chemical Computing Group Inc., version 2020.09, http://www.chemcomp.com). First, the canonical sequence of human MFN2 containing 757 amino acids was retrieved from UniProt under the ID 095140 (**Table II-3**). Then, based on this amino acid sequence, a search for possible homology candidates was performed using MOE in order to provide proper structural models (templates). The candidate list was reduced by eliminating all hits presenting a low statistical significance (BLAST E-value > 0.01) or a sequence identity <70% of the target sequence. The nucleotide-free MFN1 structure obtained by X-ray diffraction (PDB ID: 5GO4; resolution 2.20 Å) was identified as a promising template for homology modelling (see **Figure S 2A**).

A homology model of MFN2 was then generated including all regions of the canonical sequence where the predicted modified cysteine residues are located. The output model was then subject to energy minimization and the model quality was analysed using a Ramachandran plot obtained from MOE software package and by Protein Structure Analysis (ProSAweb, https://prosa.services.came.sbg.ac.at/prosa.php) which is an integrative web service for error recognition in three-dimensional (3D) protein structures [194]. The structure of glutathione (GSH) was built with MOE by importing the canonical simplified molecular-input line-entry system (SMILES) [195] (for GSH: C(CC(=O)NC(CS)C(=O)NCC(=O)O)C(C(=O)O)N) that converted the linear notation of the chemical structure into a 3D model of the molecule. To prepare the 3D structure of the MFN2 protein to use in molecular docking with GSH, all the crystallographic waters were removed, and charges and protonation states were assigned using the Protonate 3D tool implemented in MOE software package (pH 7.4). Additionally, for each cysteine residue, hydrogen atom was removed from the thiol group (formation of thiolate ($-S^-$)) and covalent docking (disulphide-bridge) between the sulphur atom of the targeted thiolate in MFN2 and the sulphur atom of GSH was performed using GOLD [196]. The ChemScore scoring function [197] was selected and 500 runs were set. The pose with the best score for each cysteine docking simulation was chosen to represent MFN2-GSH interaction. The MFN2 protein conformation was fixed while the GSH was flexible. All other parameters were set to defaults for the GOLD docking process. All structural figures were prepared with MOE and PyMol (The PyMol Molecular Graphics System, Version 2.0 Schrödinger, LLC., https://pymol.org/2/). All molecular docking calculations were performed at the Computational Medicinal Chemistry Lab (iMed.ULisboa) scientific cluster.

16. Statistical analysis

Statistical analysis of all data was performed using GraphPad Prism 8 software (San Diego, CA, USA). All values were expressed as the mean ± standard error of the mean (SEM). The differences between two groups were determined by two-tailed unpaired Student's t-test and considered statistically significant for $p < 0.05$. The one-way analysis of variance (ANOVA) with Dunnett post-hoc test was used to determined statistically significant differences between the means of three or more independent (unrelated) groups. The two-way ANOVA with Dunnett post-hoc test was used for statistical analysis of MFN2 protein expression levels.

III. RESULTS

Mitochondrial dysfunction and ROS-mediated stress accompanied with decreased glutathione levels are suggested to contribute to the structural and functional damage in the neural system in PD. To further understand how altered glutathione levels in an induced mitochondrial impairment and oxidative stress cellular environment regulate MFN2 through S-glutathionylation, an *in vitro* PD experimental model was stablished by exposing SH-SY5Y cells to the parkinsonism-triggering neurotoxin MPP^+. In parallel, SH-SY5Y cells were treated with the GSH-depletion compound BSO and/or with pro-oxidant tBHP in order to evaluate and compare the different effects on MFN2 by shifting the GSH/GSSG ratio by potentially inducing excessive ROS generation. Additionally, SH-SY5Y cells were treated with levels of GSSG comparable to the ones detected in cells under stress (0.5-1 mM) [99].

A. Cell viability, mitochondrial function, and ROS generation under the different redox-modifying agents

A series of experiments were initially conducted to determine the effects of the selected redox-modifying agents on SH-SY5Y cells' viability, mitochondrial function, and ROS generation. Firstly, MTT reduction method was used for evaluation of SH-SY5Y cell viability (**Figure III-1A**) and ATP levels for mitochondrial impairment were measured (**Figure III-1B**).

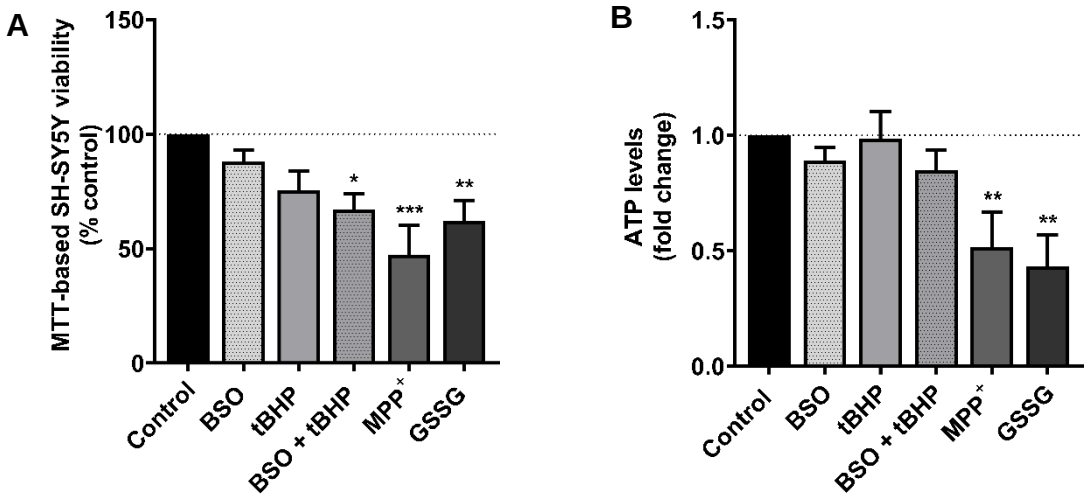

Figure III-1 Effect of the redox-modifying agents on SH-SY5Y cell viability and mitochondrial function. (A) MTT reduction assay in SH-SY5Y cells was employed to assess viability after administration of 100 µM BSO, 500 µM MPP^+ or 1 mM GSSG for 24 hours, 50 µM tBHP for 3 hours or 50 µM tBHP for 3 hours after 21 hours pre-treatment with 100 µM BSO. Cell death is represented as the percentage of MTT reduction *versus* control. **(B)** ATP content in treated SH-SY5Y cells assessed by luciferase activity was determined as fold change relative to control. All data is expressed as the mean ± SEM of triplicates of 5 independent experiments. All differences were analysed by one-way ANOVA with Dunnett post-hoc test and were considered statistically significant for $p < 0.05$. * $p < 0.05$; ** $p < 0.01$ and ******* $p < 0.001$ compared to control (untreated cells).

Results shown in **Figure III-1A** indicate that treatments with 100 µM BSO for 24 hours and 50 µM tBHP for 3 hours did not adversely impacted SH-SY5Y cell viability as well as the ATP levels (**Figure III-1B**) compared to the control. However, exposure to 50 µM tBHP for 3 hours was responsible for a significant cell loss in SH-SY5Y cells pre-conditioned with 100 µM BSO (**Figure III.1-A**), indicating that GSH depletion sensitized cells to posterior oxidative insult without significantly affecting the mitochondrial respiratory chain reported through ATP levels variations (**Figure III-1B**). On the other hand, the exposure of 500 µM MPP^+ or 1 mM GSSG for 24 hours, had a significant impact on ATP production (**Figure III-1B**) which may reflect the considerable SH-SY5Y cell loss (**Figure III-1A**).

To further understand the effects of the redox-modifying agents on mitochondrial function, protein expression of the different OXPHOS subunits was evaluated (**Figure III-2**).

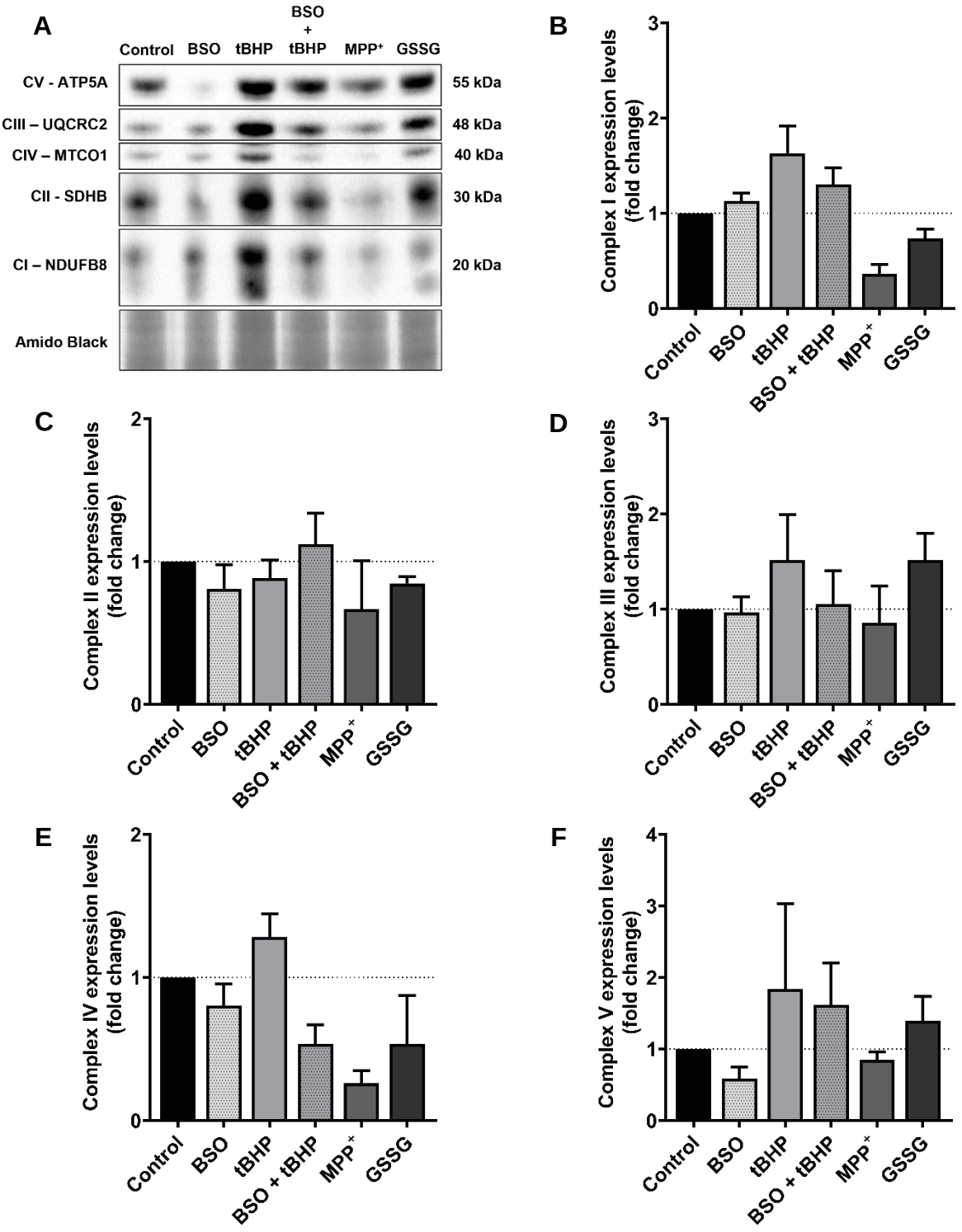

Figure III-2 OXPHOS subunits expression in SH-SY5Y cells treated with redox-modifying agents. (A) The most representative image of non-denaturing SDS-PAGE showing the immunoblots of mitochondrial OXPHOS subunits in total cell extracts of SH-SY5Y treated with 100 µM BSO, 500 µM MPP^+ or 1 mM GSSG for 24 hours, 50 µM tBHP for 3 hours or 50 µM tBHP for 3 hours after 21 hours pre-treatment with 100 µM BSO. Protein subunit ATP5A represents complex V – ATP synthase; UQCRC2 complex III – ubiquinone/cytochrome *c* oxidoreductase; MTCO1 complex IV – cytochrome *c* oxidase; SDHB complex II – succinate/ubiquinone oxidoreductase; and NDUFB8 complex I – NADH/ubiquinone oxidoreductase. Protein expression levels of the representative OXPHOS complexes were quantified using Image Lab (BioRad) and represented in quantitative histograms of the ratio of each complex normalized to the corresponding Amido Black staining and values are expressed as fold change of the control (untreated cells) of **(B)** Complex I; **(C)** Complex II; **(D)** Complex III; **(E)** Complex IV and **(F)** Complex V. Data is expressed as the mean ± SEM of 4 independent experiments.

Although the results were not considered statistically significant, we observed some potential tendencies (**Figure III-2A**). Inhibition of GSH synthesis by exposure with 100 µM BSO for 24 hours showed a tendency to decrease the expression of the complexes II, IV and V as shown in **Figure III-2C;E;F**. Previous studies had reported that the complexes I and II are more sensitive to tBHP [175,176,178]. Our results only supported the possible compromised expression of the complex II, whereas expression of complex I increased after exposure to 50 µM tBHP for 3 hours even when followed by pre-treatment with 100 µM BSO for 21 hours (**Figure III-2B;C**). Moreover, tBHP seen to upregulate the protein expression of the OXPHOS complexes III, IV and V (**Figure III-2D;E;F**) when compared to the control. These results allied with the absence of effect of tBHP exposure on ATP levels in the SH-SY5Y cells (**Figure III-1B**). Furthermore, GSH depletion before oxidant stimulus with tBHP made SH-SY5Y cells more vulnerable to the impairment of the complex IV (**Figure III-2E**). In contrast, exposure to 50 µM tBHP for 3 hours following pre-treatment with 100 µM BSO for 21 hours showed a tendency to upregulate the complexes I, II and V as indicated in **Figure III-2B;C;F**. MPP^+ is known to involve complex I activity impairment, leading to ATP depletion and alterations in cellular redox status [168,174,184]. Concordantly, our results revealed significant decrease of ATP levels (**Figure III-1B**) and general diminished OXPHOS protein expression, especially complex I, following exposure with 500 µM MPP^+ for 24 hours (**Figure III-2**). Likewise, GSSG-treated cells tend to have a decreased expression of the complexes I, II and IV (**Figure III-2B;C;E**) which can be linked with the registered energy deficit (ATP levels) (**Figure III-1B**) and to the noticeable cell death (**Figure III-1A**). Yet, administration of 1 mM GSSG for 24 hours exhibited an enrichment of complex III and V expression, although it cannot be considered statistically significant (**Figure III-2D;F**).

Furthermore, to understand if the mitochondrial impairment is related to an increase in oxidative stress in the treated SH-SY5Y cells, global (**Figure III-3A**) and mitochondrial (**Figure III-3B**) ROS generation was measured.

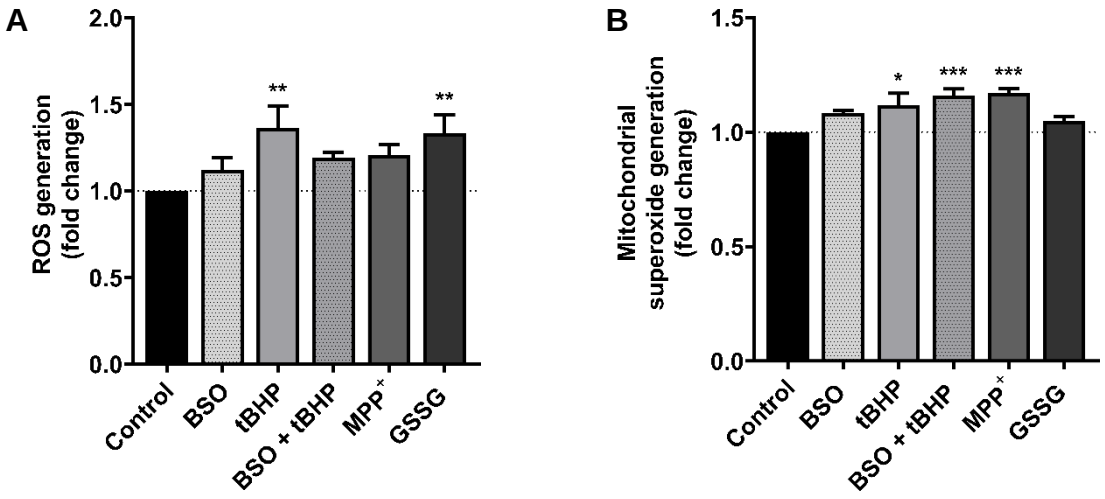

Figure III-3 Effect of the redox-modifying agents on global and mitochondrial ROS generation in SH-SY5Y cells. (A) Intracellular ROS generation measured by DCF-DA fluorescent dye and **(B)** MitoSOX-based mitochondrial superoxide generation in SH-SY5Y cells following treatment with 100 µM BSO, 500 µM MPP^+ or 1 mM GSSG for 24 hours, 50 µM tBHP for 3 hours or 50 µM tBHP for 3 hours after 21 hours pre-treatment with 100 µM BSO. Quantitative histograms are expressed as fold change of the mean fluorescence intensity of the DCF-DA and MitoSOX probes, respectively. All data is expressed as the mean ± SEM of triplicates of 5 independent experiments. All differences were analysed by one-way ANOVA with Dunnett post-hoc test and were considered statistically significant for $p < 0.05$. * $p < 0.05$; ** $p < 0.01$ and ******* $p < 0.001$ compared to control (untreated cells).

Results presented in **Figure III-3** indicate a tendency or significant increase in ROS production after exposing SH-SY5Y cells to the different redox-modifying agents. However, SH-SY5Y cells exposed to 50 µM tBHP for 3 hours exhibited significant increase in global and mitochondrial ROS generation, whereas cells treated with 1 mM GSSG for 24 hours had the most significantly increase in global ROS generation (**Figure III-3A**). On the other hand, cells exposed to 50 µM tBHP for 3 hours with a pre-treatment with 100 µM BSO for 21 hours and cells treated with 500 µM MPP^+ for 24 hours showed the most significant increase in mitochondrial superoxide generation (**Figure III-3B**). Exposure or pre-treatment with BSO led to results consistent with previous studies reporting no significant changes in mitochondrial dysfunction and ROS generation after GSH depletion with BSO [170,198]. Although, a tendency to an increased ROS generation is observed, our results suggested that BSO itself was not able to cause damage to cells but render them vulnerable to other oxidants such as tBHP, making it more evident the importance of glutathione as an efficient antioxidant molecule.

B. MFN2 expression is differentially modulated by the redox-modifying agents

To investigate whether MFN2 as a mitochondrial dynamics' regulator is modulated by the cellular redox status in the *in vitro* model, MFN2 protein expression was evaluated. The anti-MFN2 antibody used for immunoblotting (listed in **Table II-1**) was able to detect two MFN2 isoforms (isoform 1 - canonical sequence - at approximately 75 kDa and isoform 2 at 55 kDa as indicated in UniProt database). Although, both isoforms seen to have a similar pattern of expression, isoform 2 tend to be more upregulated. As shown in **Figure III-4A,** SH-SY5Y cells depleted of GSH by 100 µM BSO treatment for 24 hours presented slightly lower expression of MFN2 isoform 1, whereas expression of MFN2 isoform 2 seen to be more enhanced. However, exposure with 50 µM tBHP for 3 hours showed a tendency for upregulation of both isoforms, which was more noticeable in SH-SY5Y cells exposed to 500 µM MPP^+ or 1 mM GSSG for 24 hours (**Figure III-4A**). Additionally, exposure of SH-SY5Y cells to tBHP after a pre-treatment with 100 µM BSO for 21 hours seen to lead to a downregulation of both MFN2 isoforms (**Figure III-4A**). Overall, our data revealed a tendency of both isoforms' expression to be altered by the redox-modifying agents, *albeit* not significant, where isoform 2 seems to respond more to the treatments than isoform 1.

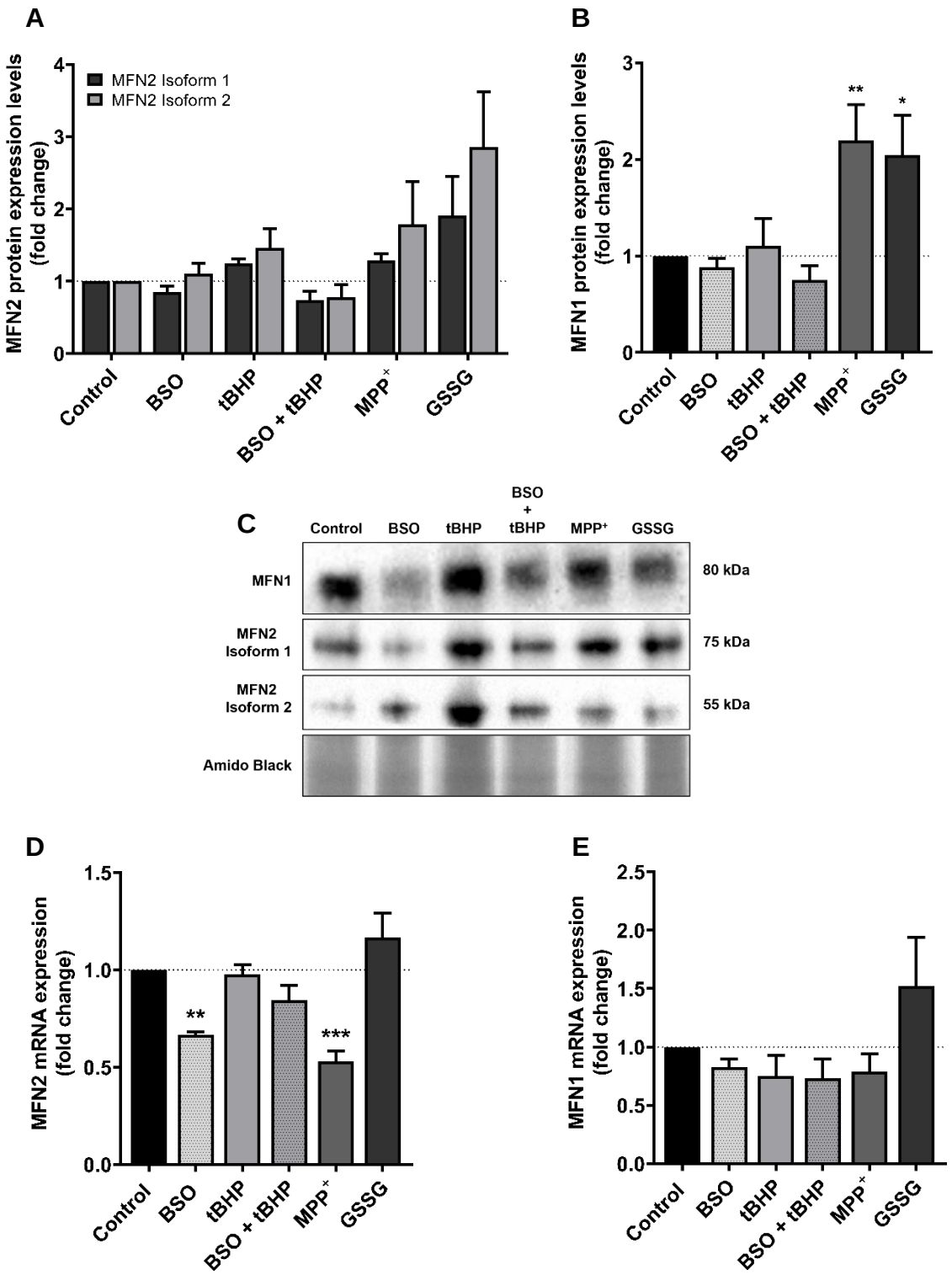

Figure III-4 Expression of mitochondrial fusion proteins MFN2 and MFN1 in SH-SY5Y cells under redox-modifying conditions. MFN2 **(A)** and MFN1 **(B)** protein expression levels are represented in quantitative histograms plotting the ratio of both MFN2 isoforms and MFN1, respectively, normalized to the corresponding Amido Black staining. All data is expressed as fold change of the control and values presented as the mean ± SEM of 7 independent experiments. **(C)** The most representative immunoblots of SDS-PAGE under reducing and denaturing conditions for protein expression levels in total cell extracts of SH-SY5Y treated with 100 µM BSO, 500 µM MPP^+ or 1 mM GSSG for 24 hours, 50 µM tBHP for 3 hours or 50 µM tBHP for 3 hours after 21 hours pre-treatment with 100 µM BSO. Levels of mRNA corresponding to MFN2 **(D)** and MFN1 **(E)** were quantified by qPCR, and data normalized to RPL19/29 as endogenous controls. All data is expressed as fold change of the control and values presented as the mean ± SEM of 3 independent experiments. All differences were analysed by two (for MFN2 protein expression) and one-way ANOVA with Dunnett post-hoc test and were considered statistically significant for $p < 0.05$. * $p < 0.05$; ** $p < 0.01$ and *** $p < 0.001$ compared to control (untreated cells).

Furthermore, when comparing MFN2 expression with its homologous MFN1 (**Figure III-4B**), results are similar with exposure or pre-treatment with 100 µM BSO leading to a tendency to decrease MFN1 protein expression, in contrast, with cells induced with 50 µM tBHP for 3 hours (**Figure III-4B**). Moreover, SH-SY5Y cells treated with MPP^+ or GSSG revealed significant upregulation of MFN1 protein expression (**Figure III-4B**). Representative immunoblots of MFN2 and MFN1 are shown in **Figure III-4C**. In addition, mRNA levels of MFN2 and MFN1 were measured (**Figure III-4D;E**). Curiously, except for the treatment with 1 mM GSSG for 24 hours, all redox-modifying agents seem to downregulate the mRNA levels of both MFNs in SH-SY5Y cells as indicated in **Figure III-4D;E**. These results, together with MFNs protein expression levels indicated a discrepancy between transcription and translation products. One of the main factors behind this variation could be the difference in the turnover time. Usually, *in vivo*, mRNA and protein levels are not necessarily proportional. The half-lives of proteins are longer than mRNAs because of the PTMs that proteins can undergo [199]. The opposite scenario can also happen where proteins degrade faster than mRNAs. Except for the induction with GSSG, our opposing results regarding mRNA and protein levels may indicate that changes in MFNs expression observed in SH-SY5Y cells might resulted from a mechanism of stabilization of the protein by PTMs which consequently led to a downregulation of MFNs transcription. Nevertheless, this hypothesis will require further clarification. On the other hand, results regarding treatment with 1 mM GSSG for 24 hours suggest that increased oxidative stress is able to upregulate significantly both transcriptional and translational products by a possible positive feedback mechanism. Taken together, these results indicated that mitochondrial fusion machinery is altered in our *in vitro* experimental model upon redox imbalance.

C. Changes in GSSG levels in SH-SY5Y cells modulate S-glutathionylation of proteins

Given that one of the earliest biochemical alterations observed in PD patients is the marked imbalance in the GSH/GSSG ratio [88,120] possibly raised from the mitochondrial impairment and excessive ROS production, the next objective was to evaluate if levels of protein S-glutathionylation were altered in the *in vitro* PD experimental model and whether it was paralleled to the exposure with other redox-modifying agents. We started by measuring the levels of both reduced (GSH) and oxidized (GSSG) forms of glutathione in the treated SH-SY5Y cells. Data from **Figure III-5A** show that exposure to 100 µM BSO for 24 hours was able to reduce GSH levels by almost 90% when comparing to the control.

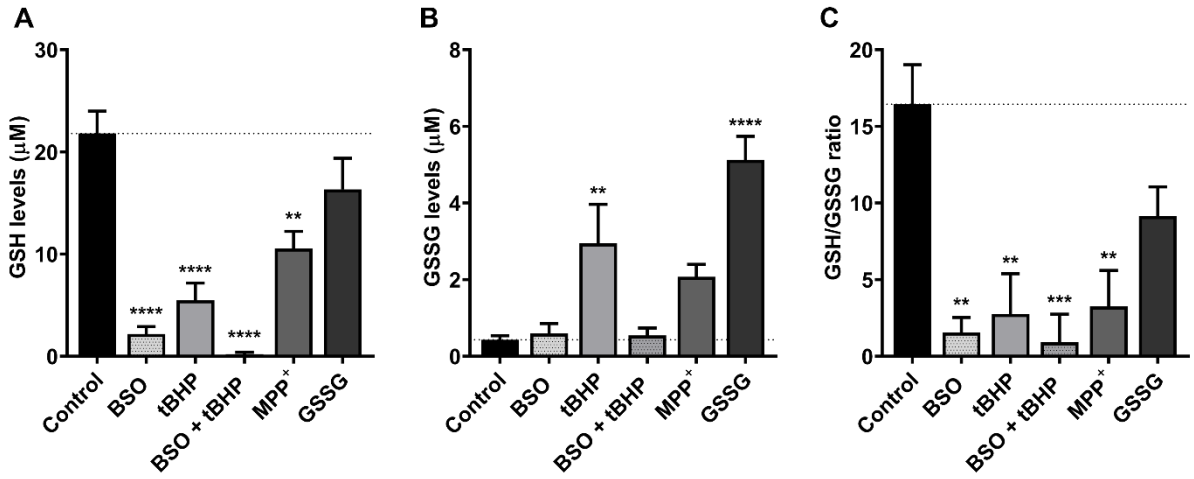

Figure III-5 Effect of the redox-modifying agents on both reduced (GSH) and oxidized (GSSG) glutathione levels. GSH **(A)** and GSSG **(B)** content in SH-SY5Y cells was measured by an enzymatic assay following the treatment with 100 µM BSO, 500 µM MPP^+ or 1 mM GSSG for 24 hours, 50 µM tBHP for 3 hours or 50 µM tBHP for 3 hours after 21 hours pre-treatment with 100 µM BSO. Concentrations of glutathione were calculated from standard curve and are represented as µM of GSH or GSSG. **(C)** The GSH/GSSG ratio. All differences were analysed by one-way ANOVA with Dunnett post-hoc test and were considered statistically significant for $p < 0.05$. ** $p < 0.01$, ******* $p < 0.001$ and **** $p < 0.0001$ compared to control (untreated cells).

In addition, SH-SY5Y cells treated with 50 µM tBHP for 3 hours showed a decrease in GSH content by almost 75% (**Figure III-5A**) but, in contrast with BSO, tBHP significantly increased the presence of GSSG in the cells, indicating that tBHP might be favouring the conversion of GSH to GSSG by producing ROS [145] as opposed to the inhibition of GSH synthesis by BSO. Pre-treatment with 100 µM BSO followed by exposure to 50 µM tBHP, reduced drastically GSH levels by almost 95% in SH-SY5Y cells (**Figure III-5A**) with no significant alterations in GSSG levels (**Figure III-5B**). Exposure to 500 µM MPP^+ for 24 hours led to a significant decrease in GSH levels by 52% (**Figure III-5A**) and an increase in GSSG content, although not statistically considerable (**Figure III-5B**). The reduced GSH levels are concordant to the reported in PD patients [88,120], but the GSSG content in MPP^+-treated cells not reaching significance could be linked to previous studies reporting decreased GSH levels without a significant increase in GSSG levels in *in vivo* PD models and in PD *post-mortem* brains [88,120]. Moreover, exposure of SH-SY5Y cells to 1 mM GSSG for 24 hours led to a significant increase of GSSG levels (**Figure III-5B**), without notably affecting GSH levels (**Figure III-5A**). Overall, results presented in **Figure III-5C** indicate a reduction in the GSH/GSSG ratio, often used as a marker of intracellular oxidative stress, in cells exposed to the redox-modifying agents.

We further analysed the effects of modulation of glutathione levels on protein S-glutathionylation in the *in vitro* model. A common mechanism proposed for S-glutathionylation is the spontaneous thiol-disulphide exchange between a reactive thiol on a

specific cysteine residue and a GSSG molecule, leading to the formation of disulphide bonds. An alternative mechanism involves the initial oxidative modification of a reduced protein-thiol, which may then react with a GSH molecule, to form the mixed disulphide via enzymatic action of GSTs such as GSTP, leading to the formation of S-glutathionylated proteins. Both reactions imply an increase of ROS level and decrease in GSH/GSSG ratio in the cells [129]. In order to evaluate if the observed changes in glutathione levels following treatment with redox-modifying agents are reflected in alterations of protein S-glutathionylation pattern in SH-SY5Y cells, levels of GSH released from protein-bound thiols (PSSG) were firstly measured. Results presented in **Figure III-6A** indicated a tendency to increased levels of GSH release from protein-thiols after the administration of 50 µM tBHP for 3 hours, 500 µM MPP^+ or 1mM GSSG for 24 hours, in contrast with the treatments with 100 µM BSO for 24 hours or 50 µM tBHP for 3 hours after pre-treatment with 100 µM BSO for 21 hours. These results ultimately indicated an enhanced number of proteins that undergone S-glutathionylation in SH-SY5Y cells under oxidative stress stimuli, without previous GSH depletion.

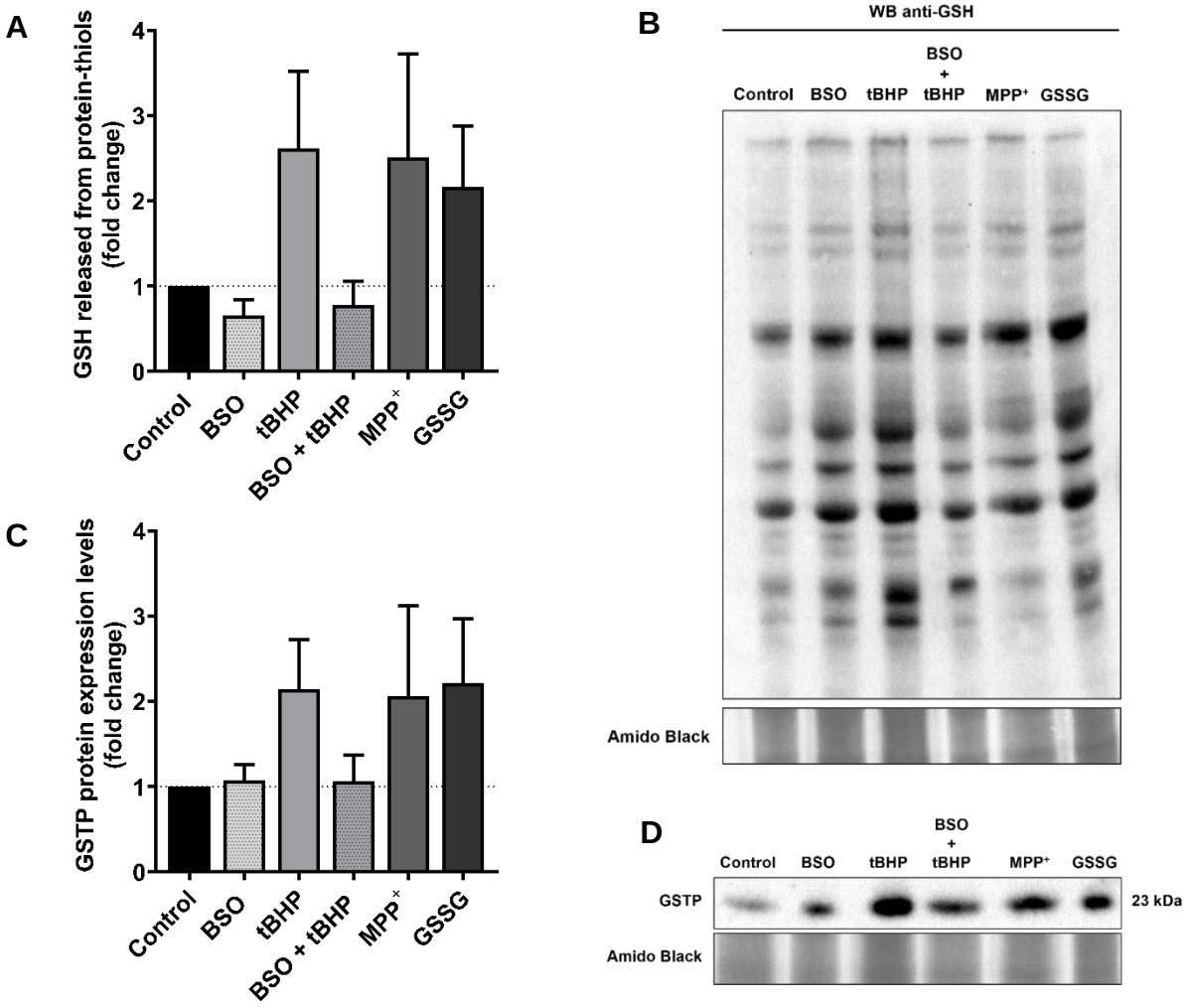

Figure III-6 Indicators for S-glutathionylation of proteins in treated SH-SY5Y cells. (A) Quantitative measurements of GSH released from protein-bound thiols (PSSG) as relative indicator of subsequent S-glutathionylation of proteins in SH-SY5Y cells following the treatment with 100 µM BSO, 500 µM MPP^+ or 1 mM GSSG for 24 hours, 50 µM tBHP for 3 hours or 50 µM tBHP for 3 hours after 21 hours pre-treatment with 100 µM BSO. Values are absorbance measurements from an enzymatic assay and are expressed as fold change of control (untreated cells). Data is expressed as the mean ± SEM of 5 independent experiments. **(B)** The most representative image of protein S-glutathionylation in SH-SY5Y cells detected by immunoblotting with anti-glutathione monoclonal antibody that detects PSSG adducts (listed in **Table II-1**). Total cell extracts were loaded and separated under non-reducing conditions. **(C)** Quantitative histogram represents protein expression of GSTP normalized to the corresponding Amido Black staining and expressed as fold change of control. Data is expressed as the mean ± SEM of 5 independent experiments. **(D)** The most representative image of reducing SDS-PAGE for the protein expression level of GSTP in total SH-SY-5Y treated cell extracts.

To further confirm the differences in protein S-glutathionylation in the *in vitro* model, non-reducing Western Blot analysis was performed using a monoclonal anti-glutathione antibody which detects PSSG adducts. As shown in **Figure III-6B**, a different pattern of protein S-glutathionylation indicated by intensity of the bands, was observed under redox stimuli compared to the control, especially, with the treatments of 50 µM tBHP for 3 hours or 1mM GSSG for 24 hours. Likewise, GSTP protein expression was found to be enhanced by

oxidant stimuli from tBHP, MPP^+ and GSSG exposures, whereas no significant differences comparing with the control were observed after GSH depletion with BSO (**Figure III-6C**). The most representative immunoblots of GSTP protein expression variation are shown in **Figure III-6D**. Inside the cell, tBHP leads to a direct increase in S-glutathionylated proteins as previously reported [145,179]. Moreover, as tBHP is able to initiate lipid peroxidation, producing radicals that can be scavenged by thiol-transferase activity such as GSTP, our results seen to demonstrate the enhance expression of GSTP under tBHP induction to protect protein thiols from irreversible oxidative insult and, thereby augmented protein S-glutathionylation. In addition, GSH depletion with BSO led to a disrupted GSH/GSSG ratio without significantly increasing the GSSG levels, which reflected in the levels of S-glutathionylation. Our results with MPP^+ exposure also indicated that depletion of GSH by around 52% was still able to tendentially increase GSSG levels that enhance the occurrence of the forward S-glutathionylation reaction, which together might reflect the biochemical cellular environment in PD.

D. S-glutathionylation of MFN2 in SH-SY5Y cells

In order to understand if alterations of GSH/GSSG levels in the *in vitro* model induced S-glutathionylation of the mitochondrial fusion regulator MFN2, co-immunoprecipitation assays of MFN2 were performed in SH-SY5Y cells treated with the different redox-modifying agents. We found that the level of S-glutathionylation of MFN2 was strengthened with the exposure of all redox-modifying agents when compared to control though, more significantly, after the exposure to 1 mM GSSG for 24 hours as detected by immunoblots analysis using anti-glutathione monoclonal antibody (**Figure III-7**). Moreover, treatment with MPP^+ treatment seen to follow GSSG induction regarding the effect of S-glutathionylation of MFN2 when compared to control (**Figure III-7**).

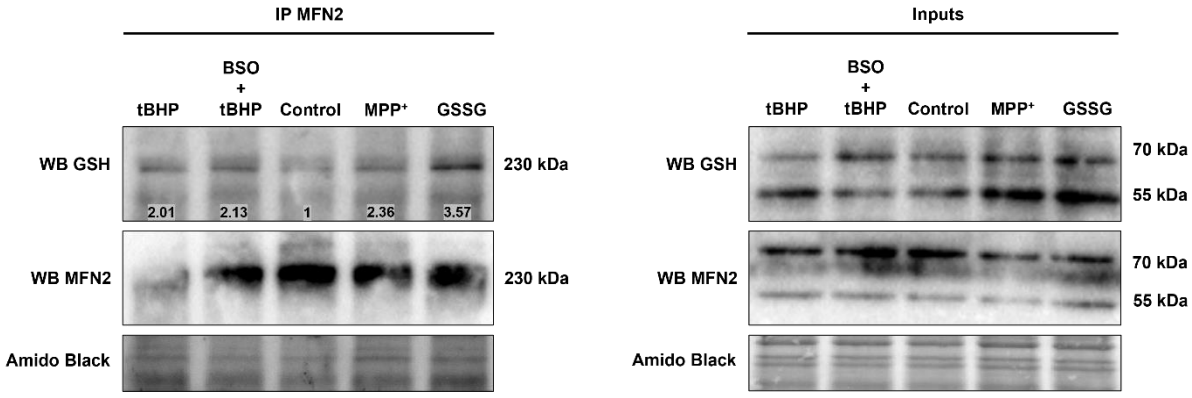

Figure III-7 S-glutathionylation of MFN2 detected by co-immunoprecipitation assay in SH-SY5Y cells exposed to 50 µM tBHP for 3 hours with and without pre-treatment with 100 µM BSO for 21 hours, 500 µM MPP^+ or 1 mM GSSG for 24 hours. Proteins separated under non-reducing conditions and S-glutathionylated MFN2 detected by Western Blot (WB) with an anti-glutathione monoclonal antibody followed by immunoblot analysis using an anti-MFN2 antibody (listed in **Table II-1**). The values correspond to the quantification of S-glutathionylated MFN2 normalized to the corresponding Amido Black staining and expressed as fold change of control.

Furthermore, biochemical and functional experiments have reported that GSSG levels induce the generation of disulphide-mediated MFN2 dimers and larger oligomers intermediated by specific cysteine residues to trigger mitochondrial fusion [53,99]. Therefore, the formation of inter- or intramolecular disulphide bridges between MFN2 monomers was analysed by the mobility of MFN2 in non-reducing gel in the absence or presence of NEM. Results shown in **Figure III-8A** revealed the gradual appearance of dimers and multimers under the exposure of all the redox-modifying agents, except for SH-SY5Y cells pre-conditioned with BSO. However, larger oligomeric species above 100 kDa, identified by the intensity of the bands seen to be preferentially formed under the treatments with 500 µM MPP^+ or GSSG 1 mM for 24 hours. The addition of the free-thiol blocking agent NEM was able to abolish the presence of these larger oligomeric forms by only revealing dimers and the monomers corresponding to both MFN2 isoforms as shown in **Figure III-8B.** Interestingly, the appearance of MFN2 dimers around 100 kDa in the presence of NEM was more noteworthy in SH-SY5Y cells exposed to 100 µM BSO for 24 hours or 50 µM tBHP compared to control (**Figure III-8B**). Additionally, the appearance of the monomer corresponding to the isoform 2, around 55 kDa, only in the presence of NEM, suggested that this isoform widely participates in the dimerization and/or oligomerization of MFN2 through formation of disulphide bridges.

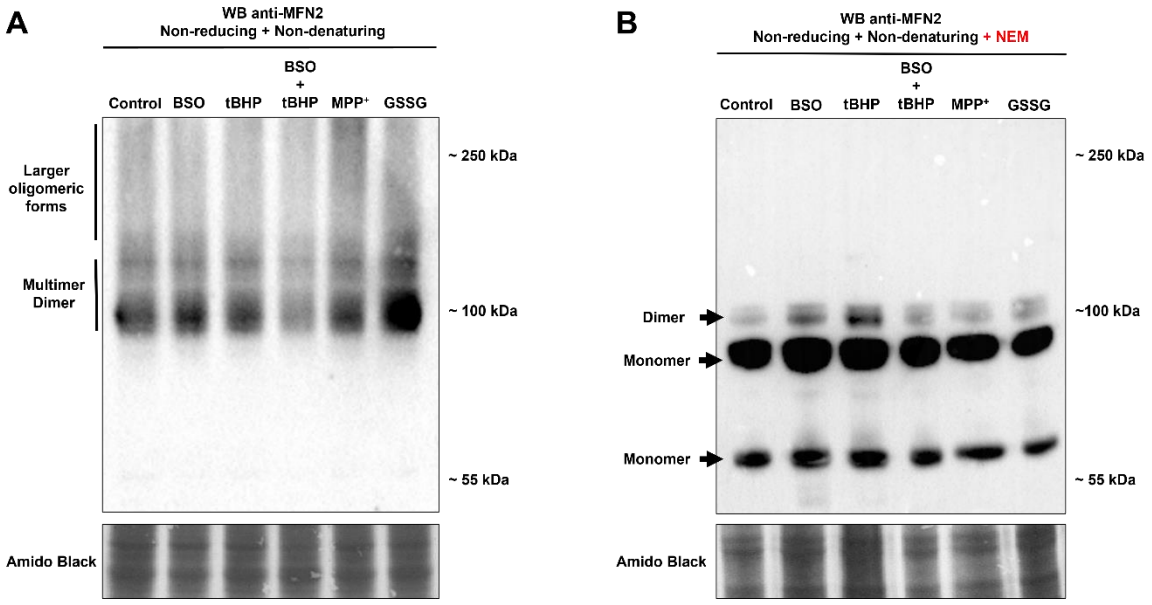

Figure III-8 Oligomerization of MFN2 in SH-SY5Y cells following treatment with redox-modifying agents. Representative non-denaturing SDS-PAGE immunoblots showing MFN2 dimers and oligomers formation under non-reducing conditions without (A) and with (B) addition of free-thiol blocking agent NEM. The left panel shows that larger oligomeric forms of MFN2 are abolished with the presence of NEM as presented in the right panel.

These observations confirmed that MFN2 oligomerization is dependent on the availability of free cysteine thiols, which in the presence of NEM were blocked; and revealed that MFN2 monomers and dimers participate in the formation of larger oligomers through disulphide bridges in the *in vitro* PD experimental model.

E. Evaluation of MFN2 and mitochondrial fusion in *post-mortem* PD brain samples

In order to understand whether mitochondrial fusion might be altered in PD, we analysed *post-mortem* mesencephalon tissue samples, at the level of the SNpc, of PD patients and non-neurological controls. Using immunofluorescence analysis, we observed the tissue distribution of MFN2 and TOM20 as well as colocalization of both proteins by measuring the fluorescence intensity of PD and control samples. To investigate the changes in the amount of MFN2 colocalizing with TOM20, indicating increased occurrence of mitochondrial fusion, a specific ImageJ macro developed by Dr. Jorge Valero Gómez-Lobo (jorge.valero@achucarro.org) was used to analyse a series of confocal microscopy images derived from merged Z-stacks. The percentage of area of occupancy for each protein, MFN2 and TOM20, and the percentage of colocalization of both were determined. As seen in **Figure III-10A**, clusters of mitochondria which are apparently undergoing fusion were detected in PD brain samples (white arrows and boxed areas) in comparison with controls.

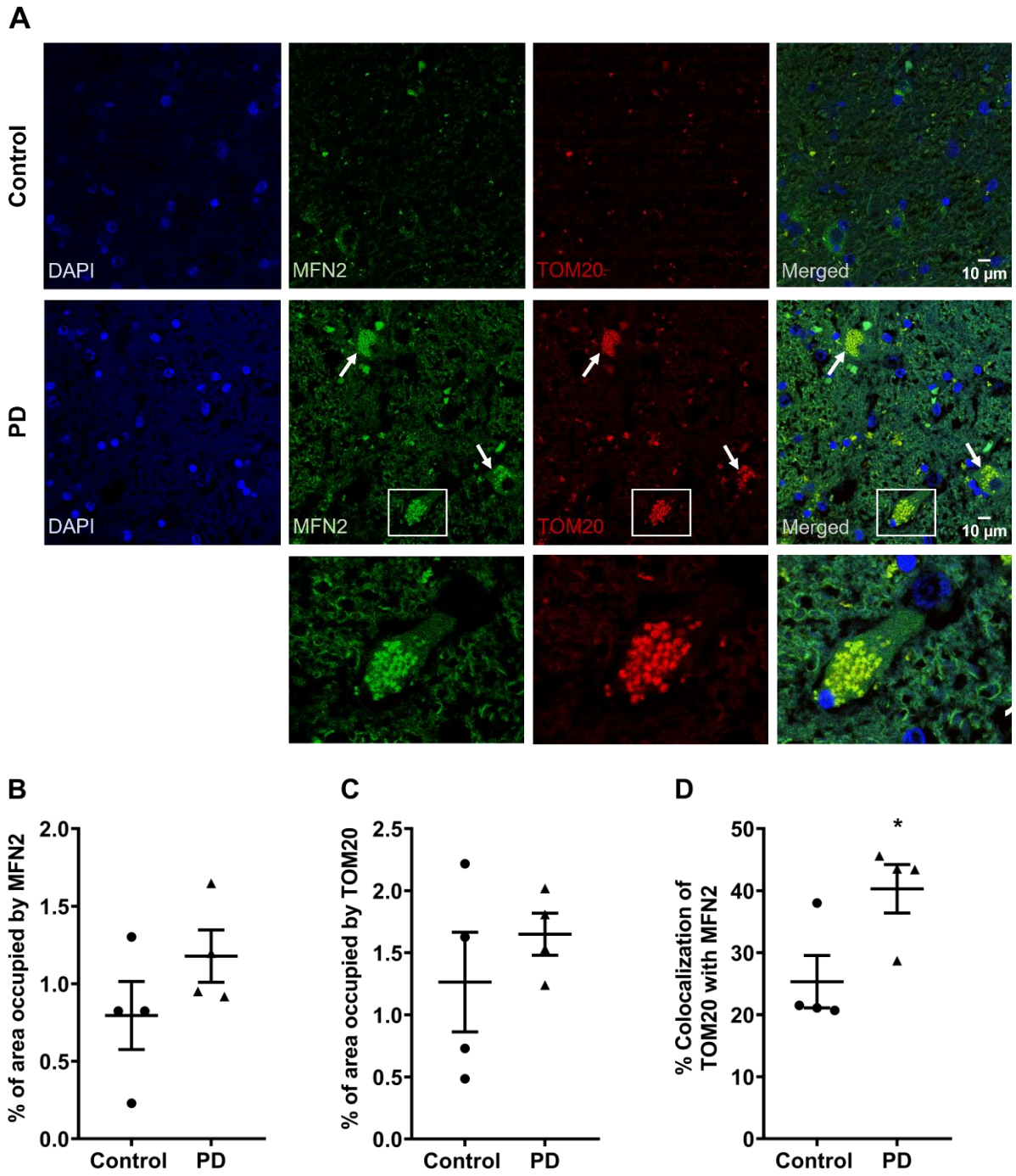

Figure III-9 Confocal analysis of control and PD mesencephalon tissue samples by targeting fusion protein MFN2 and mitochondria. (A) Representative confocal microscopy images of anti-MFN2 (green) and mitochondria marked by anti-TOM20 (red). The white arrows indicate regions of PD tissue sample where increased fluorescence of anti-MFN2 and anti-TOM20 labelling are present. Zoomed images of the boxed areas show mitochondrial protein TOM20 and fusion protein MFN2 immunostaining and colocalization of both proteins in PD samples, indicating possible mitochondrial fusion clusters. Nuclei were counterstained with DAPI (blue). Percentage of area occupied by MFN2 **(B)** and TOM20 **(C)** in relation to the total fluorescence area. **(D)** Quantification of TOM20-MFN2 colocalization expressed in percentage was based on the total area of fluorescent occupancy; control n=4; PD n=4. Significant differences were analysed by two-tailed unpaired Student's t-test; * $p < 0.05$ compared to control.

Confocal measurements indicated a tendency to a higher area of fluorescent occupancy by both MFN2 (**Figure III-10B**) and TOM20 (**Figure III-10C**) in PD compared to control individuals. Moreover, importantly significant increased colocalization of TOM20 with MFN2 in PD was detected as shown in **Figure III-10D**. Taken together, results suggested that MFN2, as a mitochondrial fusion regulator, may be enhanced in PD individuals, and colocalized with mitochondrial protein TOM20, provides evidence for potentially induced mitochondrial fusion clusters in PD.

F. Bioinformatic study identified potential different contributions to function of MFN2 isoforms

The following study was not part of the initial aims for the current dissertation. However, Western Blot analysis for MFN2 protein expression suggested that MFN2 isoform 2 is upregulated to a higher degree than the isoform 1. Therefore, in order to better understand these results, we further explored the differences between the two genomic sequences. Firstly, the FASTA format sequence of both isoforms 1 and 2 were obtained from UniProt under the protein ID O95140 and O95140-2, respectively. From the information provided in this database, it was possible to realize that isoform 2 is derived from alternative splicing and annotate the differences between the two genomic sequences (**Table III-1**).

Table III-1 Information regarding both MFN2 isoforms with the corresponding length, molecular weight, FASTA format sequence; and differences between genomic sequences. Data obtained from https://www.uniprot.org/.

MFN2_HUMAN Isoform 1 (UniProt ID: O95140)

Canonical sequence | 757 aa | 86,402 kDa

FASTA format sequence:

MSLLFSRCNSIVTVKKNKRHMAEVNASPLKHFVTAKKKINGIFEQLGAYIQESATFLEDTYRNAELDPVTTEEQVL
DVKGYLSKVRGISEVLARRHMKVAFFGRTSNGKSTVINAMLWDKVLPSGIGHTTNCFLRVEGTDGHEAFLLTEG
SEEKRSAKTVNQLAHALHQDKQLHAGSLVSVMWPNSKCPLLKDDLVLMDSPGIDVTTELDSWIDKFCLDADVF
VLVANSESTLMQTEKHFFHKVSERLSRPNIFILNNRWDASASEPEYMEEVRRQHMERCTSFLVDELGVVDRSQ
AGDRIFFVSAKEVLNARIQKAQGMPEGGGALAEGFQVRMFEFQNFERRFEECISQSAVKTKFEQHTVRAKQIAE
AVRLIMDSLHMAAREQQVYCEEMREERQDRLKFIDKQLELLAQDYKLRIKQITEEVERQVSTAMAEEIRRLSVLV
DDYQMDFHPSPVVLKVYKNELHRHIEEGLGRNMSDRCSTAITNSLQTMQQDMIDGLKPLLPVSVRSQIDMLVPR
QCFSLNYDLNCDKLCADFQEDIEFHFSLGWTMLVNRFLGPKNSRRALMGYNDQVQRPIPLTPANPSMPPLPQG
SLTQEEFMVSMVTGLASLTSRTSMGILVVGGVVWKAVGWRLIALSFGLYGLLYVYERLTWTTKAKERAFKRQFV
EHASEKLQLVISYTGSNCSHQVQQELSGTFAHLCQQVDVTRENLEQEIAAMNKKIEVLDSLQSKAKLLRNKAGW
LDSELNMFTHQYLQPSR

MFN2_HUMAN Isoform 2 (UniProt ID: O95140-2)

Alternative splicing product | 436 aa | 50,041 kDa

FASTA format sequence:

MHPHLSTLSLPRRRSMAFLSSWGALAEGFQVRMFEFQNFERRFEECISQSAVKTKFEQHTVRAKQIAEAVRLIM
DSLHMAAREQQVYCEEMREERQDRLKFIDKQLELLAQDYKLRIKQITEEVERQVSTAMAEEIRRLSVLVDDYQM
DFHPSPVVLKVYKNELHRHIEEGLGRNMSDRCSTAITNSLQTMQQDMIDGLKPLLPVSVRSQIDMLVPRQCFSL
NYDLNCDKLCADFQEDIEFHFSLGWTMLVNRFLGPKNSRRALMGYNDQVQRPIPLTPANPSMPPLPQGSLTQE
EFMVSMVTGLASLTSRTSMGILVVGGVVWKAVGWRLIALSFGLYGLLYVYERLTWTTKAKERAFKRQFVEHAS
EKLQLVISYTGSNCSHQVQQELSGTFAHLCQQVDGETLSERSMAKSTLMLLTLLFLCSFAGAQDVLTQ

Differences from canonical:

1-302: Missing

303-324:FVSAKEVLNARIQKAQGMPEGG→MHPHLSTLSLPRRRSMAFLSSW
705-757:VTRENLEQEIAAMNKKIEVLDSLQSKAKLLRNKAGWLDSELNMFTHQYLQPSR →
GETLSERSMAKSTLMLLTLLFLCSFAGAQDVLTQ

As shown in **Table III-1**, amino acids from position 1 to 302 are missing in the isoform 2. These amino acids are included in the region of the canonical sequence that encodes for the GTPase domain (from position 93 to 342). Thereby, it was possible to imply that isoform 2 is missing part of the catalytic domain. Moreover, the further amino acids, from position 303 to 324 in the canonical sequence, which differ between the two isoforms (**Table III-1** highlighted in grey), constitute the N-terminal of the isoform 2. Likewise, amino acids from position 705 to 757, which are in the hinge of the HR2 domain, also differ between the two isoforms as indicated and highlighted in blue-grey in **Table III-1**. Initially, these results suggested that isoform 2 may not play a critical role in mitochondrial fusion because of the altered GTPase domain. To clarify this notion, we further investigated if specific conserved regions were present in both isoforms that could represent significant maintenance of the protein function. After aligning both sequences using Clustal Omega Multiple Sequence Alignment (https://www.ebi.ac.uk/Tools/msa/clustalo/) and by analysing the information available in Proteomics DB[200] (https://www.proteomicsdb.org/proteomicsdb/) under the respective UniProt ID (O95140 and O95140-2), a conserved region in both isoforms was identified (**Figure III-11**). In the canonical sequence the conserved region is located between the amino acids 586-756, which corresponds to the amino acids at positions between 284-418 in isoform 2 (**Figure III-11**). Curiously, this region included the part of the C-terminal that is different between the two isoforms (from position 705 to 757). These observations might indicate that the differences within the conserved region are critical for the protein structure and function. Additionally, a recent study reported a specific and preserved region in MFN2 and MFN1 that is essential for MFNs' unique activity in mitochondrial fusion [61]. We further verified if this region identified as mitofusin isoform specific region (MISR) was also present in the MFN2 isoform 2. Indeed, results in **Figure III-11** showed that both isoforms contain the

MISR, which indicated that isoform 2, in fact, could have an important activity in mitochondrial fusion, contrasting to what was initially predicted.

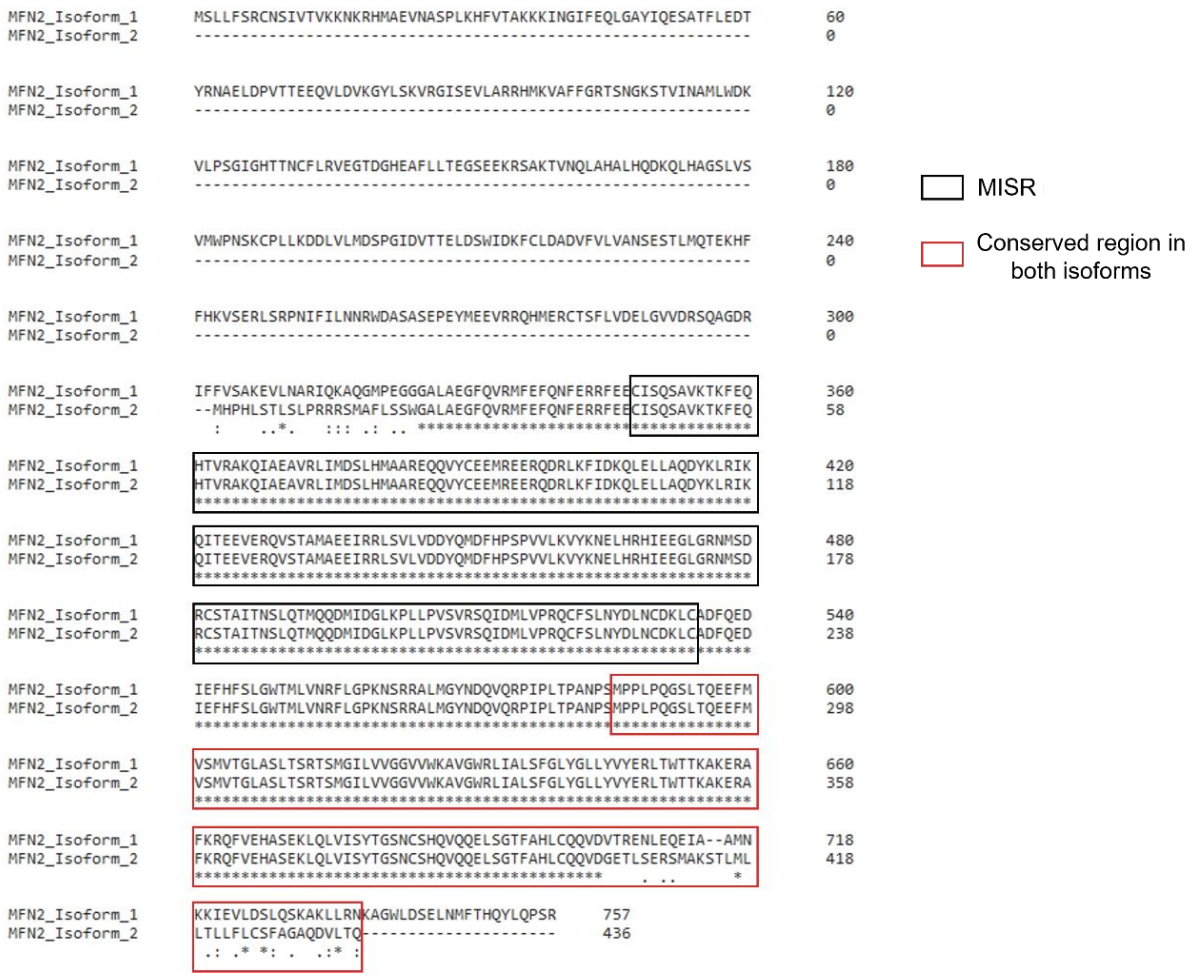

Figure III-10 Alignment of both sequences of MFN2 isoforms and identification of the conserved region and the mitofusin isoform specific region (MISR) proposed to be essential for mitochondrial fusion [61].

G. *In silico* study of the predicted S-glutathionylation sites in MFN2

S-glutathionylation is site specific, occurring only at certain cysteine residues in proteins such as MFN2. However, not all protein thiols are efficient redox sensors, as most of them have pK_a values >8.0 at neutral pH and exist in protonated forms (-SH), which are more resistant to oxidation [131,133]. Nevertheless, the specific thiols in redox-sensitive proteins are more prone to attack by oxidants, since they are more accessible to oxidant stimuli and have a decreased pK_a value because of specific amino acid charges in their vicinity, allowing them to exist in the form of thiolate anion ($-S^-$) even at neutral pH within the cytosol or in the extracellular space [133]. Therefore, a prediction of such specific protein thiols in MFN2 was performed in order to identify possible cysteine residues that may undergo S-

glutathionylation. Three bioinformatics tools, DeepGSH [190], iCysMod [191] and pCysMod [192] were used to predict S-glutathionylated cysteine residues and additional redox-PTMs mediated by thiol groups. The FASTA format of the canonical sequence of MFN2 was retrieved from UniProt (ID O95140) and submitted for all the web servers/databases to predict potential redox-modified sites. Moreover, the three bioinformatics tools provided information regarding values of disorder corresponding to the estimation of cysteine located in a region where protein have no single well-defined tertiary structure in their native and functional state; and protein secondary structure. All the results are presented in **Table III-2**. Consistently, among the 13 cysteines present in MFN2, only 8 were predicted to be S-glutathionylated (**Table III-2**). All potentially S-glutathionylated cysteines are considered to be in an ordered tendency position as evidenced by the lower score values (<0.5 - score corresponds to a threshold at which 5% of the positions of globular proteins were predicted as being disordered) and are also prominently at α-helix structural arrangement (**Table III-2**). Most of the cysteine residues have near them basic amino acids such as lysine (K), arginine (R) and histidine (H), which have been suggested to stabilize the thiolate anion by decreasing its pK_a and increasing the reactivity of cysteine [138,201].

Table III-2 Cysteine residues in MFN2 predicted to be modified by S-glutathionylation and other additional redox-PTMS. This table contains 7 columns, including the position of cysteine residues in the canonical sequence of MFN2, the peptide sequence window, the predicted redox-PTMs, the corresponding false positive rate (FPR %), the domain in which the respective residue is located, the disorder region values that were calculated by IUPred [202] and the secondary structure that was predicted by NetSurfP [203].

Cysteine position	Peptide	Redox PTMs	FPR (%)	Domain	Disorder value	Secondary structure
8	MSLLFSR**C**NSIVTVK	S-palmitoylation	4.44	Inter-domain space	0.1643	Coil
		S-glutathionylation	0.18			
132	GIGHTTN**C**FLRVEGT	S-sulphenylation	4.49	GTPase	0.3807	β-strand
		S-palmitoylation	4.44			
		S-glutathionylation	0.12			
281	RRQHMER**C**TSFLVDE	S-glutathionylation	0.06	GTPase	0.1969	α-helix
		Oxidation [204]				
348	FERRFEE**C**ISQSAVK	S-sulphenylation	0.18	Inter-domain space	0.1942	α-helix
		S-glutathionylation	0.12			
		S-palmitoylation	0.12			
		Oxidation [205]				
390	AREQQVY**C**EEMREER	S-glutathionylation	0.06	HR1	0.4541	α-helix
		S-nitrosylation [206,207]	0.00			
482	GRNMSDR**C**STAITNS	S-palmitoylation	2.03	Inter-domain space	0.4409	α-helix
		S-glutathionylation	0.06			
684	ISYTGSN**C**SHQVQQE	S-glutathionylation	1.84	~HR2	0.2436	Coil
700	SGTFAHL**C**QQVDVTR	S-glutathionylation	1.17	HR2	0.2129	α-helix

Next, molecular docking of the predicted cysteines with GSH molecule was performed. Nonetheless, the crystallographic structures of MFN2[59] (PDB IDs: 6JFM,

resolution 2.09 Å; 6JFL, resolution 2.806 Å, and 6JFK, resolution 1.997 Å) available in PDB were only partially resolved. The three structures had the limitation of missing variable regions of the genomic sequence, where some of the predicted cysteine residues are located (i.e., Cys8, Cys482, Cys684, and Cys700); and, additionally, a large part of the sequence encoding for the GTPase domain, presenting truncated residues at the domain boundaries. Therefore, to obtain the 3D structure of the MFN2 protein without missing gaps, a homology modelling strategy was implemented combining the structure with the highest sequence similarity, the MFN1 protein (PDB ID: 5GO4; resolution 2.202 Å) (**Figure S 2A**) and the partial nucleotide-free structure of the MFN2 protein (PDB ID: 6JFL) (**Figure S 2B**), using MOE (as described in **II.B.15**). In order to validate the model, the Ramachandran plot of the homology model created with MOE software package identified the number of outliers (4 amino acids) and confirmed that the amino acids residues were mainly localized in energetically favourable regions of the plot (**Figure S 3A**). In addition, through the ProSA web server[194], the quality of the MFN2 homology model was assessed, and validated, using the normalized z-score (**Figure S 3B**) whose result indicates the overall model quality. The z-score of the input structure indicates, within the range of scores typically found for proteins of similar size, the deviation of the total energy of the structure with respect to an energy distribution derived from random conformations [194]. The z-score of -6.55 indicated that our output homology model is in the range of native conformations. Moreover, the energy plot (**Figure S 3C**) which demonstrates the local model quality/stability by plotting energies as a function of amino acid sequence position, showed some fluctuations; and the 3D visualization suggested a few residues with unusually high energies that are highlighted in the **Figure S 3D** by red colour. However, combining all the validation data allowed the final homology model (**Figure III-12A**) to be used in further studies.

Identification of the predicted cysteine residues on the molecular surface of the homology model, as represented in **Figure III-12B**, allowed us to recognize that Cys348, Cys390, Cys482, Cys684 and Cys700 are on the surface of the protein more prone to interact with molecules such as GSH. In contrast, residues Cys8, Cys132, and Cys281 (not represented) are buried inside the protein core which may result in difficult GSH accessibility. To confirm these observations, molecular docking calculations of the identified cysteine residues with GSH molecule (structure previously prepared using MOE surface package) were performed using GOLD software (as described in **II.B.15**). From the 8 predicted cysteine residues (**Table III-2**), only 5 cysteines that are on the molecular surface of MFN2 (i.e., Cys348, Cys390, Cys482, Cys684, and Cys700) were able to be docked with GSH molecule by covalent binding and the calculations were successfully accomplished. Together with the findings described above and the molecular docking stimulations, our

results suggested that these 5 particular cysteine residues are highly probable to be modified by S-glutathionylation. In **Figure III-13** the best binding pose, obtained from docking calculations with GOLD, is presented for each cysteine together with the ChemScore[197] score for the cysteine-GSH affinity calculations.

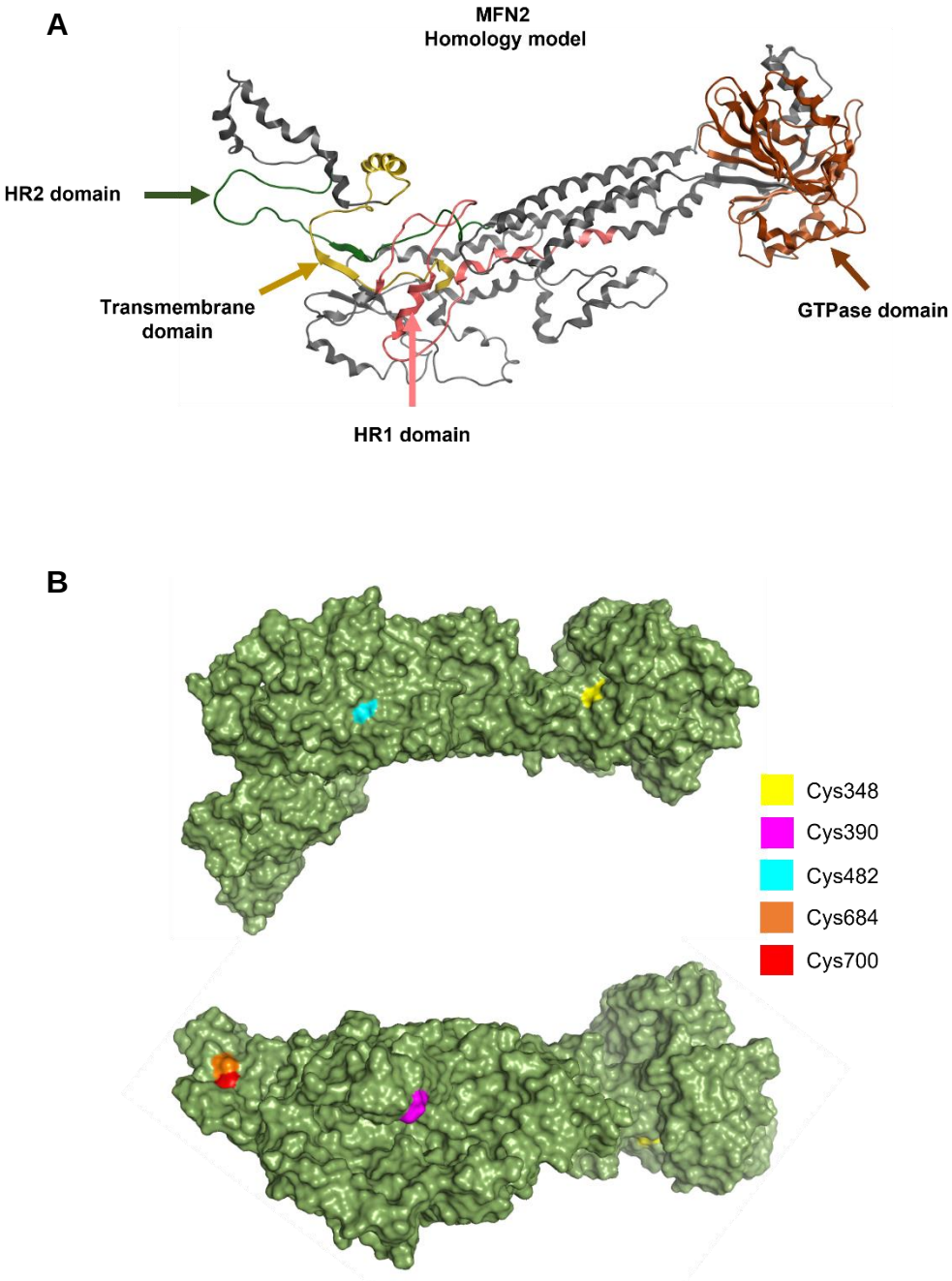

Figure III-11 (A) Graphical representation of the MFN2 homology model with the respective domains obtained with MOE software package. **(B)** Molecular surface of the MFN2 homology model and the identified cysteine residues which are on the surface of the protein and are highly probable to undergo S-glutathionylation.

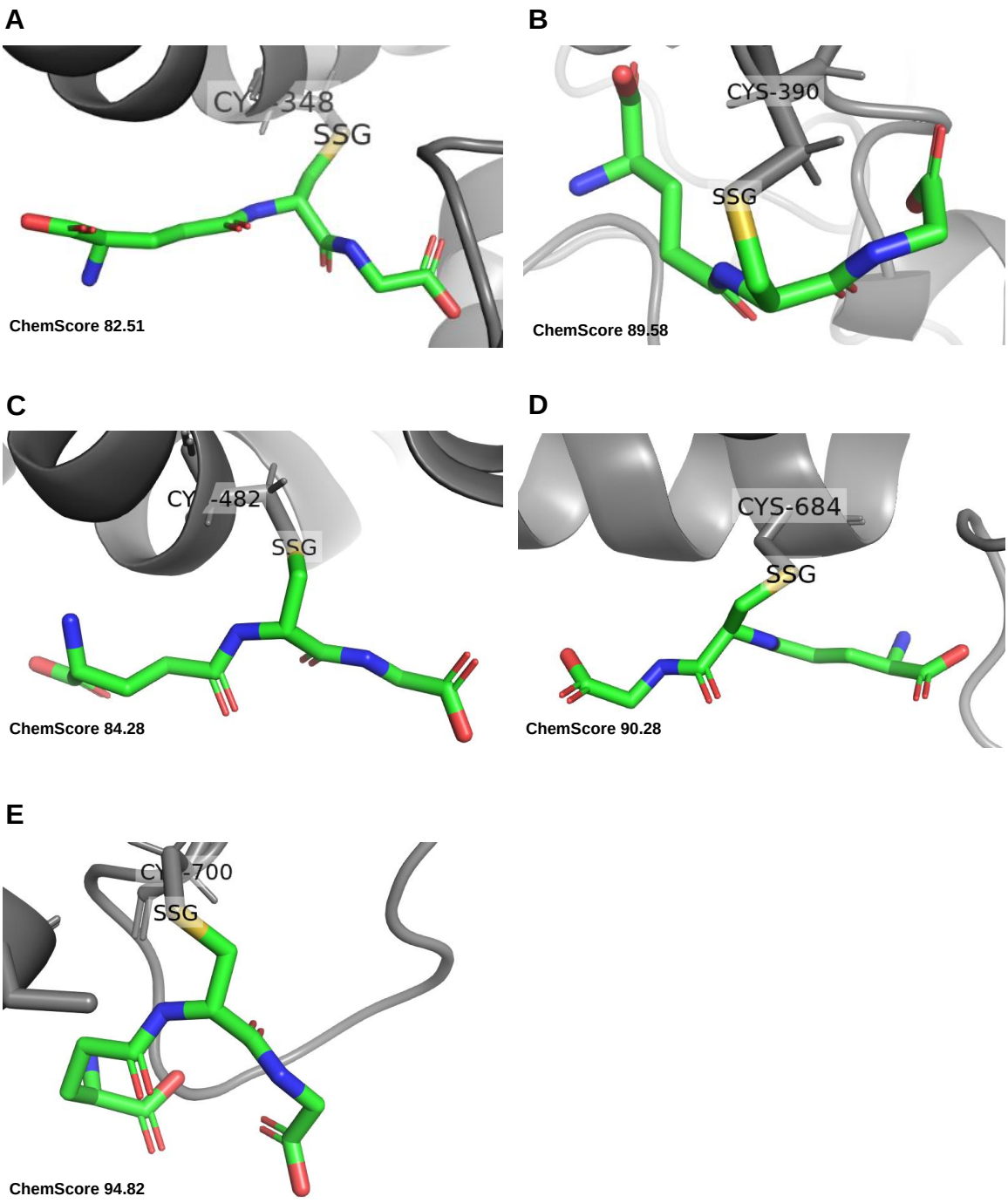

Figure III-12 Docking simulation support the ability of GSH to trigger MFN2 S-glutathionylation in the predicted cysteine residues. Best docking pose for GSH (green) covalent binding with Cys348 **(A)**; Cys390 **(B)**; Cys482 **(C)**; Cys684 **(D)** and Cys700 **(E)**. Covalent docking between sulphur atom of each cysteine residue and sulphur atom of GSH molecule is identified as SSG (disulphide bridge). Hydrogen atoms were omitted for sake of clarity. ChemScore values for each docked calculation was generated by GOLD software.

IV. DISCUSSION

Neurodegenerative diseases are debilitating and largely untreatable conditions that constitute a leading medical, economical and societal challenge faced by the European society. The existent therapies are mainly symptomatic being unable to prevent neurodegeneration that drives the progression of these diseases. Therefore, the identification of novel therapeutic targets to achieve neuroprotection is of the utmost importance.

While affecting different brain regions and causing diverse disabilities, most neurodegenerative disorders share common pathological features such as mitochondrial dysfunction and oxidative stress, that have emerged as important contributing factors for the neuropathogenesis of these diseases. In addition, antioxidant defences involving the action of molecules such as glutathione, have been demonstrated to be disrupted in the neurodegenerative context. Ultimately, this implies that the increasing production of reactive species in neurons is defectively controlled and enhances the damage accumulation in mitochondria. On the other hand, mitochondrial function largely depends on a tight control of structure, localization and balance between biogenesis and degradation of dysfunctional mitochondria. The redox regulation of mitochondrial dynamics upon rising oxidative stress is being increasingly recognized as an important antioxidant signalling mechanism, involving PTMs of proteins that rely on the redox status of cysteine residues, which act as stress sensors. In this regard, protein S-glutathionylation triggered by increased GSSG levels during oxidative stress appears to be one of the predominant modifications as it serves both to protect proteins from irreversible oxidative damage and to modify structure/function relationship. MFN2, as an important mediator of mitochondrial fusion, has been reported to undergo S-glutathionylation, which acts to functionalize MFN2 in the sense of driving the fusion of dysfunctional mitochondria with healthy mitochondria, under stress induction, in order to dilute damaged components. Moreover, previous studies have shown that MFN2 has an essential role in maintaining the balance of mitochondrial dynamics in DAergic neurons and its depletion causes neuronal loss [97,98]. Additionally, MFN2 overexpression was shown to be involved in a protective mechanism against cell apoptosis and mitochondrial dysfunction during oxidative stress [208,209]. Therefore, we suggest that redox regulation of MFN2 upon mitochondrial impairment could play a key neuroprotective role in the complex interplay of mitochondrial dynamics and oxidative stress involved in the neuropathogenesis of PD.

In the current dissertation, the central aim was to understand how the extent of MFN2 S-glutathionylation under induced mitochondrial dysfunction and oxidative stress, modulates

MFN2 expression and potential function as mitochondrial fusion mediator in an *in vitro* PD experimental model and upon exposure to different compounds that alter the intracellular redox *milieu*. To further reveal possible changes in mitochondrial morphology linked to the mitochondrial fusion regulator MFN2 in PD, confocal microscopy analysis of *post-mortem* mesencephalon tissue samples was performed. Additionally, bioinformatic studies were made to (1) understand the potential structural and function differences between MFN2 isoforms; and (2) to identify cysteine residues in MFN2 that are predicted to undergo S-glutathionylation. Finally, these residues were targeted in the 3D structure of MFN2 for molecular docking simulations with GSH molecule using *in silico* approaches, to predict S-glutathionylation by scoring cysteine-GSH interaction.

The initial results from this study, suggested that S-glutathionylation of MFN2 is favourably driven by GSSG levels raised from mitochondrial impairment together with increased oxidative stress in the *in vitro* PD model. Mitochondrial dysfunction leads to an increase in ROS generation which consequently act as second messengers able to regulate intracellular signal transduction under a variety of physiological and pathological conditions. Overproduction of ROS leads to the conversion of GSH to GSSG, shifting GSH/GSSG ratio into a more oxidizing cellular environment. Consequently, the accumulation of GSSG levels enhances S-glutathionylation of proteins to protect them from irreversible oxidative damage. Our data indicated that elevated levels of GSSG triggered by significant ROS production after treatments with tBHP, MPP^+ or GSSG, led to an increase in levels of protein S-glutathionylation with a concomitant induction of GSTP protein expression as previously reported, for instance, in MPTP-treated mice [210]. Moreover, co-immunoprecipitation of MFN2 in SH-SY5Y cells treated with MPP^+ revealed a tendency to enhanced S-glutathionylation, similiar to the level of S-glutathionylation seen after GSSG treatment [99]. These results involving MPP^+ could be related with a recent study reporting greater S-glutathionylation of MFN2 under oxidative stress caused by a pollutant [211]. Environmental toxins are considered to be one of the possible causes for sporadic PD. Therefore, our results led us propose that S-glutathionylation of MFN2, that is apparently prompted under MPP^+ neurotoxicity, is possibly driven by the accumulation of GSSG levels triggered by the overproduction of ROS by the direct impairment of complex I in the mitochondrial respiratory chain. These observations could be also supported by the reported decrease in GSH/GSSG ratio preceding impairments of OXPHOS in PD [121,212,213]. Besides, as MPP^+ exposure produced similar effects in SH-SY5Y cells as the treatment with GSSG, it is likely that the changes at the level of stress induction, GSH/GSSG ratio and consequent S-glutathionylation of MFN2 under GSSG exposure reflect the neuronal environment seen in PD patients with

mitochondrial dysfunction associated, for instance, to deficiency in PD-related proteins involved in mitochondrial dynamics.

Mitochondrial fusion has been proposed to be mediated through MFN2 oligomerization triggered by increased GSSG levels. The formation of dimeric antiparallel coiled-coil structures (*cis*-oligomerization) of either homodimers (MFN1-MFN1 or MFN2-MFN2) or heterodimers (MFN1-MFN2) [55,74] has been demonstrated to be important for mitochondrial tethering. The initial MFN2 dimerization through formation of disulphide bridges [53,99], suggests that the generation of larger disulphide-induced oligomers may act to "prime" them to bind in *trans* (*trans*-oligomerization) and drive mitochondrial fusion of opposing OMM [99,214]. Thus, the involvement of glutathione in MFN2 di/oligomerization suggests a direct link between the rates of mitochondrial fusion and the level of cellular stress. Our results from the Western Blot under non-reducing conditions of SH-SY5Y cells treated with the different redox-modifying agents, revealed a significant GSSG-dependent shift of MFN2 immunoreactivity into distinct dimeric and oligomeric species, running between 70 and 250 kDa. However, immunoblotting with anti-MFN2 directly showed that the free-thiol blocking agent NEM largely prevented the formation of higher molecular weight oligomers via disulphide bridges. The appearance of several oligomeric species could represent multimers of MFN2 with altered mobility due to distinct disulphide species, or could reflect the presence of additional, unknown partners within these complexes. These observations verified that MFN2 oligomerization is dependent on the availability of free cysteine thiols. Previous studies had reported that cysteine residues Cys684 and Cys700 in MFN2 are critical for the GSSG-induced formation of disulphide-linked oligomers driving mitochondrial fusion and the respiratory response to oxidative stress [99,153,154,214]. Here, we demonstrated *in silico* that these two cysteine residues together with the three predicted Cys348, Cys390 and Cys482 undergo S-glutathionylation either by thiol-disulphide exchange or by enzymatic action of GSTP or Grx. The thiolates of the targeted cysteines in the 3D structure of MFN2 were put under molecular docking simulations with GSH molecule, which showed potentially high scoring for the cysteine-GSH docking calculations. Altogether, these results suggested that critical cysteine residues in MFN2 play key regulatory roles in redox-PTMs through S-glutathionylation and MFN2 oligomerization that drive mitochondrial fusion under oxidative stress.

Consistent with the results from co-immunoprecipitation of MFN2, GSSG-dependent oligomerization underlined here, is possibly triggered by GSSG levels raised from ROS burden from the direct mitochondrial impairment in the *in vitro* PD model and not only by the disrupted GSH/GSSG ratio through GSH decline in PD context. These conclusions are deduced from the following observations: under the exposure to all redox-modifying agents

which decreased the GSH/GSSG ratio, dimerization of MFN2 was observed; however, a prevalent formation of larger MFN2 oligomers was only possible under MPP^+ or GSSG treatment. Depletion of GSH synthesis *per se* was not sufficient to cause significant mitochondrial damage as well as oxidative stress and pro-oxidant tBHP stimulus, although significantly increasing GSSG levels in comparison to untreated or to BSO-treated SH-SY5Y cells, also did not affected mitochondrial function. Importantly, exposure to MPP^+ or GSSG similarly impacted mitochondrial function as revealed through ATP production and the OXPHOS subunits expression, in particular complex I, by either direct inhibition or possible inactivation by S-glutathionylation. Previous studies have shown that treatment of isolated mitochondria with GSSG resulted in S-glutathionylation of the complex I on the 75 kDa subunit at Cys531 and Cys704 resulting in loss of activity [215,216]. Subsequently, the reported increase in ROS together with accentuated reduction in the GSH/GSSG ratio led to the formation of larger MFN2 oligomers compared to the untreated or BSO-treated cells. Taken together, these results indicated that MFN2 oligomerization is highly dependent not only on the GSH/GSSG ratio but more importantly, on whether the signalling for increase GSSG content surges from impairment of mitochondria and not only from GSH depletion. These findings ultimately revealed the importance of mitochondrial fusion induction through redox signals in MFN2, especially, under pathological conditions such as PD.

Curiously, we observed that the increased GSSG levels upon PD-related neurotoxin MPP^+ or GSSG treatments which led to S-glutathionylation of MFN2, also tend to upregulate MFN2 protein expression. Interestingly, both treatments also enhanced the expression of the analogous mitochondrial fusion mediator MFN1. Accordingly, these results give insights to a GSSG-dependent upregulation of mitochondrial fusion machinery in PD in order to drive remodelling of a damaged mitochondrial network. These findings suggest that PD-associated environmental neurotoxins could contribute to redox-PTMs as well as to changes in the expression of important mitochondrial dynamics mediators. Further results from *post-mortem* PD mesencephalon tissue immunofluorescence analysis, demonstrated possible enhanced mitochondrial fusion clusters revealed by the significant colocalization of MFN2 and TOM20 proteins. Although a recent study has demonstrated decreased levels of both MFNs in SNpc of sporadic PD patients without reaching any significance [217], results from the current study indicate an opposite scenario. The area of occupancy of MFN2 tend to be enhanced in *post-mortem* PD samples and mitochondrial morphology was preferentially changed for fusion. Our findings suggested that enhanced mitochondrial fusion mediated by MFN2 is a potential neuroprotective mechanism triggered by neurons against increased oxidative stress and mitochondrial impairment in PD. Prior studies based on genetic factors associated with monogenic PD suggested that disturbed mitochondrial dynamics is likely

involved in the neuropathogenesis of PD [36,38,218]. However, detailed studies on changes in mitochondrial dynamics, especially in mitochondrial fusion, in sporadic PD are scarce. At the time of this study, we did not had access to the clinical report of the selected donors and therefore we do not known whether the patients whose tissue samples were analysed presented mainly sporadic or monogenic forms of PD. This information could be important for better interpretation of these preliminary results, providing more definite and direct evidence of mitochondrial morphology changes in DAergic neurons in both monogenic and sporadic forms of PD.

Taken together the results from the *in vitro* PD experimental model and the analysis of *post-mortem* PD samples, it is reasonable to assume that a regulatory pathway which might contribute to PD progression, will involve mitochondrial dysfunction leading to increased oxidative stress, and consequent oxidation of GSH which in turn will potentiate S-glutathionylation of mitochondrial dynamics regulators such as MFN2, that plays a determinant role in the remodelling of dysfunctional mitochondria.

In the second part of the current study, we started by analysing the genomic sequences of the two MFN2 isoforms (isoform 1 – canonical sequence, isoform 2 – alternative splicing product) as some differences in the protein expression were observed. This analysis provided a few insights into the potential structural and functional variations between the two MFN2 isoforms. The biological properties of the isoform 2 are not described in literature, thereby, the conclusions from this study were based on the information available in databases and from interconnection with previous reports involving isoform 1 structure and function. By comparing the two genomic sequences, it was possible to mark that (1) isoform 2 is missing large part of the GTPase domain, with some of the final 21 amino acids corresponding to its N-terminal differing from the canonical sequence; and (2) the C-terminal of both isoforms also differs in amino acid sequence. However, two crucial regions were identified in both isoforms: one conserved region that, curiously, includes part of the C-terminal that differs in amino acids between the two isoforms; and a mitofusin isoform-specific region (MISR) which was recently identified to contribute to MFN-specific function by Hoppins and colleagues [61]. To note that the term «mitofusin isoform» in the study from Hoppins and colleagues refers to MFN1 and MFN2, differently from the terminology used in the current study, where we indicate MFN2 isoforms as the same protein with different structures (MFN2 isoform 1 and MFN2 isoform 2). Given that MISR includes the loop and α-helices that compose part of the hinge of HR1 domain (near the GTPase domain), Hoppins and colleagues proposed that MISR could impact conformational changes in full-length MFN and thus influence nucleotide-dependent assembly. The GTPase catalytic cycle is expected to control MFN activity through modulation of its self-assembly and conformational changes

that together drive membrane remodelling [56,61]. Given the possible differences in the MFN2 conformational states, it is likely that the MFN2 oligomers observed in this study represent multimers of both isoforms in different conformational states. Moreover, the appearance of the monomer corresponding to the isoform 2, around 55 kDa, only in the presence of the free-thiol blocking agent NEM, suggested that this isoform widely participates in the oligomerization of MFN2 through formation of disulphide bridges. Therefore, as MISR is present in both isoforms but only isoform 1 carries the complete GTPase domain, from this viewpoint it can be proposed that isoform 2 could contribute to specific conformational flexibility by forming multimers with the isoform 1 through GSSG-dependent bonds between the potentially identified S-glutathionylated cysteine residues and, thereby, contribute to the nucleotide-dependent assembly of isoform 1. In fact, from our *in silico* study, three of the five cysteine residues (i.e., Cys348, Cys390 and Cys482) present in both isoforms which are potentially S-glutathionylated, are located in the identified MISR, suggesting that these specific residues could be critical for the mitochondrial fusion event, as had already been proposed for Cys684 [99,154]. Moreover, it cannot be excluded the possibility of the formation of homodimers through inter- or intramolecular disulphide-bonds even between isoform 2 or heterodimers with homologous proteins such as MFN1.

Up-to-date, two different MFN2 topologies has been proposed: N_{out}-C_{out} topology, where the C-terminal and the HR1/2 domains are cytoplasmic and TMDs cross the OMM, which would result from a hairpin transmembrane anchor mediating the fusion process [55,58]; and N_{out}-C_{in} topology where the membrane anchor is a single pass transmembrane helix, with the C-terminal and HR2 domain residing in the IMS [53]. The latter predicted topology was demonstrated biochemically and revealed that the C-terminal includes the redox-sensitive cysteine residues, Cys684 and Cys700 within the IMS, which have been proposed to be important for the mitochondrial docking by *cis*-oligomerization. Although, *cis*-oligomerization is currently lacking structural insights, it has been linked to the MFNs with N_{out}-C_{in} topology which might act as cofactors for MFNs with N_{out}-C_{out} topology, as suggested by comparing with yeast mitochondrial fusion regulators Ugo1 and Fzo1 [44]. From this analysis, we may suggest the possibility of isoform 2 participating in mitochondrial fusion even with conditioned catalytic domain, by acting as cofactor for isoform 1. This could justify the tendency towards elevated protein expression in the SH-SY5Y cells treated with tBHP, MPP^+ and GSSG, where the increased GSSG levels potentially drive mitochondrial fusion. In fact, GTPase domain has been shown to be only critical for mitochondrial fusion completion [55]. Previous studies had also demonstrated that mutant isoform of MFN2 (with inactivated GTPase) was able to participate in mitochondrial fusion [219]. The hydrolysis-deficient mutant of MFN2, $MFN2_{RasG12V}$, equally promoted stimulation of mitochondrial fusion [219] and, in

addition, showed a significant protection of neurons against stress-induced cell death [220]. Hence, in this study we suggest the potential relevance of isoform 2 as part of mitochondrial fusion machinery and propose that the structural differences between both isoforms may be essential for the efficiency of mitochondrial fusion stimulation upon cellular stress induction. Nevertheless, further biochemical and structural investigation are required to confirm the preliminary results reported here.

The results from this study bring important insights into the complex regulatory pathway of mitochondrial fusion through S-glutathionylation of critical cysteine residues in MFN2. Although a few studies have reported the functional importance of certain conserved cysteine residues in MFN2, the majority of identified residues have never been under further investigation. So far, the relevance of cysteine residues in MFN2 in the context of PD is still an underexplored research area, where numerous steps of regulatory pathways remain to be investigated. Importantly, understanding the redox regulation of mitochondrial fusion in PD through S-glutathionylation of MFN2, could potentiate the discovery of new biomarkers and uncover novel therapeutic targets. Therefore, in the near future, it will be important to study the functional importance of the identified cysteine residues in MFN2 by generating mutants in *in vitro* PD models and further *in vivo* models; and understand if S-glutathionylation of these specific residues is able to impact MFN2 function as mitochondrial fusion mediator under mitochondrial dysfunction and oxidative stress. Furthermore, our preliminary results from the genomic sequence analysis of the two MFN2 isoforms brought some attention to the importance of the structural characteristics within the same protein and how evolutionary conserved regulators from mitochondrial dynamics machinery can suffer genomic alterations in order to render their function more efficient. In addition, as the overall knowledge of cysteine based reversible modifications is still quite limited due to the challenges associated with isolation, site-specific identification, and quantification, new techniques should continue to evolve to selectively identify specific S-glutathionylated proteins in a quantitative fashion related to changes in cellular functions. Thus, the use of *in silico* approaches combined with proteomics for identification of S-glutathionylated proteins such as MFN2 will be crucial for better understanding of the protein regulation by redox-PTMs; and additionally use S-glutathionylated MFN2 as a potential biomarker.

Altogether, results from this dissertation provide novel perspectives on the mechanisms coupling mitochondrial dynamics to the cellular stress response in the brain, thereby, contributing to clarify the features underlying PD progression in relation to mitochondrial dysfunction and oxidative stress. Specifically, these results may offer additional evidence that induction of mitochondrial fusion could be one of the neuronal

responses to a redox imbalance state and bring new insights to PD neuropathogenesis together with future novel approaches to therapeutic development.

V. REFERENCES

1. Dickson, D. W. Neuropathology of Parkinson disease. *Parkinsonism Relat Disord* **46 Suppl 1**, S30–S33 (2018).
2. Iwatsubo, T. Aggregation of α-synuclein in the pathogenesis of Parkinson's disease. *Journal of Neurology, Supplement* **250**, 11–14 (2003).
3. The Project Gutenberg eBook of An Essay on the Shaking Palsy, by James Parkinson. https://www.gutenberg.org/files/23777/23777-h/23777-h.htm.
4. Parkinson's Disease Information Page | National Institute of Neurological Disorders and Stroke. https://www.ninds.nih.gov/Disorders/All-Disorders/Parkinsons-Disease-Information-Page.
5. Tysnes, O. B. & Storstein, A. Epidemiology of Parkinson's disease. *J Neural Transm (Vienna)* **124**, 901–905 (2017).
6. Hayes, M. T. Parkinson's Disease and Parkinsonism. *Am J Med* **132**, 802–807 (2019).
7. Poewe, W. *et al.* Parkinson disease. *Nat Rev Dis Primers* **3**, 1–21 (2017).
8. Weintraub, D. *et al.* The neuropsychiatry of Parkinson's disease: advances and challenges. *Lancet Neurol* **21**, 89 (2022).
9. Aarsland, D. *et al.* Parkinson disease-associated cognitive impairment. *Nat Rev Dis Primers* **7**, (2021).
10. JW, H. *et al.* Psychiatric Manifestation in Patients with Parkinson's Disease. *J Korean Med Sci* **33**, (2018).
11. Park, J. S., Davis, R. L. & Sue, C. M. Mitochondrial Dysfunction in Parkinson's Disease: New Mechanistic Insights and Therapeutic Perspectives. *Curr Neurol Neurosci Rep* **18**, (2018).
12. Chang, K. H. & Chen, C. M. The role of oxidative stress in Parkinson's disease. *Antioxidants* vol. 9 1–32 Preprint at https://doi.org/10.3390/antiox9070597 (2020).
13. Cookson, M. R. Parkinsonism Due to Mutations in PINK1, Parkin, and DJ-1 and Oxidative Stress and Mitochondrial Pathways. *Cold Spring Harb Perspect Med* **2**, (2012).
14. Ge, P., Dawson, V. L. & Dawson, T. M. PINK1 and Parkin mitochondrial quality control: a source of regional vulnerability in Parkinson's disease. *Molecular Neurodegeneration 2020 15:1* **15**, 1–18 (2020).
15. Manzoni, C. *et al.* Pathogenic parkinson's disease mutations across the functional domains of LRRK2 alter the autophagic/lysosomal response to starvation. *Biochem Biophys Res Commun* **441**, 862–866 (2013).
16. Panicker, N., Ge, P., Dawson, V. L. & Dawson, T. M. The cell biology of Parkinson's disease. *Journal of Cell Biology* vol. 220 Preprint at https://doi.org/10.1083/jcb.202012095 (2021).
17. Trist, B. G., Hare, D. J. & Double, K. L. Oxidative stress in the aging substantia nigra and the etiology of Parkinson's disease. *Aging Cell* **18**, (2019).
18. Sheng, Z. H. & Cai, Q. Mitochondrial transport in neurons: impact on synaptic homeostasis and neurodegeneration. *Nature Reviews Neuroscience 2012 13:2* **13**, 77–93 (2012).
19. Celsi, F. *et al.* Mitochondria, calcium and cell death: A deadly triad in neurodegeneration. *Biochim Biophys Acta* **1787**, 335 (2009).
20. Ransohoff, R. M. How neuroinflammation contributes to neurodegeneration. *Science* **353**, 777–783 (2016).
21. Yin, F., Sancheti, H., Liu, Z. & Cadenas, E. Mitochondrial function in ageing: Coordination with signalling and transcriptional pathways. *Journal of Physiology* vol. 594 2025–2042 Preprint at https://doi.org/10.1113/JP270541 (2016).

22. Haddad, F., Sawalha, M., Khawaja, Y., Najjar, A. & Karaman, R. Dopamine and Levodopa Prodrugs for the Treatment of Parkinson's Disease. *Molecules* **23**, (2017).

23. Tan, Y. Y., Jenner, P. & Chen, S. di. Monoamine Oxidase-B Inhibitors for the Treatment of Parkinson's Disease: Past, Present, and Future. *J Parkinsons Dis* **12**, 477–493 (2022).

24. Pilipovich, A. A. & Golubev, V. L. [The agonist of dopamine receptors piribedil in treatment of Parkinson's disease]. *Zh Nevrol Psikhiatr Im S S Korsakova* **117**, 83–90 (2017).

25. Fejeran, J., Salazar, F., Alvarez, C. M. & Jahangiri, F. R. Deep Brain Stimulation and Microelectrode Recording for the Treatment of Parkinson's Disease. *Cureus* **14**, (2022).

26. Marras, C., Canning, C. G. & Goldman, S. M. Environment, lifestyle, and Parkinson's disease: Implications for prevention in the next decade. *Mov Disord* **34**, 801–811 (2019).

27. Henchcliffe, C. & Sarva, H. Restoring Function to Dopaminergic Neurons: Progress in the Development of Cell-Based Therapies for Parkinson's Disease. *CNS Drugs* **34**, 559–577 (2020).

28. Freya, T. G. & Mannellab, C. A. The internal structure of mitochondria. *Trends Biochem Sci* **25**, 319–324 (2000).

29. Picard, M., Shirihai, O. S., Gentil, B. J. & Burelle, Y. Mitochondrial morphology transitions and functions: Implications for retrograde signaling? *Am J Physiol Regul Integr Comp Physiol* **304**, 393–406 (2013).

30. Annesley, S. J. & Fisher, P. R. Mitochondria in Health and Disease. *Cells* **8**, (2019).

31. Cogliati, S. *et al.* Mitochondrial Cristae Shape Determines Respiratory Chain Supercomplexes Assembly and Respiratory Efficiency. *Cell* **155**, 160–171 (2013).

32. Kann, O. & Kovács, R. Mitochondria and neuronal activity. *Am J Physiol Cell Physiol* **292**, 641–657 (2007).

33. Li, Z., Okamoto, K. I., Hayashi, Y. & Sheng, M. The Importance of Dendritic Mitochondria in the Morphogenesis and Plasticity of Spines and Synapses. *Cell* **119**, 873–887 (2004).

34. Tilokani, L., Nagashima, S., Paupe, V. & Prudent, J. Mitochondrial dynamics: Overview of molecular mechanisms. *Essays in Biochemistry* vol. 62 341–360 Preprint at https://doi.org/10.1042/EBC20170104 (2018).

35. Frederick, R. L. & Shaw, J. M. Moving Mitochondria: Establishing Distribution of an Essential Organelle. *Traffic* **8**, 1668–1675 (2007).

36. Burté, F., Carelli, V., Chinnery, P. F. & Yu-Wai-Man, P. Disturbed mitochondrial dynamics and neurodegenerative disorders. *Nature Reviews Neurology* vol. 11 11–24 Preprint at https://doi.org/10.1038/nrneurol.2014.228 (2015).

37. Chan, D. C. Mitochondrial Dynamics and Its Involvement in Disease. *Annu Rev Pathol* **15**, 235–259 (2020).

38. Gao, J. *et al.* Abnormalities of mitochondrial dynamics in neurodegenerative diseases. *Antioxidants* vol. 6 Preprint at https://doi.org/10.3390/antiox6020025 (2017).

39. Mishra, P. & Chan, D. C. Mitochondrial dynamics and inheritance during cell division, development and disease. *Nature Reviews Molecular Cell Biology 2014 15:10* **15**, 634–646 (2014).

40. Chan, D. C. Fusion and Fission: Interlinked Processes Critical for Mitochondrial Health. *http://dx.doi.org/10.1146/annurev-genet-110410-132529* **46**, 265–287 (2012).

41. Santetl, A. *et al.* Mitofusin-1 protein is a generally expressed mediator of mitochondrial fusion in mammalian cells. *J Cell Sci* **116**, 2763–2774 (2003).

42. Filadi, R., Pendin, D. & Pizzo, P. Mitofusin 2: from functions to disease. *Cell Death Dis* **9**, 330 (2018).

43. Ishihara, N., Fujita, Y., Oka, T. & Mihara, K. Regulation of mitochondrial morphology through proteolytic cleavage of OPA1. *EMBO J* **25**, 2966–2977 (2006).

44. Cohen, M. M. & Tareste, D. Recent insights into the structure and function of Mitofusins in mitochondrial fusion. *F1000Res* **7**, (2018).

45. Smirnova, E., Griparic, L., Shurland, D.-L. & Bliek, A. M. van der. Dynamin-related Protein Drp1 Is Required for Mitochondrial Division in Mammalian Cells. *https://doi.org/10.1091/mbc.12.8.2245* **12**, 2245–2256 (2017).

46. Losó n, O. C., Song, Z., Chen, H. & Chan, D. C. Fis1, Mff, MiD49, and MiD51 mediate Drp1 recruitment in mitochondrial fission. *Mol Biol Cell* **24**, 659–667 (2013).

47. Twig, G. & Shirihai, O. S. The Interplay Between Mitochondrial Dynamics and Mitophagy. *https://home.liebertpub.com/ars* **14**, 1939–1951 (2011).

48. Lewis, S. C., Uchiyama, L. F. & Nunnari, J. ER-mitochondria contacts couple mtDNA synthesis with Mitochondrial division in human cells. *Science (1979)* **353**, (2016).

49. Twig, G. *et al.* Fission and selective fusion govern mitochondrial segregation and elimination by autophagy. *EMBO J* **27**, 433–446 (2008).

50. Detmer, S. A. & Chan, D. C. Functions and dysfunctions of mitochondrial dynamics. *Nature Reviews Molecular Cell Biology 2007 8:11* **8**, 870–879 (2007).

51. Baker, N., Patel, J. & Khacho, M. Linking mitochondrial dynamics, cristae remodeling and supercomplex formation: How mitochondrial structure can regulate bioenergetics. *Mitochondrion* **49**, 259–268 (2019).

52. Chandhok, G., Lazarou, M. & Neumann, B. Structure, function, and regulation of mitofusin-2 in health and disease. *Biol Rev Camb Philos Soc* **93**, 933 (2018).

53. Mattie, S., Riemer, J., Wideman, J. G. & McBride, H. M. A new mitofusin topology places the redox-regulated C terminus in the mitochondrial intermembrane space. *Journal of Cell Biology* **217**, 507–515 (2018).

54. Qi, Y. *et al.* Structures of human mitofusin 1 provide insight into mitochondrial tethering. *Journal of Cell Biology* **215**, 621–629 (2016).

55. Koshiba, T. *et al.* Structural Basis of Mitochondrial Tethering by Mitofusin Complexes. *Science (1979)* **305**, 858 (2004).

56. Daumke, O. & Roux, A. Mitochondrial Homeostasis: How Do Dimers of Mitofusins Mediate Mitochondrial Fusion? *Current Biology* **27**, R353–R356 (2017).

57. Franco, A. *et al.* Correcting mitochondrial fusion by manipulating mitofusin conformations. *Nature* **540**, 74 (2016).

58. Rojo, M., Legros, F., Chateau, D. & Lombès, A. Membrane topology and mitochondrial targeting of mitofusins, ubiquitous mammalian homologs of the transmembrane GTPase Fzo. *J Cell Sci* **115**, 1663–1674 (2002).

59. Li, Y.-J. *et al.* Structural insights of human mitofusin-2 into mitochondrial fusion and CMT2A onset. *Nat Commun* **10**, 4914 (2019).

60. Cao, Y.-L. *et al.* MFN1 structures reveal nucleotide-triggered dimerization critical for mitochondrial fusion. *Nature 2017 542:7641* **542**, 372–376 (2017).

61. Sloat, S. R., Whitley, B. N., Engelhart, E. A. & Hoppins, S. Identification of a mitofusin specificity region that confers unique activities to Mfn1 and Mfn2. *Mol Biol Cell* **30**, 2309 (2019).

62. Züchner, S. *et al.* Mutations in the mitochondrial GTPase mitofusin 2 cause Charcot-Marie-Tooth neuropathy type 2A. *Nat Genet* **36**, 449–451 (2004).

63. Loiseau, D. *et al.* Mitochondrial coupling defect in Charcot–Marie–Tooth type 2A disease. *Ann Neurol* **61**, 315–323 (2007).

64. Mourier, A. *et al.* Mitofusin 2 is required to maintain mitochondrial coenzyme Q levels. *Journal of Cell Biology* **208**, 429–442 (2015).

65. Chen, H., Chomyn, A. & Chan, D. C. Disruption of Fusion Results in Mitochondrial Heterogeneity and Dysfunction. *Journal of Biological Chemistry* **280**, 26185–26192 (2005).

66. Sebastián, D. *et al.* Mitofusin 2 (Mfn2) links mitochondrial and endoplasmic reticulum function with insulin signaling and is essential for normal glucose homeostasis. *Proceedings of the National Academy of Sciences* **109**, 5523–5528 (2012).

67. de Brito, O. M. & Scorrano, L. Mitofusin 2 tethers endoplasmic reticulum to mitochondria. *Nature* **456**, 605–610 (2008).

68. Schrepfer, E. & Scorrano, L. Mitofusins, from Mitochondria to Metabolism. *Mol Cell* **61**, 683–694 (2016).

69. Yang, Y. *et al.* MFN2 ameliorates cell apoptosis in a cellular model of Parkinson's disease induced by rotenone. *Exp Ther Med* **16**, 3680–3685 (2018).

70. Chen, L. *et al.* Mitochondrial Fusion Protein Mfn2 and Its Role in Heart Failure. *Front Mol Biosci* **8**, 372 (2021).

71. Chen, Y. & Dorn, G. W. PINK1-phosphorylated mitofusin 2 is a parkin receptor for culling damaged mitochondria. *Science (1979)* **340**, 471–475 (2013).

72. Misko, A., Jiang, S., Wegorzewska, I., Milbrandt, J. & Baloh, R. H. Mitofusin 2 Is Necessary for Transport of Axonal Mitochondria and Interacts with the Miro/Milton Complex. *The Journal of Neuroscience* **30**, 4232 (2010).

73. Soriano, F. X. *et al.* Evidence for a Mitochondrial Regulatory Pathway Defined by Peroxisome Proliferator–Activated Receptor-γ Coactivator-1α, Estrogen-Related Receptor-α, and Mitofusin 2. *Diabetes* **55**, 1783–1791 (2006).

74. Chen, H. *et al.* Mitofusins Mfn1 and Mfn2 coordinately regulate mitochondrial fusion and are essential for embryonic development. *Journal of Cell Biology* **160**, 189–200 (2003).

75. Sandoval, H. *et al.* Mitochondrial fusion but not fission regulates larval growth and synaptic development through steroid hormone production. *Elife* **3**, (2014).

76. Chen, H., McCaffery, J. M. & Chan, D. C. Mitochondrial Fusion Protects against Neurodegeneration in the Cerebellum. *Cell* **130**, 548–562 (2007).

77. Grünewald, A., Kumar, K. R. & Sue, C. M. New insights into the complex role of mitochondria in Parkinson's disease. *Prog Neurobiol* **177**, 73–93 (2019).

78. Mailloux, R. J. An update on mitochondrial reactive oxygen species production. *Antioxidants* vol. 9 Preprint at https://doi.org/10.3390/antiox9060472 (2020).

79. Liu, Y., Fiskum, G. & Schubert, D. Generation of reactive oxygen species by the mitochondrial electron transport chain. *J Neurochem* **80**, 780–787 (2002).

80. Kussmaul, L. & Hirst, J. The mechanism of superoxide production by NADH:ubiquinone oxidoreductase (complex I) from bovine heart mitochondria. *Proc Natl Acad Sci U S A* **103**, 7607–7612 (2006).

81. Pryde, K. R. & Hirst, J. Superoxide Is Produced by the Reduced Flavin in Mitochondrial Complex I: A SINGLE, UNIFIED MECHANISM THAT APPLIES DURING BOTH FORWARD AND REVERSE ELECTRON TRANSFER *. *Journal of Biological Chemistry* **286**, 18056–18065 (2011).

82. Grivennikova, V. G., Kozlovsky, V. S. & Vinogradov, A. D. Respiratory complex II: ROS production and the kinetics of ubiquinone reduction. *Biochim Biophys Acta Bioenerg* **1858**, 109–117 (2017).

83. Muller, F. L., Liu, Y. & van Remmen, H. Complex III Releases Superoxide to Both Sides of the Inner Mitochondrial Membrane *. *Journal of Biological Chemistry* **279**, 49064–49073 (2004).

84. Sies, H. & Jones, D. P. Reactive oxygen species (ROS) as pleiotropic physiological signalling agents. *Nature Reviews Molecular Cell Biology 2020 21:7* **21**, 363–383 (2020).

85. Hemmati-Dinarvand, M. *et al.* Oxidative stress and Parkinson's disease: conflict of oxidant-antioxidant systems. *Neurosci Lett* **709**, 134296 (2019).

86. Neves Carvalho, A., Firuzi, O., Joao Gama, M., van Horssen, J. & Saso, L. Oxidative Stress and Antioxidants in Neurological Diseases: Is There Still Hope? *Curr Drug Targets* **18**, 705–718 (2017).

87. Khan, Z. & Ali, S. A. Oxidative stress-related biomarkers in Parkinson's disease: A systematic review and meta-analysis. *Iran J Neurol* **17**, 137 (2018).

88. Sofic, E., Lange, K. W., Jellinger, K. & Riederer, P. Reduced and oxidized glutathione in the substantia nigra of patients with Parkinson's disease. *Neurosci Lett* **142**, 128–130 (1992).

89. Edmondson, D. Hydrogen peroxide produced by mitochondrial monoamine oxidase catalysis: biological implications. *Curr Pharm Des* **20**, 155–160 (2014).

90. Monzani, E. *et al.* Dopamine, Oxidative Stress and Protein-Quinone Modifications in Parkinson's and Other Neurodegenerative Diseases. *Angew Chem Int Ed Engl* **58**, 6512–6527 (2019).

91. Willems, P. H. G. M., Rossignol, R., Dieteren, C. E. J., Murphy, M. P. & Koopman, W. J. H. Redox Homeostasis and Mitochondrial Dynamics. *Cell Metabolism* vol. 22 207–218 Preprint at https://doi.org/10.1016/j.cmet.2015.06.006 (2015).

92. Eisner, V., Picard, M. & Hajnóczky, G. Mitochondrial dynamics in adaptive and maladaptive cellular stress responses. *Nature Cell Biology* vol. 20 755–765 Preprint at https://doi.org/10.1038/s41556-018-0133-0 (2018).

93. Hao, L. Y., Giasson, B. I. & Bonini, N. M. DJ-1 is critical for mitochondrial function and rescues PINK1 loss of function. *Proc Natl Acad Sci U S A* **107**, 9747–9752 (2010).

94. O'Hara, D. M., Pawar, G., Kalia, S. K. & Kalia, L. v. LRRK2 and α-Synuclein: Distinct or Synergistic Players in Parkinson's Disease? *Front Neurosci* **14**, 577 (2020).

95. Filograna, R. *et al.* Mitochondrial dysfunction in adult midbrain dopamine neurons triggers an early immune response. *PLoS Genet* **17**, e1009822 (2021).

96. Gautier, C. A. *et al.* The endoplasmic reticulum-mitochondria interface is perturbed in PARK2 knockout mice and patients with PARK2 mutations. *Hum Mol Genet* **25**, 2972–2984 (2016).

97. Lee, S. *et al.* Mitofusin 2 is necessary for striatal axonal projections of midbrain dopamine neurons. *Hum Mol Genet* **21**, 4827–4835 (2012).

98. Pham, A. H., Meng, S., Chu, Q. N. & Chan, D. C. Loss of Mfn2 results in progressive, retrograde degeneration of dopaminergic neurons in the nigrostriatal circuit. *Hum Mol Genet* **21**, 4817–4826 (2012).

99. Shutt, T., Geoffrion, M., Milne, R. & McBride, H. M. The intracellular redox state is a core determinant of mitochondrial fusion. *EMBO Rep* **13**, 909–915 (2012).

100. Holmström, K. M. & Finkel, T. Cellular mechanisms and physiological consequences of redox-dependent signalling. *Nature Reviews Molecular Cell Biology* vol. 15 411–421 Preprint at https://doi.org/10.1038/nrm3801 (2014).

101. Levonen, A. L., Hill, B. G., Kansanen, E., Zhang, J. & Darley-Usmar, V. M. Redox regulation of antioxidants, autophagy, and the response to stress: Implications for electrophile therapeutics. *Free Radic Biol Med* **71**, 196–207 (2014).

102. van Laer, K., Hamilton, C. J. & Messens, J. Low-Molecular-Weight Thiols in Thiol–Disulfide Exchange. *https://home.liebertpub.com/ars* **18**, 1642–1653 (2013).

103. Ulrich, K. & Jakob, U. The role of thiols in antioxidant systems. *Free Radic Biol Med* **140**, 14–27 (2019).

104. Wu, G., Fang, Y.-Z., Yang, S., Lupton, J. R. & Turner, N. D. Glutathione Metabolism and Its Implications for Health. *J Nutr* **134**, 489–492 (2004).

105. Forman, H. J., Zhang, H. & Rinna, A. Glutathione: Overview of its protective roles, measurement, and biosynthesis. *Mol Aspects Med* **30**, 1–12 (2009).

106. Schafer, F. Q. & Buettner, G. R. Redox environment of the cell as viewed through the redox state of the glutathione disulfide/glutathione couple. *Free Radic Biol Med* **30**, 1191–1212 (2001).

107. Iskusnykh, I. Y., Zakharova, A. A. & Pathak, D. Glutathione in Brain Disorders and Aging. *Molecules* vol. 27 Preprint at https://doi.org/10.3390/molecules27010324 (2022).

108. Bachhawat, A. K. & Yadav, S. The glutathione cycle: Glutathione metabolism beyond the γ-glutamyl cycle. *IUBMB Life* **70**, 585–592 (2018).

109. Lu, S. C. Glutathione synthesis. *Biochimica et Biophysica Acta (BBA) - General Subjects* **1830**, 3143–3153 (2013).

110. Lu, S. C. REGULATION OF GLUTATHIONE SYNTHESIS. *Mol Aspects Med* **30**, 42 (2009).

111. Oestreicher, J. & Morgan, B. Glutathione: subcellular distribution and membrane transport 1. *Biochem Cell Biol* **97**, 270–289 (2019).

112. Calabrese, G., Morgan, B. & Riemer, J. Mitochondrial Glutathione: Regulation and Functions. *Antioxidants and Redox Signaling* vol. 27 1162–1177 Preprint at https://doi.org/10.1089/ars.2017.7121 (2017).

113. Scirè, A. *et al.* Glutathione compartmentalization and its role in glutathionylation and other regulatory processes of cellular pathways. *BioFactors* vol. 45 152–168 Preprint at https://doi.org/10.1002/biof.1476 (2019).

114. Kumar, A. *et al.* Mammalian proapoptotic factor ChaC1 and its homologues function as γ-glutamyl cyclotransferases acting specifically on glutathione. *EMBO Rep* **13**, 1095–1101 (2012).

115. Kaur, A. *et al.* ChaC2, an Enzyme for Slow Turnover of Cytosolic Glutathione. *J Biol Chem* **292**, 638–651 (2017).

116. Aoyama, K. Glutathione in the Brain. *Int J Mol Sci* **22**, 22 (2021).

117. Matsumura, N., Kinoshita, C. & Aoyama, K. [Mechanism of glutathione production in neurons]. *Nihon Yakurigaku Zasshi* **156**, 26–30 (2021).

118. Huang, J. & Philbert, M. A. Distribution of glutathione and glutathione-related enzyme systems in mitochondria and cytosol of cultured cerebellar astrocytes and granule cells. *Brain Res* **680**, 16–22 (1995).

119. Ballatori, N. *et al.* Glutathione dysregulation and the etiology and progression of human diseases. *Biol Chem* **390**, 191–214 (2009).

120. Pearce, R. K. B., Owen, A., Daniel, S., Jenner, P. & Marsden, C. D. Alterations in the distribution of glutathione in the substantia nigra in Parkinson's disease. *Journal of Neural Transmission 1997 104:6* **104**, 661–677 (1997).

121. Sian, J. *et al.* Alterations in glutathione levels in Parkinson's disease and other neurodegenerative disorders affecting basal ganglia. *Ann Neurol* **36**, (1994).

122. Paik, S. R., Lee, D., Cho, H. J., Lee, E. N. & Chang, C. S. Oxidized glutathione stimulated the amyloid formation of α-synuclein. *FEBS Lett* **537**, 63–67 (2003).

123. Gökçe Çokal, B. *et al.* Serum glutathione peroxidase, xanthine oxidase, and superoxide dismutase activities and malondialdehyde levels in patients with Parkinson's disease. *Neurol Sci* **38**, 425–431 (2017).

124. Asanuma, M. & Miyazaki, I. Glutathione and related molecules in parkinsonism. *International Journal of Molecular Sciences* vol. 22 Preprint at https://doi.org/10.3390/ijms22168689 (2021).

125. Bjørklund, G., Peana, M., Maes, M., Dadar, M. & Severin, B. The glutathione system in Parkinson's disease and its progression. *Neuroscience and Biobehavioral Reviews* vol. 120 470–478 Preprint at https://doi.org/10.1016/j.neubiorev.2020.10.004 (2021).

126. Garrido, M. *et al.* Glutathione depletion and overproduction both initiate degeneration of nigral dopaminergic neurons. *Acta Neuropathol* **121**, 475–485 (2011).

127. Finkel, T. Signal transduction by reactive oxygen species. *Journal of Cell Biology* **194**, 7–15 (2011).

128. Harmel, R. & Fiedler, D. Features and regulation of non-enzymatic post-translational modifications. *Nature Chemical Biology 2018 14:3* **14**, 244–252 (2018).

129. Musaogullari, A. & Chai, Y. C. Redox regulation by protein s-glutathionylation: From molecular mechanisms to implications in health and disease. *International Journal of Molecular Sciences* vol. 21 1–25 Preprint at https://doi.org/10.3390/ijms21218113 (2020).

130. Miseta, A. & Csutora, P. Relationship Between the Occurrence of Cysteine in Proteins and the Complexity of Organisms. *Mol Biol Evol* **17**, 1232–1239 (2000).

131. Paulsen, C. E. & Carroll, K. S. Cysteine-Mediated Redox Signaling: Chemistry, Biology, and Tools for Discovery. *Chem Rev* **113**, 4633–4679 (2013).

132. Requejo, R., Hurd, T. R., Costa, N. J. & Murphy, M. P. Cysteine residues exposed on protein surfaces are the dominant intramitochondrial thiol and may protect against oxidative damage. *FEBS J* **277**, 1465–1480 (2010).

133. Poole, L. B. The basics of thiols and cysteines in redox biology and chemistry. *Free Radic Biol Med* **80**, 148–157 (2015).

134. Moran, L., Gutteridge, J. & Quinlan, G. Thiols in Cellular Redox Signalling and Control. *Curr Med Chem* **8**, 763–772 (2012).

135. Chung, H. S., Wang, S.-B., Venkatraman, V., Murray, C. I. & van Eyk, J. E. Cysteine Oxidative Posttranslational Modifications. *Circ Res* **112**, 382–392 (2013).

136. lo Conte, M. & Carroll, K. S. The Redox Biochemistry of Protein Sulfenylation and Sulfinylation *. *Journal of Biological Chemistry* **288**, 26480–26488 (2013).

137. Groitl, B. & Jakob, U. Thiol-based redox switches. *Biochimica et Biophysica Acta (BBA) - Proteins and Proteomics* **1844**, 1335–1343 (2014).

138. Kalinina, E. & Novichkova, M. Glutathione in Protein Redox Modulation through S-Glutathionylation and S-Nitrosylation. *Molecules* **26**, (2021).

139. Mieyal, J. J., Gallogly, M. M., Qanungo, S., Sabens, E. A. & Shelton, M. D. Molecular Mechanisms and Clinical Implications of Reversible Protein S-Glutathionylation. *https://home.liebertpub.com/ars* **10**, 1941–1988 (2010).

140. Townsend, D. M. *et al.* Novel Role for Glutathione S-Transferase π: REGULATOR OF PROTEIN S-GLUTATHIONYLATION FOLLOWING OXIDATIVE AND NITROSATIVE STRESS *. *Journal of Biological Chemistry* **284**, 436–445 (2009).

141. Tew, K. D. Redox in redux: Emergent roles for glutathione S-transferase P (GSTP) in regulation of cell signaling and S-glutathionylation. *Biochem Pharmacol* **73**, 1257–1269 (2007).

142. Matsui, R. *et al.* Redox Regulation via Glutaredoxin-1 and Protein S-Glutathionylation. *Antioxid Redox Signal* **32**, 677–700 (2020).

143. Beer, S. M. *et al.* Glutaredoxin 2 Catalyzes the Reversible Oxidation and Glutathionylation of Mitochondrial Membrane Thiol Proteins: IMPLICATIONS FOR MITOCHONDRIAL REDOX REGULATION AND ANTIOXIDANT DEFENSE *. *Journal of Biological Chemistry* **279**, 47939–47951 (2004).

144. Vaish, S., Gupta, D., Mehrotra, R., Mehrotra, S. & Basantani, M. K. Glutathione S-transferase: a versatile protein family. *3 Biotech 2020 10:7* **10**, 1–19 (2020).

145. di Simplicio, P., Lupis, E. & Rossi, R. Different mechanisms of formation of glutathione-protein mixed disulfides of diamide and tert-butyl hydroperoxide in rat blood. *Biochim Biophys Acta* **1289**, 252–260 (1996).

146. Ogata, F. T., Branco, V., Vale, F. F. & Coppo, L. Glutaredoxin: Discovery, redox defense and much more. *Redox Biol* **43**, (2021).

147. Lillig, C. H. & Berndt, C. Glutaredoxins in thiol/disulfide exchange. *Antioxid Redox Signal* **18**, 1654–1665 (2013).

148. Arnér, E. S. J. & Holmgren, A. Physiological functions of thioredoxin and thioredoxin reductase. *Eur J Biochem* **267**, 6102–6109 (2000).

149. Findlay, V. J. *et al.* A Novel Role for Human Sulfiredoxin in the Reversal of Glutathionylation. *Cancer Res* **66**, 6800 (2006).

150. Matsusaki, M. *et al.* The Protein Disulfide Isomerase Family: from proteostasis to pathogenesis. *Biochim Biophys Acta Gen Subj* **1864**, (2020).

151. Grek, C. L., Zhang, J., Manevich, Y., Townsend, D. M. & Tew, K. D. Causes and consequences of cysteine s-glutathionylation. *Journal of Biological Chemistry* vol. 288 26497–26504 Preprint at https://doi.org/10.1074/jbc.R113.461368 (2013).

152. Zhang, J., Ye, Z. wei, Singh, S., Townsend, D. M. & Tew, K. D. An evolving understanding of the S-glutathionylation cycle in pathways of redox regulation. *Free Radical Biology and Medicine* vol. 120 204–216 Preprint at https://doi.org/10.1016/j.freeradbiomed.2018.03.038 (2018).

153. Wolf, C. *et al.* Redox Modifications of Proteins of the Mitochondrial Fusion and Fission Machinery. *Cells* **9**, 815 (2020).

154. Thaher, O. *et al.* The thiol switch C684 in Mitofusin-2 mediates redox-induced alterations of mitochondrial shape and respiration. *Neurochem Int* **117**, 167–173 (2018).

155. Sabens Liedhegner, E. A., Gao, X. H. & Mieyal, J. J. Mechanisms of altered redox regulation in neurodegenerative diseases-focus on S-glutathionylation. *Antioxidants and Redox Signaling* vol. 16 543–566 Preprint at https://doi.org/10.1089/ars.2011.4119 (2012).

156. Lind, C. *et al.* Identification of S-glutathionylated cellular proteins during oxidative stress and constitutive metabolism by affinity purification and proteomic analysis. *Arch Biochem Biophys* **406**, 229–240 (2002).

157. Nonaka, K. *et al.* Serum Levels of S-Glutathionylated Proteins as a Risk-Marker for Arteriosclerosis Obliterans. *Circulation Journal* **71**, 100–105 (2007).

158. Grek, C. L., Reyes, L., Townsend, D. M. & Tew, K. D. S-glutathionylation of buccal cell proteins as biomarkers of exposure to hydrogen peroxide. *BBA Clin* **2**, 31–39 (2014).

159. Sánchez-Gómez, F. J., Espinosa-Díez, C., Dubey, M., Dikshit, M. & Lamas, S. S-glutathionylation: Relevance in diabetes and potential role as a biomarker. *Biol Chem* **394**, 1263–1280 (2013).

160. Wang, H.-L., Zhang, J., Li, Y.-P., Dong, L. & Chen, Y.-Z. Potential use of glutathione as a treatment for Parkinson's disease. *Exp Ther Med* **21**, (2021).

161. Mallach, A. *et al.* Post mortem examination of Parkinson's disease brains suggests decline in mitochondrial biomass, reversed by deep brain stimulation of subthalamic nucleus. *FASEB J* **33**, 6957–6961 (2019).

162. Norat, P. *et al.* Mitochondrial dysfunction in neurological disorders: Exploring mitochondrial transplantation. *npj Regenerative Medicine* vol. 5 Preprint at https://doi.org/10.1038/s41536-020-00107-x (2020).

163. Reddy, P. H. Inhibitors of Mitochondrial Fission as a Therapeutic Strategy for Diseases with Oxidative Stress and Mitochondrial Dysfunction. *Journal of Alzheimer's Disease* **40**, 245–256 (2014).

164. Falkenburger, B. H., Saridaki, T. & Dinter, E. Cellular models for Parkinson's disease. *J Neurochem* **139**, 121–130 (2016).

165. Xicoy, H., Wieringa, B. & Martens, G. J. M. The SH-SY5Y cell line in Parkinson's disease research: a systematic review. *Mol Neurodegener* **12**, 10 (2017).

166. Xie, H. R., Hu, L. sen & Li, G. Y. SH-SY5Y human neuroblastoma cell line: In vitro cell model of dopaminergic neurons in Parkinson's disease. *Chin Med J (Engl)* **123**, 1086–1092 (2010).

167. Påhlman, S. *et al.* Differentiation and survival influences of growth factors in human neuroblastoma. *Eur J Cancer* **31**, 453–458 (1995).

168. Lee, H. S., Park, C. W. & Kim, Y. S. MPP(+) increases the vulnerability to oxidative stress rather than directly mediating oxidative damage in human neuroblastoma cells. *Exp Neurol* **165**, 164–171 (2000).

169. Buthionine sulfoximine | C8H18N2O3S - PubChem. https://pubchem.ncbi.nlm.nih.gov/compound/Buthionine-sulfoximine.

170. Chen, J., Small-Howard, A., Yin, A. & Berry, M. J. The responses of Ht22 cells to oxidative stress induced by buthionine sulfoximine (BSO). *BMC Neurosci* **6**, 10 (2005).

171. Salvi, A., Patki, G., Khan, E., Asghar, M. & Salim, S. Protective Effect of Tempol on Buthionine Sulfoximine-Induced Mitochondrial Impairment in Hippocampal Derived HT22 Cells. *Oxid Med Cell Longev* **2016**, (2016).

172. Pileblad, E., Magnusson, T. & Fornstedt, B. Reduction of brain glutathione by L-buthionine sulfoximine potentiates the dopamine-depleting action of 6-hydroxydopamine in rat striatum. *J Neurochem* **52**, 978–980 (1989).

173. Slott, V. L. & Hales, B. F. Effect of glutathione depletion by buthionine sulfoximine on rat embryonic development in vitro. *Biochem Pharmacol* **36**, 683–688 (1987).

174. Wüllner, U. *et al.* Glutathione depletion potentiates MPTP and MPP+ toxicity in nigral dopaminergic neurones. *Neuroreport* **7**, 921–923 (1996).

175. Kučera, O. *et al.* The effect of tert -butyl hydroperoxide-induced oxidative stress on lean and steatotic rat hepatocytes in vitro. *Oxid Med Cell Longev* **2014**, (2014).

176. Kanupriya *et al.* Mechanism of tert-butylhydroperoxide induced cytotoxicity in U-937 macrophages by alteration of mitochondrial function and generation of ROS. *Toxicology in Vitro* **21**, 846–854 (2007).

177. Nishida, K., Ohta, Y. & Ishiguro, I. Modulating role of endogenous reduced glutathione in tert-butyl hydroperoxide-induced cell injury in isolated rat hepatocytes. *Free Radic Biol Med* **23**, 453–462 (1997).

178. Drahota, Z. *et al.* Tert-Butyl Hydroperoxide Selectively Inhibits Mitochondrial Respiratory-Chain Enzymes in Isolated Rat Hepatocytes. *Physiol. Res* **54**, 67–72 (2005).

179. Crane, D., Hüussinger, D., Graf, P. & Sies, H. Decreased Flux through Pyruvate Dehydrogenase by Thiol Oxidation during t-Butyl Hydroperoxide Metabolism in Perfused Rat Liver. *Hoppe Seylers Z Physiol Chem* **364**, 977–988 (1983).

180. Rush, G. F. & Alberts, D. tert.-Butyl hydroperoxide metabolism and stimulation of the pentose phosphate pathway in isolated rat hepatocytes. *Toxicol Appl Pharmacol* **85**, 324–331 (1986).

181. Langston, J. W., Ballard, P., Tetrud, J. W. & Irwin, I. Chronic Parkinsonism in humans due to a product of meperidine-analog synthesis. *Science (1979)* **219**, 979 (1983).

182. Meredith, G. & Rademacher, D. MPTP mouse models of Parkinson's disease: An update. *J Parkinsons Dis* **1**, 19–33 (2011).

183. Dauer, W. & Przedborski, S. Parkinson's disease: Mechanisms and models. *Neuron* **39**, 889–909 (2003).

184. Ali, S. F., David, S. N., Newport, G. D., Cadet, J. L. & Slikker Jr., W. MPTP-induced oxidative stress and neurotoxicity are age-dependent: Evidence from measures of reactive oxygen species and striatal dopamine levels. *Synapse* **18**, 27–34 (1994).

185. Nakai, M., Mori, A., Watanabe, A. & Mitsumoto, Y. 1-Methyl-4-phenylpyridinium (MPP+) decreases mitochondrial oxidation-reduction (REDOX) activity and membrane potential (Δψm) in rat striatum. *Exp Neurol* **179**, 103–110 (2003).

186. Murphy, M. P. *et al.* Guidelines for measuring reactive oxygen species and oxidative damage in cells and in vivo. *Nat Metab* **4**, 651–662 (2022).

187. Rahman, I., Kode, A. & Biswas, S. K. Assay for quantitative determination of glutathione and glutathione disulfide levels using enzymatic recycling method. *Nat Protoc* **1**, 3159–3165 (2006).

188. MM, B. A rapid and sensitive method for the quantitation of microgram quantities of protein utilizing the principle of protein-dye binding. *Anal Biochem* **72**, 248–254 (1976).

189. Livak, K. J. & Schmittgen, T. D. Analysis of relative gene expression data using real-time quantitative PCR and the 2(-Delta Delta C(T)) Method. *Methods* **25**, 402–408 (2001).

190. Li, S. *et al.* Deep learning based prediction of species-specific protein S-glutathionylation sites. *Biochimica et Biophysica Acta (BBA) - Proteins and Proteomics* **1868**, 140422 (2020).

191. Wang, P. *et al.* iCysMod: an integrative database for protein cysteine modifications in eukaryotes. *Brief Bioinform* (2021) doi:10.1093/bib/bbaa400.

192. Li, S. *et al.* pCysMod: Prediction of Multiple Cysteine Modifications Based on Deep Learning Framework. *Front Cell Dev Biol* **9**, 117 (2021).

193. Jones, G., Willett, P., Glen, R. C., Leach, A. R. & Taylor, R. Development and validation of a genetic algorithm for flexible docking. *J Mol Biol* **267**, 727–748 (1997).

194. Wiederstein, M. & Sippl, M. J. ProSA-web: interactive web service for the recognition of errors in three-dimensional structures of proteins. *Nucleic Acids Res* **35**, W407 (2007).

195. Weininger, D. Smiles. 3. Depict. Graphical Depiction of Chemical Structures. *J Chem Inf Comput Sci* **30**, 237–243 (1990).

196. *GOLD User Guide GOLD User Guide iii*. www.ccdc.cam.ac.uk (2019).

197. Verdonk, M. L., Cole, J. C., Hartshorn, M. J., Murray, C. W. & Taylor, R. D. Improved protein–ligand docking using GOLD. *Proteins: Structure, Function, and Bioinformatics* **52**, 609–623 (2003).

198. Seyfried, J. *et al.* Differential effects of L-buthionine sulfoximine and ethacrynic acid on glutathione levels and mitochondrial function in PC12 cells. *Neurosci Lett* **264**, (1999).

199. Greenbaum, D., Colangelo, C., Williams, K. & Gerstein, M. Comparing protein abundance and mRNA expression levels on a genomic scale. *Genome Biol* **4**, (2003).

200. Schmidt, T. *et al.* ProteomicsDB. *Nucleic Acids Res* **46**, D1271–D1281 (2018).

201. Marino, S. M. & Gladyshev, V. N. Analysis and Functional Prediction of Reactive Cysteine Residues *. *Journal of Biological Chemistry* **287**, 4419–4425 (2012).

202. Dosztányi, Z., Csizmók, V., Tompa, P. & Simon, I. The pairwise energy content estimated from amino acid composition discriminates between folded and intrinsically unstructured proteins. *J Mol Biol* **347**, 827–839 (2005).

203. Klausen, M. S. *et al.* NetSurfP-2.0: Improved prediction of protein structural features by integrated deep learning. *Proteins* **87**, 520–527 (2019).

204. H, X. *et al.* A Quantitative Tissue-Specific Landscape of Protein Redox Regulation during Aging. *Cell* **180**, 968-983.e24 (2020).

205. Bak, D. W., Pizzagalli, M. D. & Weerapana, E. Identifying Functional Cysteine Residues in the Mitochondria. *ACS Chem Biol* **12**, 947–957 (2017).

206. Mnatsakanyan, R. *et al.* Proteome-wide detection of S-nitrosylation targets and motifs using bioorthogonal cleavable-linker-based enrichment and switch technique. *Nat Commun* **10**, 2195 (2019).

207. Satohisa, S. *et al.* Endogenous NO upon estradiol-17β stimulation and NO donor differentially regulate mitochondrial S-nitrosylation in endothelial cells. *Endocrinology* **155**, 3005–3016 (2014).

208. Zhao, F., Austria, Q., Wang, W. & Zhu, X. Mfn2 Overexpression Attenuates MPTP Neurotoxicity In Vivo. *Int J Mol Sci* **22**, 1–14 (2021).

209. Huang, P., Yu, T. & Yoon, Y. Mitochondrial clustering induced by overexpression of the mitochondrial fusion protein Mfn2 causes mitochondrial dysfunction and cell death. *Eur J Cell Biol* **86**, 289–302 (2007).

210. Castro-Caldas, M. *et al.* Glutathione S-transferase pi mediates MPTP-induced c-Jun N-terminal kinase activation in the nigrostriatal pathway. *Mol Neurobiol* **45**, 466–477 (2012).

211. Che, L. *et al.* Mitochondrial redox-driven mitofusin 2 S-glutathionylation promotes neuronal necroptosis via disrupting ER-mitochondria crosstalk in cadmium-induced neurotoxicity. *Chemosphere* **262**, (2021).

212. Sian, J. *et al.* Glutathione-related enzymes in brain in Parkinson's disease. *Ann Neurol* **36**, 356–361 (1994).

213. Jenner, P., Dexter, D. T., Sian, J., Schapira, A. H. v & Marsden, C. D. Oxidative stress as a cause of nigral cell death in Parkinson's disease and incidental lewy body disease. *Ann Neurol* **32**, S82–S87 (1992).

214. Ryan, M. T. & Stojanovski, D. Mitofusins 'bridge'' the gap between oxidative stress and mitochondrial hyperfusion'. *EMBO Rep* **13**, 870 (2012).

215. Hurd, T. R. *et al.* Complex I within oxidatively stressed bovine heart mitochondria is glutathionylated on Cys-531 and Cys-704 of the 75-kDa subunit: Potential role of Cys residues in decreasing oxidative damage. *Journal of Biological Chemistry* **283**, 24801–24815 (2008).

216. Taylor, E. R. *et al.* Reversible glutathionylation of complex I increases mitochondrial superoxide formation. *J Biol Chem* **278**, 19603–19610 (2003).

217. Zhu, X. *et al.* Mfn2 protects dopaminergic neurons exposed to paraquat both in vitro and in vivo: Implications for idiopathic Parkinson's disease. *Biochim Biophys Acta Mol Basis Dis* **1863**, 1359–1370 (2017).

218. Chen, H. & Chan, D. C. Mitochondrial dynamics--fusion, fission, movement, and mitophagy--in neurodegenerative diseases. *Hum Mol Genet* **18**, (2009).

219. Neuspiel, M., Zunino, R., Gangaraju, S., Rippstein, P. & McBride, H. Activated Mitofusin 2 Signals Mitochondrial Fusion, Interferes with Bax Activation, and Reduces Susceptibility to Radical Induced Depolarization. *Journal of Biological Chemistry* **280**, 25060–25070 (2005).

220. Jahani-Asl, A. *et al.* Mitofusin 2 protects cerebellar granule neurons against injury-induced cell death. *Journal of Biological Chemistry* **282**, 23788–23798 (2007).

VI. ANNEXES

Supplementary Data

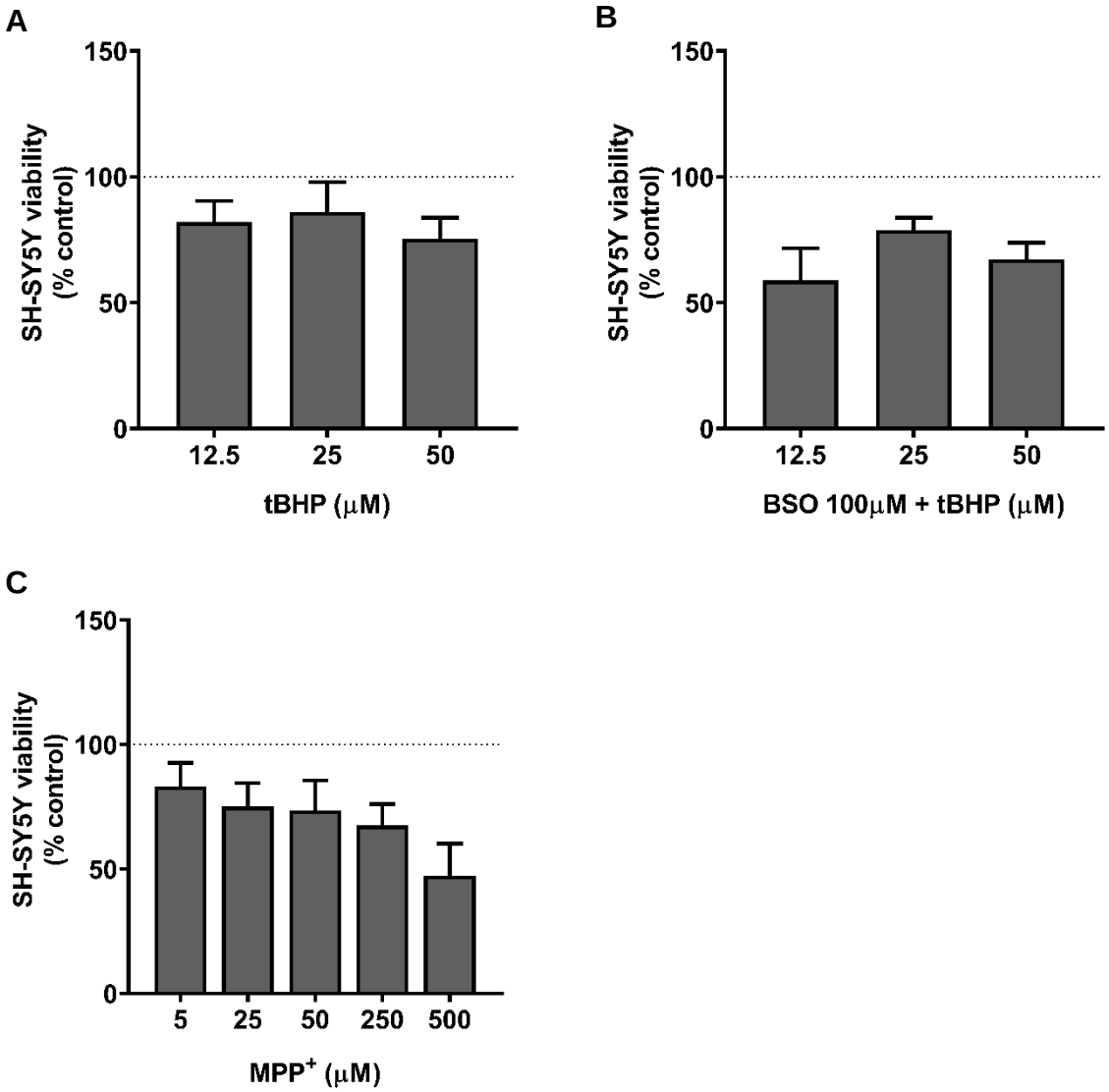

Figure S 1 Dose-dependent MTT-based SH-SY5Y cell viability assays in the *in vitro* model. (A) 12.5; 25 and 50 µM tBHP for 3 hours or with **(B)** pre-treatment with BSO 100 µM for 24 hours. **(C)** 5; 25; 50; 250; 500 µM MPP^+ for 24 hours.

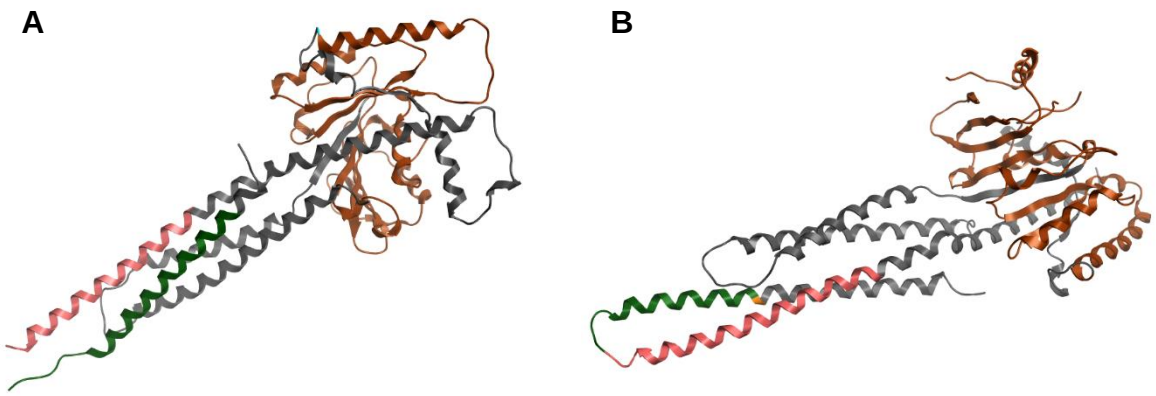

Figure S 2 (A) Graphical representation of the MFN1 protein structure (PDB ID: 5GO4, resolution 2.202 Å) and **(B)** MFN2 (PDB ID: 6JFL, resolution 2.806 Å) used for homology modelling with MOE software. Domains are identified in both structures with different colours.

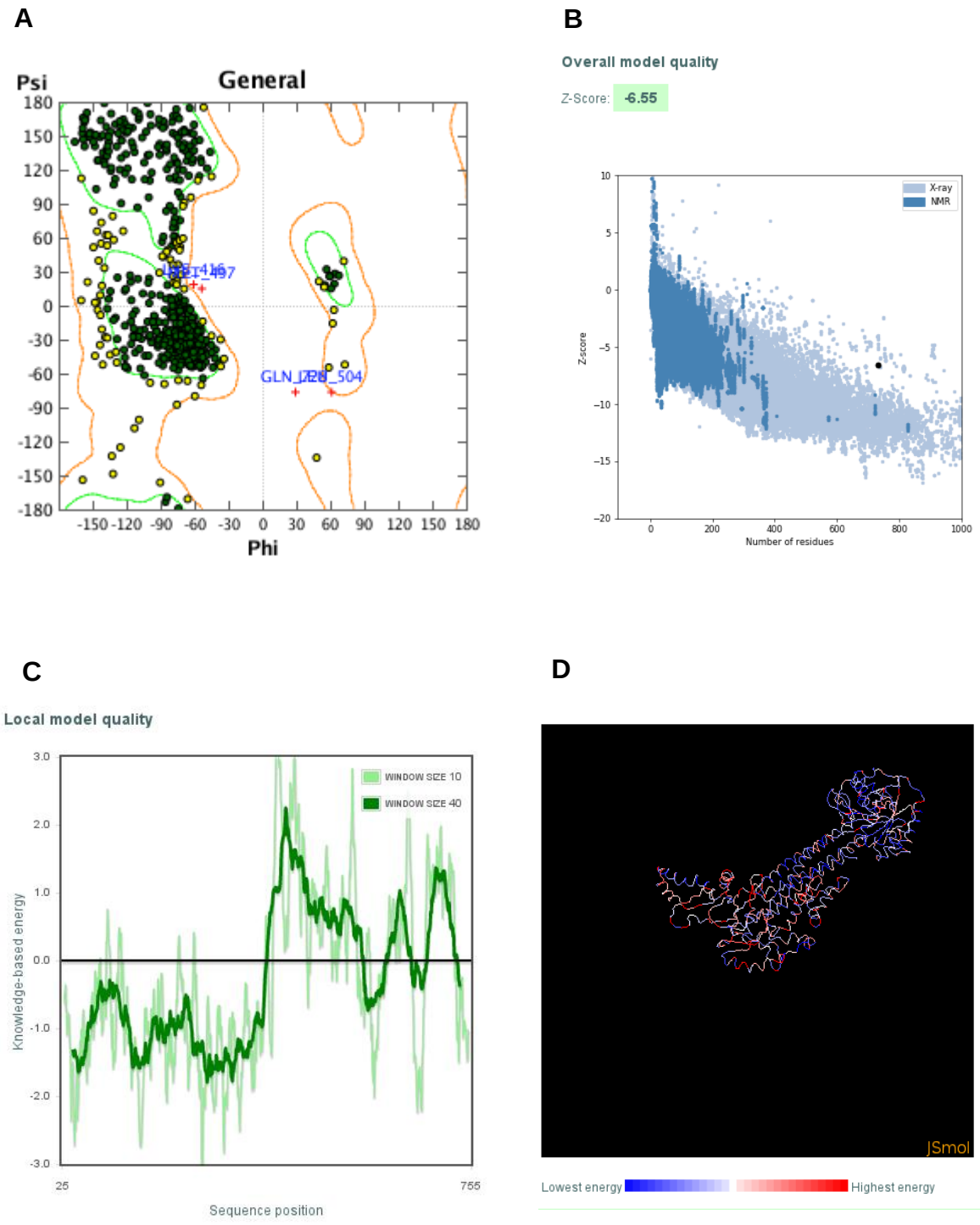

Figure S 3 Validation of the MFN2 homology model. (A) Ramachandran plot; **(B)** Overall model quality with the respective z-score; **(C)** energy plot as a function of amino acid sequence position; and **(D)** 3D visualization using molecule viewer Jmol (http://www.jmol.org) of the energy distribution for each amino acid in the homology model.